Tailored Flow Behavior of Biogenic Suspensions and Oils

Zur Erlangung des akademischen Grades eines
DOKTORS DER INGENIEURWISSENSCHAFTEN (Dr.-Ing.)

der Fakultät für Chemieingenieurwesen und Verfahrenstechnik
des Karlsruher Instituts für Technologie (KIT)
vorgelegte

genehmigte
DISSERTATION

von
Dipl.-Ing. Leon Jampolski
aus Tscheljabinsk (Russland)

Referent:	Prof. Dr. N. Willenbacher
Korreferent:	Prof. Dr.-Ing. T. Kolb
Tag der mündlichen Prüfung:	14.06.2018

Preface

This publication based thesis contains the main results of my experimental investigations obtained during 2013 and 2017 at the Karlsruhe Institute of Technology, Institute for Mechanical Process Engineering and Mechanics in the group of Applied Mechanics.
First of all I want to thank my supervisor Prof. Dr. Norbert Willenbacher for giving me the opportunity to work on an exiting research topic. With your patience and advices you helped me to develop and grow with the incoming tasks.
Many thanks also to Prof. Dr. Thomas Kolb for being the co-supervisor of this thesis as well as the possibility to perform experimental measurements at your institute. Simultaneously I want to thank Alexander Sänger and Dr. Tobias Jakobs for their help and support regarding measurements and discussions. Thanks also to Christian Hotz and Dr. Sabine Fleck for the usage of their apertures and to Mark Eberhard for providing materials.
Thank you also to Prof. Dr. Gisela Guthausen for her support and advices regarding the MRI experiments.
Special thanks to Marco Tomasi Morgano for the introduction into pyrolysis oils and the time during the Bio Fuels Conference.
Furthermore I want to thank Dr. Bernhard Hochstein for the discussions and the scientific exchange. Thanks also to Astrid Huber and Klaus Hirsch for the support and the particle size measurements.
Also I would like to thank my students Björn Baumgarten, Pedro Andrade, Katrin Becker, Rafael Gonzalez Mayorga, Karin Wang, Karim Abdel Aal und Ronald Gordon for their contribution.
I want to thank Susanne Wollgarten, Monica Schneider and Dirk Sachsenheimer for the intellectual discussions during lunch and other activities.
Moreover I like to thank my family for their support during my time at the university.
Especially I want to thank Clara for your support, the proofreading, your advice and your patience.

Notations

Latin symbols

symbol	description
A	Area of projection
A_H	Hamaker constant
B_0	Magnetic flux density
c	Constant, see Eq. 4.10
c_{ero}	Erosional constant
C	Circularity
$d_{particle}$	Particle diameter
d_{16}	Particle size at cumulated PSD of 16%
d_{50}	Particle size at cumulated PSD of 50%
d_{84}	Particle size at cumulated PSD of 84%
D_{dr}	Diameter of a single drop
D_{liq}	Diameter of undisturbed liquid jet
E_A	Activation energy
F_c	Capillary force
$F_{c_{close}}$	Capillary force for spheres in contact
f_{prim}	Primary instability frequency
F_{vdW}	van-der-Waals force
g	Constant of gravitation
$g(\phi^*_{sf}, s^*)$	Functional correlation
G'	Storage modulus
G''	Loss modulus
K_S	Consistency index
L_C	Characteristic length
m	Flow index
m_{liquid}	Mass of liquid phase
m_{solid}	Mass of solid phase
M_W	Molecular weight

n	Number of revolutions
N_1	First normal stress difference
N_{pic}	Number of images
q_0	Differential circulation distribution
q_3	Differential particle size distribution
Q_3	Cumulated particle size distribution
r	Rotor radius
R	Ideal gas constant
Re	Reynolds number
s	Distance between two particles
s^*	Normalized particle distance
SMD	Sauter mean diameter
t_{mill}	Milling time
t	Time
δt	Time difference
T	Temperature
T_0	Reference temperature
T_{pyro}	Pyrolysis temperature
Th_{sp}	Threshold value
$V_{capillary}$	Capillary bridge volume
v_{gas}	Gas phase velocity
v_{jet}	Mean jet velocity
v_{liq}	Liquid phase velocity
V_{liquid}	Volume of liquid phase
V_{pore}	Particle pore volume
v_{rel}	Relative velocity
V_{solid}	Volume of solid phase
We	Weber number
x	x-axis coordinate
y	y-axis coordinate
z	z-axis coordinate

Greek symbols

symbol	**description**
$\overline{\alpha}_{sp}$	Time averaged spray angle
$\dot{\gamma}$	Shear rate
$\dot{\gamma}_{high}$	Shear rate at a value of 1000 s^{-1}
$\dot{\gamma}_{low}$	Shear rate at a value of 1.1 s^{-1}
Γ	Interfacial tension
ε	Porosity
η	Dynamic viscosity
η_{fluid}	Bulk viscosity
η_{red}	Reduced viscosity
η_{rel}	Relative viscosity
η_{infty}	Infinite shear rate viscosity
$[\eta]$	Intrinsic viscosity
$\theta_{(S,B)}$	Contact angle of the bulk to the solid
ρ	Density
ρ_{avg}	Average density of a multiphase system
ρ_{gas}	Gas density
ρ_{liquid}	Density of the liquid
ρ_{solid}	Solid density
ρ_{susp}	Suspension density
σ	Shear stress
σ_0	Stress amplitude
σ_{PSD}	Width of the PSD
$\Delta\sigma$	Shear stress difference
ϕ_m	Mass fraction
ϕ_{sf}	Second fluid fraction
ϕ^*_{sf}	Normalized second fluid fraction
ϕ_V	Volume fraction
$\phi_{V_{max}}$	Maximal packing fraction
ω	Angular velocity

Abbreviations

ATMO	Atmospheric spray test rig
BW	Beech wood
BWCS	Beech wood coke slurry
CM	Chicken manure
CMC	Carboxymethyl cellulose
DME	Dimethyl ether
EFG	Entrained flow gasification
GC-MS	Gas chromatography coupled with mass spectroscopy
GLR	Gas-to-liquid ratio
HHV	Higher heating value
HPLC	High performance liquid chromatography
IGCC	Integrated gasification combined cycle
LHV	Lower heating value
LPG	Liquefied petroleum gas
MRI	Magnetic resonance imaging
NMR	Nuclear magnetic resonance
PAA	Poly acrylic acid
PSD	Particle size distribution
PTFE	Polytetrafluoroethylene
RARE	Rapid acquisition with relaxation enhancement
RCF	Relative centrifugal force
SEC	Size-exclusion chromatography
SEM	Scanning electron microscope
SNG	Synthetic natural gas
SS	Sewage sludge
THF	Tetrahydrofuran
vdW	van-der-Waals
WS	Wheat straw
WSCS	Wheat straw coke slurry

Contents

Preface i

Notations ii

1 Introduction 1

1.1 Flow behavior of suspensions . . . 3

1.1.1 Sedimentation and capillary suspensions . . . 4

1.1.2 Rheology of anisotropic particle suspensions . . . 7

1.2 Atomization . . . 10

1.2.1 Atomization for EFG within the bioliq®-process . . . 12

1.3 Pyrolysis oils . . . 13

2 Manuscript overview and scope of the work 16

3 Improving the Processability of Coke Water Slurries for Entrained Flow Gasification 18

3.1 Abstract . . . 18

3.2 Introduction . . . 19

3.3 Materials and methods . . . 21

3.3.1 Materials . . . 21

3.3.2 Sample preparation . . . 22

3.3.3 Rheological characterization . . . 22

3.3.4 Sedimentation stability . . . 23

3.3.5 Atomization . . . 24

3.4 Results and discussion . . . 26

3.4.1 Rheological characterization . . . 26

3.4.2 Sedimentation stability . . . 27

3.4.3 Atomization . . . 31

3.5 Conclusion . . . 38

3.6 Acknowledgement . . . 39

4 Influence of particle shape on the rheology of high solids coke water slurries 40
4.1 Abstract . . . 40
4.2 Introduction . . . 40
4.3 Materials and methods . . . 43
4.3.1 Materials . . . 43
4.3.2 Particle size and shape design . . . 44
4.3.3 Particle shape determination . . . 44
4.3.4 Sample preparation . . . 45
4.3.5 Rheological characterization . . . 45
4.3.6 Intrinsic viscosity . . . 46
4.4 Results and discussion . . . 47
4.4.1 Milling influence . . . 47
4.4.2 Influence of mass and volume fraction on flow behavior . . . 50
4.4.3 Influence of particle shape on viscosity in the low and high shear regime . . . 54
4.5 Conclusion . . . 56
4.6 Acknowledgement . . . 58

5 Flow Behavior and Aging of Pyrolysis Oils from Different Feedstocks 59
5.1 Abstract . . . 59
5.2 Introduction . . . 60
5.3 Materials and methods . . . 62
5.3.1 Materials . . . 62
5.3.2 Rheological measurements . . . 62
5.3.3 Instrumental analysis . . . 65
5.3.4 SEC . . . 67
5.4 Results and discussion . . . 68
5.4.1 Flow behavior . . . 68
5.4.2 Temperature dependency . . . 69
5.4.3 Aging under a free surface . . . 71
5.4.4 Aging under an inert gas atmosphere . . . 73
5.4.5 GC-MS and SEC analyses . . . 75
5.5 Conclusion . . . 77
5.6 Supporting information . . . 79
5.7 Acknowledgments . . . 82

6 Summary 83

7 Outlook **87**

8 Kurzfassung **88**

Bibliography **93**

1 Introduction

Centuries ago wood was the principal energy source for domestic life as well as for the then-heavy industry. The world population was just a fraction of the one nowadays and completely dependent on renewables [Henrich et al., 2015]. With progressively increasing industrialization fossil fuels have taken the role of the main energy supply. Today, with a world population of more than 7 billion people and an energy consumption of 600 EJ a^{-1} over 80 % of this energy mixture is provided by fossil fuels and only 10 % by bioenergy [Kaltschmitt et al., 2009]. Due to the expected exponential growth of the population a doubling of the energy consumption to 1200 EJ a^{-1} is estimated during the next century. If the extraction of fossil fuels will be enhanced or maintained, resources like crude oil or natural gas could be probably exhausted within this century, whilst coal deposits could last for approximately a millennium [Dahmen et al., 2016]. A certain amount of the fossil fuels have to be replaced by renewable energy to prevent their depletion. Electricity, which is about 40 % of the consumed total secondary energy, can be generated effectively by using primary energy sources like wind and solar power systems [Patel, 2006]. Utilization of different biomass can be applied by thermochemical, physico-chemical and biochemical conversion into force and heat as schematically shown in 1.1. However, the only renewable carbonaceous source is biomass (phyto- and zoomass, including their excrements).

Since the first decade of the new millennium the growth of global biofuel production is expanding. The government policies target different objectives such as promotion of rural economic growth, suppressing global warming or reducing the use of fossil fuels [Hochman et al., 2010]. Currently commercialized biofuels are first-generation biofuels based on food crops [Sims et al., 2010]. As a consequence thereof a price boost of food commodity appeared. A more ethical way to produce biofuels or hydrocarbons is provided by the biomass to liquid bioliq®-process developed in Karlsruhe [Dahmen et al., 2012]. It is a new path to use residual biomass in a two-step procedure. First a decentralized pretreatment of non-eatable biomass takes place. Low grade coproducts of biomass production from agriculture and forestry, e.g. wheat straw are the basic raw material. Energy densification takes place via pyrolysis, the biomass is converted into a high energy density biogenic fluid. The intermediate products, resulting from the py-

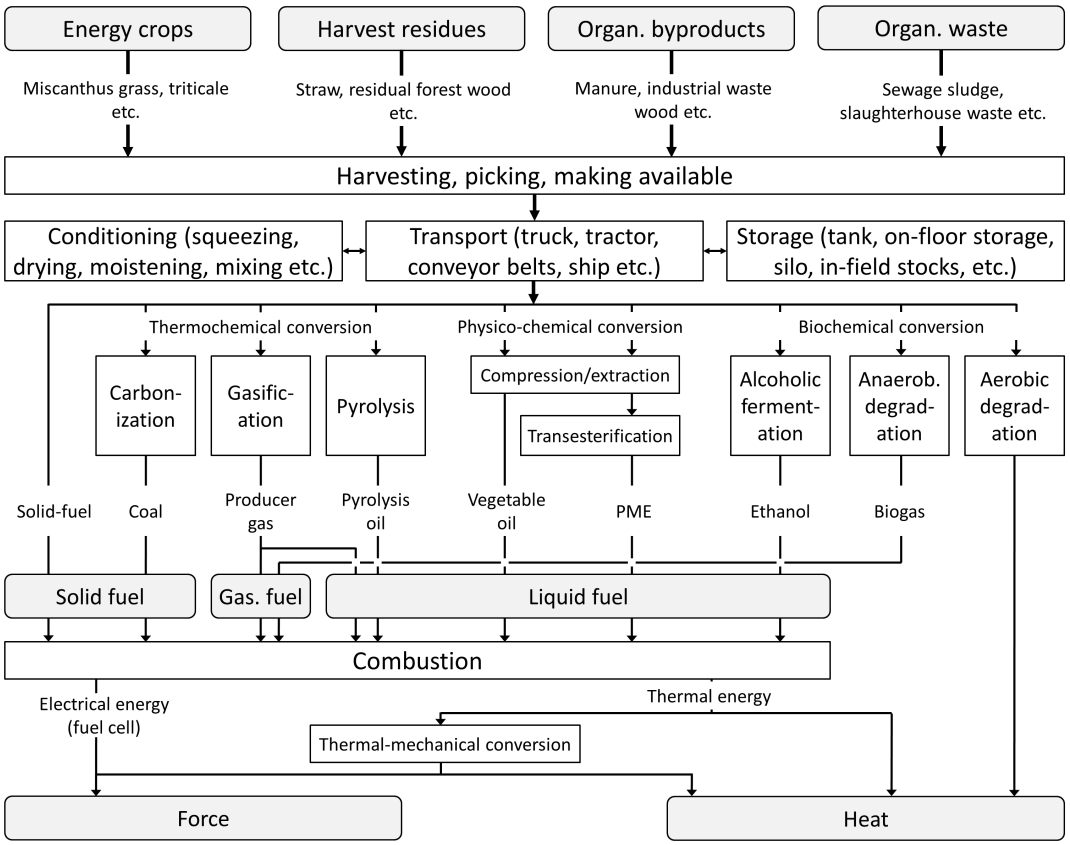

Figure 1.1: Schematic supply chain of energy delivery from biomass (gray boxes: energy sources; white boxes: conversion processes; simplified illustration without light as useful energy) after [Kaltschmitt et al., 2009].

rolysis, have to be transported in a large mass scale at reasonable transportation costs to a central gasification plant. This previously produced slurry is used as fuel for a high pressure entrained flow gasifier (EFG) [Higman and Burgt, 2003, Dahmen et al., 2012]. A flow sheet of the subsequent treatment of the biogenic fluid is shown in in Figure 1.2, focusing on the EFG. The slurry is stored in tanks, which have to be permanently stirred to prevent sedimentation of the dispersed solids (coke). Stirring results in a steady energy consumption, which influences the process efficiency in a negative way. Afterwards a pumping of the slurry to the EFG takes place. Additives for improvement of the flow behavior can be added here, followed by an atomization of the liquid in the gasifier. The here-from produced synthesis gas can be converted by a subsequent gas cleaning and a synthesis step into a broad range of (synthetic) fuels and carbon-based chemicals, which

are accessible through this process [Dahmen et al., 2015].
The flow behavior of the pyrolysis products, especially the coke slurries, plays an important role within this process and a wide range of shear rates are relevant. Low shear rates control sedimentation, the intermediate shear rate regime is relevant for unit operations like pumping and mixing, finally the flow behavior at high shear rates is decisive for atomization in the burner nozzle of an EFG.

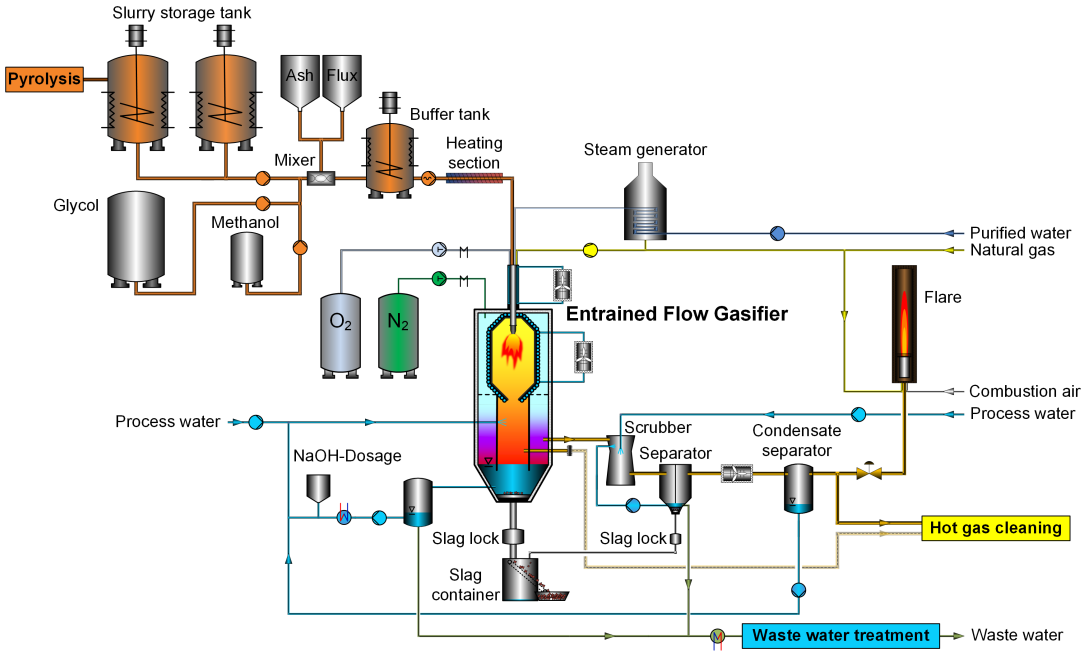

Figure 1.2: Flow sheet of the bioliq® EFG-process [Bioliq, 2017].

1.1 Flow behavior of suspensions

Dispersions are heterogeneous mixtures of a dispersed phase in a bulk fluid phase. Solid/liquid (suspensions) and liquid/liquid (emulsions) combinations are the most known representatives for technical applications. The rheology of suspensions is mainly controlled by the volume fraction ϕ_V of solids in the liquid bulk but several forces acting among particles are simultaneously present. They result in a dominating repulsion or attraction and can affect the flow of the suspensions. The attractive van-der-Waals interaction is always present, additional electrostatic or steric repulsive forces may act. Brownian force has to be taken into account for particles of all shapes randomizing their spatial distribution and orientation, but is most dominant for particles below 1 μm.

While Brownian motion and the above mentioned particle interactions are present at rest, additional hydrodynamic forces occur when the fluid flows. Furthermore, particle shape, and at high volume fractions also particle size distribution, have a significant effect on suspension rheology. Broadening of the particle size distribution increases the maximum packing fraction $\phi_{V_{max}}$ at which the viscosity diverges [Farris, 1968]. This can lead to a higher solids loading of a suspension while the viscosity remains constant.

1.1.1 Sedimentation and capillary suspensions

Repulsive electrostatic or steric interactions may be employed to prevent particle agglomeration and keep particles suspended , on the other hand dominating van-der-Waals attraction can lead to the formation of a sample-spanning particle network preventing particle sedimentation or creaming. Here a new concept for stabilization of particles, which are not affected by Brownian motion, suspended in low viscosity fluids is presented. This concept is based on capillary forces acting among particles due to addition of a small amount of a second immiscible fluid. Focusing on prevention of particle sedimentation of carbonaceous slurries following statements are valid:
Unstable slurries prone to sedimentation require a high energy input and accordingly significant operating costs due to *permanent* stirring of storage tanks. Settling rate decreases with decreasing particle size and increasing anisotropy as shown for coal particles suspended in water [Turian et al., 1992]. Sedimentation can also be delayed by increasing the viscosity of the continuous phase using polymeric thickeners (e.g. CMC, rhamsan gum or PAA) [Dinçer et al., 2003, Usui et al., 1997, Umar et al., 2009]. Organic solvents can also be used to prevent settling of coal particles leading to weak gel structures as the coal is swelled by the solvents [Shin and Shen, 2007]. Amphilic additives with low molecular weight are utilized to control the flocculation and network structure of coal water slurries. The settling rate, as well as concentration profile and compression strength of the sediment can be controlled by change of the coverage of the particle surface with non-ionic surfactant and upon addition of non-adsorbing polymer to the continuous phase [Tudor et al., 1996].

A new innovative way of preventing particle sedimentation is based on the capillary suspension phenomenon [Koos and Willenbacher, 2011]. Capillary suspensions are a ternary system and a mixture of one solid and two immiscible liquid phases. Adding a small amount of a secondary fluid into a suspension results in a sample-spanning and stable particle network controlled by capillary forces. Capillary forces also occur in wet granular material between particles as a bridging mechanism. A scheme of forces acting between two equally sized spherical particles with diameter $d_{particle}$ is shown in Figure

1.3.

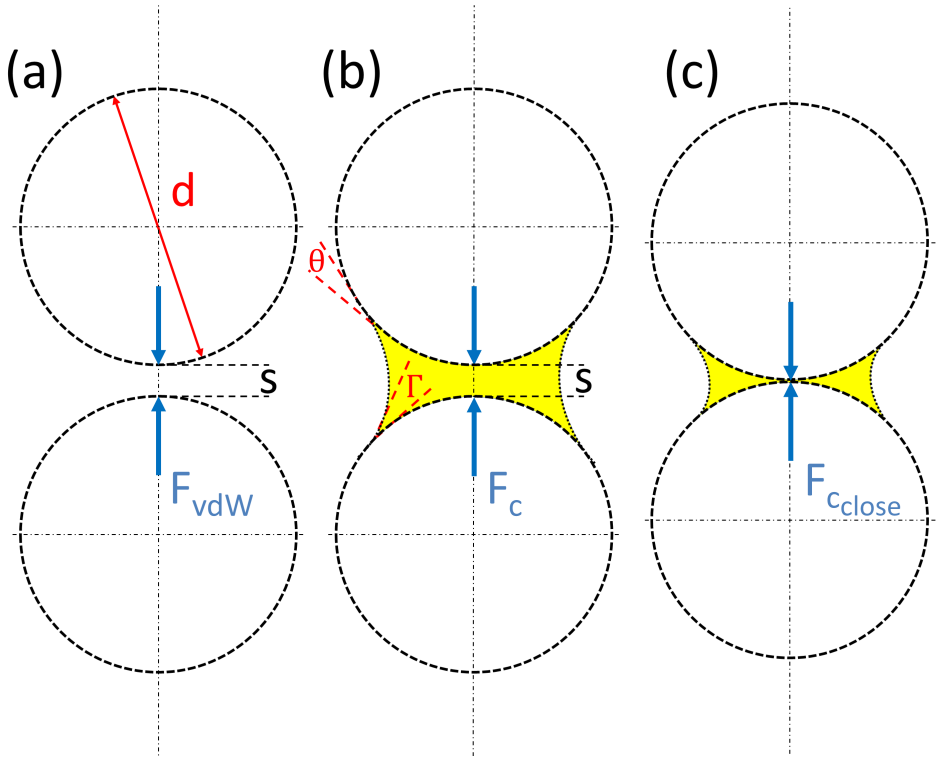

Figure 1.3: Scheme of a forces interacting between two equally sized adjacent particles (a) van-der-Waals force (b) capillary force and (c) capillary force while the particles are in contact.

The van-der-Waals force F_{vdW} is displayed in Figure 1.3 (a). This kind of particle particle interaction can also be used for stabilization of suspensions and for $s << d_{particle}$ F_{vdW} can be calculated as follows [Hamaker, 1937]:

$$F_{vdW} = \frac{A_H d_{particle}}{24 s^2} \tag{1.1}$$

Here A_H is the Hamaker constant and s the distance between two particle surfaces. The capillary force F_c for the same conditions, shown in Figure 1.3 (b), is given as follows [Pietsch and Rumpf, 1967, Schubert, 1984]:

$$F_c = g(\phi^*_{sf}, s^*) \frac{d_{particle}}{2} \Gamma cos\theta_{(S,B)} \tag{1.2}$$

Where ϕ^*_{sf} and s^* are the normalized volume of the capillary bridge $\phi^*_{sf} = V_{capillary}/(d_{particle}/2)^3$ and the normalized particle distance $s^* = s/(d_{particle}/2)$, respectively. The functional correlation $g(\phi^*_{sf}, s^*)$ describes the dependency of the cap-

illary force on the volume of the capillary bridge and the distance between the particles. Γ is the interfacial tension and $\theta_{(S,B)}$ the contact angle of the bulk to the solid. For spheres, which are in contact, toroidal capillary bridges with a small volumes occur and the functional correlation $g(\phi^*_{sf}, s^*)$ becomes 2π and Eq. 1.2 reduces to:

$$F_{c_{close}} = \pi d_{particle} \Gamma cos\theta_{(S,B)} \tag{1.3}$$

Typically F_c is two or three orders of magnitude higher than F_{vdW} [Koos, 2014]. Sedimentation and phase separation can be more effectively suppressed with the capillary suspension concept than using van-der-Waals forces to create a sample-spanning network.

Two different types of capillary suspensions are observed, depending on the wetting behavior of the ternary system. The wetting behavior is characterized by the three-phase contact angle $\theta_{(S,B)}$, which the secondary fluid forms against the particle surface surrounded by the primary or bulk fluid. The pendular state sets in for $\theta_{(S,B)} < 90°$ and forms pendular bridges connecting the particles resulting in a percolating network. In the so-called capillary state $\theta_{(S,B)} > 90$ ° clusters of particles are formed around a single drop of the secondary fluid, these clusters are the building blocks of the sample-spanning network [Bossler and Koos, 2016]. More detailed insight into the structure of capillary suspensions is given by Koos [Koos, 2014].

A drastic increase in low shear viscosity and a pronounced shear thinning results through the build-up of a network of capillary bridges between the particles. The high shear viscosity is unaffected due to the break up of the capillary bridges through high hydrodynamic forces. Those unique flow properties allow for good processing properties while simultaneously a sedimentation stability is given. An adjustment or tailoring of the flow behavior of capillary suspensions is easily achieved. Accordingly, capillary suspensions are established for a broad range of new and innovative formulations and materials for a wide field of applications, such as novel fat-free food formulations [Hoffmann et al., 2014], pastes for printed electronics providing unique shape accuracy and surface uniformity [Bitsch et al., 2014, Schneider et al., 2016] or foams based on this phenomenon [Zhang et al., 2014, Zhang et al., 2015b]. They can even be used as precursors for highly porous, high mechanical strength membranes made of ceramics or glass [Dittmann et al., 2013, Maurath et al., 2015, Dittmann et al., 2016]. Structure formation of particle-laden polymer blends [Domenech and Velankar, 2014] or assembling of metals or nanoparticles into novel nanocomposites superstructures [Xu et al., 2013a] can also be controlled or improved by the capillary suspension concept.

1.1.2 Rheology of anisotropic particle suspensions

As already mentioned before, the flow behavior of suspensions is strongly dependent on the volume fraction of suspended particles ϕ_V. Particle shape affects the intrinsic viscosity $[\eta]$ as well as the maximum packing fraction $\phi_{V_{max}}$ [Barnes et al., 1989, Donev et al., 2004, Weitz, 2004]. The latter is also depending on particle size distribution and both parameters enter into physical and/or phenomenological models describing the volume fraction dependence of the viscosity. For dilute suspensions the relative viscosity $\eta_{rel} = \frac{\eta}{\eta_{fluid}}$ is given in Eq. 1.4 which is relevant for $\phi_V \leq 1$ % [Einstein, 1906, Einstein, 1911]. The disturbance of the flow field around one particle does not affect other particles [Tadros, 2010]:

$$\eta_{rel} = 1 + [\eta]\,\phi_V \tag{1.4}$$

Eq. 1.5, proposed by Batchelor, is covering a volume concentration range from 1 to 10 % [Batchelor, 1977] and takes into account two-body hydrodynamic interactions:

$$\eta_{rel} = 1 + [\eta]\,\phi_V + [\eta]^2\,\phi_V^2 \tag{1.5}$$

Both equations (1.4 and 1.5) are derived from physical first principles and are valid for spheres with $[\eta] = 2.5$. Many phenomenological relations for η_{rel} as a function of ϕ_V and $[\eta]$ including $\phi_{V_{max}}$ can be found in the literature [Eilers, 1943, Maron and Pierce, 1956, Krieger and Dougherty, 1959, Zarraga et al., 2000] covering the range of higher ϕ_V. An overview of those relations is given in Table 1.1.

Table 1.1: Overview of different empirical models describing the relative viscosity η_{rel}.

Eilers [Eilers, 1943]	$\eta_{rel} = (1 + \frac{2.5\phi_V}{2(1-1.35\phi_V}))^2$
Maron Pierce [Maron and Pierce, 1956]	$\eta_{rel} = (1 - \frac{\phi_V}{\phi_{V_{max}}})^{-2}$
Krieger Dougherty [Krieger and Dougherty, 1959]	$\eta_{rel} = (1 - \frac{\phi_V}{\phi_{V_{max}}})^{-[\eta]\phi_{V_{max}}}$
Santamaria-Holek [Santamaría-Holek and Mendoza, 2010]	$\eta_{rel} = (1 - \frac{\phi_V}{\frac{1-\phi_{V_{max}}}{\phi_{V_{max}}}\phi_V})^{-[\eta]}$

Measurements of $[\eta]$ can be conducted using an Ubbelohde viscometer. The reduced

viscosity η_{red} is defined as:

$$\eta_{red} = \frac{\eta_{rel} - 1}{\phi_V} \tag{1.6}$$

and $[\eta]$ is given by:

$$[\eta] = \lim_{\phi_V \to 0} \eta_{red} \tag{1.7}$$

Accordingly, the intrinsic viscosity can be extracted from a diagram of η_{red} as a function of ϕ_V as the intersection of the graph and the y-axis. Those kind of measurements can be performed for polymers [Tadros, 2010] as well as solid particles [Rubio-Hernández et al., 2006]. Values below the rigid sphere limit of 2.5 for $[\eta]$ can be achieved for highly porous particles where the fluid is immobilized inside the particles [Nawab and Mason, 1958]. Non-spherical particles exhibit $[\eta]$ values > 2.5 and $[\eta]$ is a simple measure for the degree of anisotropy.

Since many particles, used in industrial (flow) processes, are not spherical but anisotropic, the interest in investigations was already early awoken. Many studies have been carried out of anisotropic, non-Brownian particles dealing with flow behavior of suspensions in theoretical, experimental and numerical ways [Jeffery, 1922, Taylor, 1932, Rallison, 1978, Haber and Brenner, 1984, Brenner, 1974, Santamaría-Holek and Mendoza, 2010, Giesekus, 1983, Brown et al., 2000, Yamamoto and Matsuoka, 1999, Pabst et al., 2006]. Low shear viscosity increases with increasing particle anisotropy. Rod-like particle suspensions show a faster rise in viscosity level over the whole shear rate range than suspensions made out of plate-like particles and equal volume fraction [Barnes et al., 1989, Yamamoto and Matsuoka, 1999]. Carbonaceous suspensions like coke slurries, as well as their fossil counterpart coal slurries, include non-spherical and non-colloidal particles [Turian et al., 2002]. As already mentioned, the intrinsic viscosity as well as the maximum packing fraction are strongly dependent on the anisotropy of the particles [Barnes, 1981]. Additionally the porosity of those carbonaceous particles has a significant influence on the effective volume fraction, since the liquid inside the pores is immobilized. Milling or grinding can also expose internal pores and increase the interfacial area which might influence the flow behavior [Turian et al., 2002]. Most of the works found in the literature focus on the flow behavior of coal slurries with water or oil as bulk phase. Investigations regarding the packing of non-porous spherical coal particles in aqueous slurries showed that the so-called reachable concentration, i.e. the particle concentration at which an upper viscosity limit for processing those slurries is

reached, could be increased by using particles with distinctly different sizes in various mixing ratios. In particular viscosity minimum were reached with mixtures containing a large size ratio (≈ 1:10) [Tu et al., 2015, Yang et al., 2016]. This effect is traced back to the above mentioned Farris Effect, which describes the increase of $\phi_{V_{max}}$ for particles with a transition from a unimodal to a multimodal particle size distribution. The rheology of coal oil mixtures was discussed covering a broad range of different coals, where the Newtonian flow behavior was observed up to mass fractions of $\phi_m = 30$ %. Beyond this point the viscosity function was described with the Bingham plastic model [Bingham, 1917] due to the occurring yield stress, which is a consequence of the dominant vdW-Interactions among the particles. With increasing particle size a decrease in viscosity and yield stress occurred, most notably for high particle loadings, as a result of the $d_{particle}^{-1}$ scaling of the stress related to the vdW attractions [Papachristodoulou and Trass, 1984]. Similar results were obtained using biochar as solid phase. Viscosity reduction of those biochar suspensions was achieved using polymeric additives, providing steric stabilization [Shivaram et al., 2013]. Many investigations on coal water slurries revealed that they exhibit shear thinning flow behavior. Further viscosity decrease was achieved using different surface active additives as dispersing or wetting agents to prevent agglomeration of particles. An increased solids loading could be reached due to reduced attractive interactions among particles [Roh et al., 1995, Aktas and Woodburn, 2000, Tiwari et al., 2004, Chen et al., 2011a, Pawlik et al., 1997, Pawlik, 2005, Xu et al., 2009a].

Porosity of coal particles has a major influence on the flow behavior of slurries, since the immobilized bulk in those particle pores increases ϕ_V. Dry coal particles (lignite) adsorbed only partially. The water sealed the pores and trapped air inside them. The effective particle porosity is reduced through this phenomenon and the viscosity is decreased at a given solids content as the particles occupy a lower volume. Activated carbon and coke particles do not show this effect, as the whole pore volume was filled with the adsorbed water [Zhang et al., 2016]. Other investigations regarding the effect of porosity on flow behavior of carbonaceous slurries revealed that the porosity remains constant upon treatment in a laboratory scale ball mill, while the particle size distribution (PSD) changes. Slurry viscosity decreased here for coals from lower to higher rank at a constant volume fraction as the surface loading of those coals differ. However, although a dependency of the slurry viscosity on particle shape was hypothesized (e.g. sphericity) no systematic data were presented [Boylu et al., 2004]. Milling of petroleum coke for petroleum coke oil slurries resulted in an increased viscosity, which was attributed to the decreasing width of the PSD [He et al., 2011].

1.2 Atomization

Formation of a spray is mostly known as atomization. With this technique it is possible to access a high surface in liquids or distribute matter finely. For several industrial processes the transformation of bulk liquid into sprays or other physical dispersions of small droplets is important [Lefebvre, 1990]. Disturbances of the liquid jet are necessary to generate a spray and even small perturbations can have a major impact on a liquid ejected through a nozzle into a gaseous environment, forming a spray [Ashgriz, 2011]. The dimensionless Weber number We describes the ratio of the inertia to the surface force for a liquid released out of a nozzle. It can be defined as follows:

$$We = \frac{\rho_{liquid} v_{jet}^2 D_{liq}}{\Gamma} \tag{1.8}$$

Where ρ_{liquid} is the liquid density, v_{jet} the mean jet velocity, D_{liq} the diameter of the undisturbed liquid jet and Γ the surface tension. The ratio of the interia to the viscous force is described as the dimensionless Reynolds number Re:

$$Re = \frac{\rho_{liquid} v_{jet} D_{liq}}{\eta} \tag{1.9}$$

First instability investigations were performed by applying of a harmonic disturbance signal on the jet, varying amplitude and intensity. The resulting axial disruption of the jet is caused by a capillary instability which leads to spherical droplets as the surface disturbance grows [Rayleigh, 1878]. This is distinct for the Rayleigh capillary mechanism which appears at low We and Re numbers of the liquid. An aerodynamic interaction with the ambient gas does not occur and the droplets diameter is in the same range as the jet diameter. Three more distinct regimes of round jet break up can be found in a log-log plot of We and Re (see Figure1.4). A similar result as for the Rayleigh mechanism appears for the first wind-induced region where sinusoidal oscillations generate droplet sizes of almost the same size. While smaller droplets arise in the second wind-induced region with increasing external forces. At high We and Re numbers the atomization regime is reached. Through high aerodynamic interactions between liquid and gas the smallest droplet size can be achieved here at the orifice exit [Sirignano and Mehring, 2000]. An overview of the disintegration modes is given in Figure 1.4.

The disintegration systems are called atomizers or injectors and droplet formation is controlled by the kinetic energy of the liquid itself, by exposure to high-velocity air or gas, or through external mechanical energy input provided by rotating or vibrating devices [Lefebvre, 1990]. The application for atomization is found in many fields, like industrial

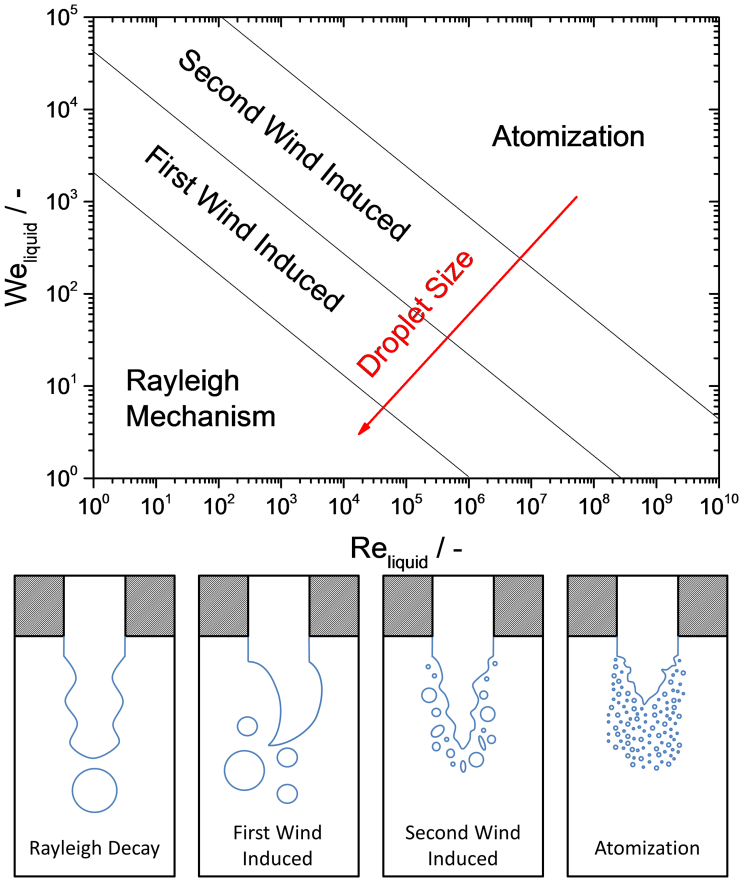

Figure 1.4: Modes of jet disintegration in depencency on liquid Weber and Reynolds number [Reitz, 1978, Sirignano and Mehring, 2000].

painting (e.g. in the automotive section) via high-speed rotary bell-cup atomizers [Im et al., 2004], creating powdered food through a rotary atomizer with a co-current airflow [Abadio et al., 2004] or exhaust cleaning and combustion [Kufferath et al., 1999]. An overview of atomizers is given in Figure 1.5, where (a), (b) and (c) are pressure driven, (d) rotary and (e) as well as (f) are twin fluid atomizers.

Internal mixing atomizer operate, as given by the name, with internal mixing configurations. The blending of the air and liquid happens before discharging through an outlet orifice. For the external mixing form of twin-fluid atomizers the interaction of the fluids happens outside of the orifice. If the twin-fluid atomizers are operated with air as gas phase, they are named air-assisted atomizers [Lefebvre, 1990]. The advantage of external mixing air-assisted atomizers is that erosion can be avoided. For the boundary that the liquid velocity $v_{liq} \ll \frac{c_{ero}}{\sqrt{\rho_{avg}}}$ no erosion occurs. Here c_{ero} is the erosional constant

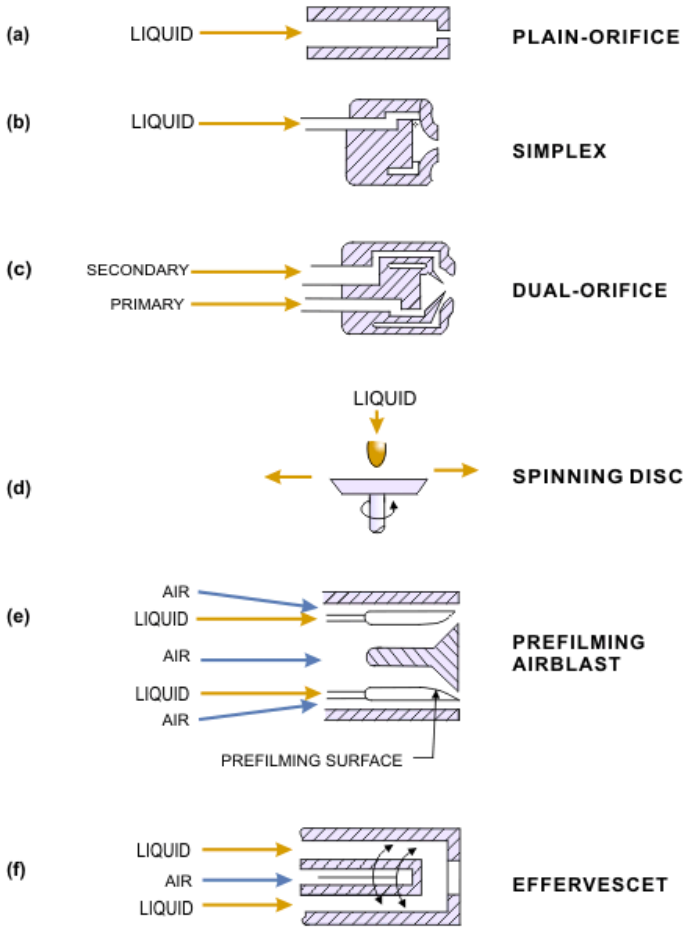

Figure 1.5: Overview of different atomizers after [Lefebvre, 2006].

(e.g. 250 for corrosion resistant alloys or corrosion inhibitor at intermittent service) and ρ_{avg} the average density of a multiphase system. [Coulson et al., 1999] This and the beneficial lack of back pressure problems are reason why those nozzles are used for the atomization of highly viscous liquids and especially suspensions, which are the feed for EFG in the bioliq®-process.

1.2.1 Atomization for EFG within the bioliq®-process

The atomization of non-Newtonian fluids, like coke suspensions, is a very challenging endeavor. The spray quality is mainly determined by the high shear limiting value of the apparent viscosity [Mansour and Chigier, 1995]. Former work with internal mixing twin-fluid jet atomizer confirmed that slurry viscosity has a strong impact on air assisted

atomization quality but also emphasizes the relevance of particle size distribution [Tsai and Vu, 1986]. Investigations of the break-up regimes and jet break-up length in highly viscous coal water slurries processed by a coaxial two-fluid atomizer exhibited that the Rayleigh type break-up is dominant for these systems and jet break-up length as well as droplet size increase with increasing viscosity [Zhao et al., 2012]. The spray structure is also controlled by viscoelasticity, namely the first normal stress difference N_1 of the slurries determined via rotational rheometry. At low viscoelasticity shear wave structures are present while jet oscillation is mainly found at high viscoelasticity. Additionally, the occurrence of periodic spray structures in dependency of the slurry viscosity has been reported [Zhao et al., 2014]. Since most EFG operate at an increased ambient pressure to account for the demand of process steps spray investigations under those real conditions were performed by Jakobs et al. Those atomization experiments with an external mixing twin-fluid atomizer in a reactor with increased pressure revealed an increase of droplet size with increasing ambient pressure at a constant aerodynamic We number [Jakobs et al., 2015]. Furthermore, it has been reported that the atomization mode (e.g. flapping or pulsating) has also a high impact on the disintegration of the jet. The membrane type break-up, which forms bag-like membranes that disintegrate into small droplets usually dominates in the range of the aerodynamic We number between 20 and 80. The flapping mode, driven by a non-axisymmetric oscillatory instability, is the reason for the fine droplets that result by the periodical transversal movement of the jet into the rapid gas stream close to the nozzle. The pulsating mode is the more continuous form of atomization, whereas here the disintegration due to the shear instability analogous to the Kelvin-Helmholtz-Instability is mainly responsible for the spray droplet size while mixtures of the flapping as well as pulsing mode can occur [Sänger et al., 2014]. The influence of stabilization via the capillary suspension phenomenon on the spray quality of an external mixing twin-fluid atomizer is examined in chapter 3.

1.3 Pyrolysis oils

Pyrolysis is defined as a thermochemical process breaking up the molecular bonds of the fuel molecules (i.e. cracking of those bonds) at typical temperatures of 250 - 1200°C. In the case of biomass, that is lignocellulosic, the converted products are solid (char/coke) and liquid [Bridgwater, 1999, Bridgwater and Peacocke, 2000]. Pyrolysis oil is the organic liquid product. It has a dark brown color, a pronounced smoky odor and consists of a large number of organic compounds [Ortega et al., 2011]. The liquid is of moderate higher heating value and can be burnt directly in thermal power stations or used as feed

for EFG [Hogan, 1997, Santo et al., 2006]. This alternative carbonaceous fuel can be used in the future additionally as a replacement or blending agent of abating fossil fuels in the field of transportation and gasification [Alonso et al., 2010, Higman and Burgt, 2003, Jiang and Ellis, 2010]. Pyrolyzed biomass used as feed for gasification can be reformed into synthesis gas with a subsequent gas cleaning and synthesis step to produce synthetic fuels or hydrocarbons, as in the bioliq®-process where synthetic fuels are made out of dimethyl ether(DME) [Dahmen et al., 2012, Wright et al., 2008]. The oil is not in a stable thermodynamic equilibrium since it is rapidly cooled or quenched from the high production temperatures [Zhang et al., 2007], this is a reason why many pyrolysis oils tend to become unstable or exhibit phase separation during storage [Oasmaa, A., Kuoppala, 2003]. A lot of efforts have been spent to upgrade and stabilize pyrolysis oils through catalysis [Zhang et al., 2006, Fisk et al., 2009, Widayatno et al., 2016, Koike et al., 2016, Xu et al., 2009b, Oh et al., 2016]. The properties of those oils are mostly improved by this treatment but it is sophisticated, time-consuming and therefore expensive. The need of such a catalytic treatment has to be examined for each oil individually. The flow behavior of pyrolysis oils is a key parameter for handling and processing [Yang et al., 2015]. During storage and transportation of pyrolysis oil instabilities of physical and chemical nature may occur, such as phase separation, increase of molecular weight or viscosity increase [Batts and Fathoni, 1991, Pfitzer et al., 2016].

Aging of pyrolysis oils

Thermal stability tests were performed, measuring the variation in viscosity, molecular weight distribution and water content of different wood-based pyrolysis oils at increased temperatures for certain time periods with a spindle in cup viscometer. A viscosity increase was accompanied by a decrease of volatile ingredients (small molecules) while the amount of high molecular weight compounds increased, indicating polymerization [Chaala et al., 2004]. Similar observations were reported by others and polymerization turned out to be more pronounced at increased aging temperatures [Diebold and Czernik, 1997, Junming et al., 2008, Alsbou and Helleur, 2014]. The increased average molecular weight is another characteristic of the aging process. As indicated before, the main reason for the increase are condensation and especially polymerization reactions of the low molecular weight compounds [Diebold, 2000, Oasmaa, A., Kuoppala, 2003], which can be measured via size exclusion chromatography (SEC). Identification and quantification of volatiles which are evaporating during aging can be achieved with Gas Chromatograph Mass Spectrometry (GC-MS) [Scholze and Meier, 2001]. Viscosity was

determined at only one shear rate and one temperature in the before mentioned works. One of the first works investigating the viscosity as function of shear rate at various temperatures was performed by Nolte and Liberatore [Nolte and Liberatore, 2010]. Oils from wood based raw material were found to be non-Newtonian at lower temperatures and oils from switch grass and wheat straw turned out to be biphasic and shear thinning in the whole investigated temperature range. Biochar can act as a catalyst and boost reactions within the pyrolysis oil resulting in an increased water content and thus a decreased viscosity in the examined shear rate range from 100 to 500 s^{-1} [Zhang et al., 2013]. Furthermore, investigations of the flow behavior of blends of pyrolysis oil, char and additives were performed showing a viscosity reduction due to those additives [Gao et al., 2016]. For in-situ measurements of the viscosity during the accelerated aging procedure a sealed pressure cell in a rheometer was used, which yields similar results as common aging experiments where viscosity measurements are performed after different storage time [Nolte and Liberatore, 2011]. A treatment of the pyrolysis oil at 80°C for 24 h was found to be equivalent to an aging of the oil for approximately 1 year at room temperature in a sealed reservoir [Trinh et al., 2013].

2 Manuscript overview and scope of the work

The following main part of this thesis is structured into three publications dealing with the application of a new stabilization concept for aqueous coke slurries and its influence on atomization (Improving the processability of coke water slurries for entrained flow gasification [Jampolski et al., 2016]), the design and influence of particle shape on the flow behavior of coke water slurries (Coke slurries with improved higher heating value and good processability via particle shape design [Jampolski et al., 2017a]) and the rheology of pyrolysis oils (Flow Behavior and Aging of Pyrolysis Oils from Different Feedstocks [Jampolski et al., 2017b]).

As already stated in the introduction knowledge of the flow behavior of biomass slurries and oils in a wide shear rate range is important for the optimal process design and control of technical processes, applying those facts, e.g. entrained flow gasification for synthesis gas production. The viscosity of biogenic slurries is strongly dependent from its composition and the flow conditions within the process. While low shear rates occur during sedimentation at storage, intermediate shear rates are present during pumping operations. As a high hydrodynamic force appears during the atomization process high shear rates are predominant during this process step.

In order to control the viscosity only at low shear rates the capillary suspension phenonmenon [Koos and Willenbacher, 2011] was applied to prevent sedimentation within the storage tanks. Adding a small amount of an immiscible, secondary fluid to the coke water slurry results in the formation of a sample-spanning particle network controlled by capillary forces increasing the low shear viscosity for several orders of magnitude while not affecting the high shear viscosity. Optical as well as gravimetric sedimentation stability tests were conducted to quantify sedimentation. Atomization experiments with stabilized slurries were performed to evaluate the effect of this new stabilization concept on the spray quality regarding the sauter mean diameter, the spray angle as well as the dominating primary instability process leading to droplet formation [Sänger et al., 2014].

In order to obtain viscosity control over the whole shear rate range the effect of the particles on the flow behavior was investigated. Particle size distribution and shape have a strong impact on the high shear viscosity as well as on the maximum packing fraction at which the slurries are immobilized [Farris, 1968, Weitz, 2004, Santamaría-Holek and

Mendoza, 2010]. Combining the effects of particle size distribution and shape result in a specifically tailored viscosity function of biogenic suspensions for the special needs of the bioliq®-process. Circularity was chosen as particle shape indicator, as it is easily obtained with a high accuracy from light microscopic images, and clearly correlates with the viscosity curves of the corresponding aqueous coke slurries. A physico-mathematical description of the viscosity functions and of the viscosity dependency on volume fraction were made to quantify the influence of the parameters particle size distribution and shape.

The bulk phase for those biogenic suspensions can be the aqueous condensate of the pyrolysis, which has a HHV of ~ 5 MJ kg^{-1} [Nicoleit et al., 2016] and almost the same rheological properties as water (Newtonian flow behavior and a viscosity of 1 mPa s at a temperature of 20°C). The organic pyrolysis condensate, which is also called pyrolysis oil, can serve as a bulk fluid for the biomass slurries but also as a stand-alone feed for the gasification, since its HHV is sufficiently high ($>$ 20 MJ kg^{-1}) [Nicoleit et al., 2016, Jampolski et al., 2017b]. Investigations of the flow behavior and temperature dependency of pyrolysis oils from different feedstocks produced at different temperatures were performed to get further insight into the processing of such fluids. Moreover, pyrolysis oils are non-equilibrium liquids and there are always ongoing reactions inside them which lead to an increase of the viscosity or even a phase separation during storage [Oasmaa, A., Kuoppala, 2003]. Therefore, the effect of time and temperature on the rheology of those biogenic oils at process relevant shear rates and temperatures was examined.

3 Improving the Processability of Coke Water Slurries for Entrained Flow Gasification

Full title	Improving the processability of coke water slurries for entrained flow gasification
Authors	Leon Jampolski, Alexander Sänger, Tobias Jakobs, Gisela Guthausen, Thomas Kolb, Norbert Willenbacher
Status	published
Bibliographic data	Fuel 185, 102-111, 2016 DOI: 10.1016/j.fuel.2016.07.102

3.1 Abstract

A new stabilization concept for coke water slurries based on the capillary suspension phenomenon [Koos and Willenbacher, 2011] is presented. Adding a small amount of an immiscible, secondary fluid to the slurry results in the formation of a sample-spanning particle network controlled by capillary forces. This is accompanied by a strong increase in low shear viscosity controlling sedimentation, whereas the viscosity at high shear rates, relevant for twin-fluid atomization, remains unchanged. Wheat straw and beech wood coke, from fast pyrolysis, suspended in water (mass fraction $\phi_m = 20$ %) have been used as model systems and octanol-1 was added as secondary fluid ($\phi_{sf} = 0$ - 3.1 vol.%) to proof this concept. Visual inspection, centrifugation experiments as well as nuclear magnetic resonance imaging confirm the drastically increased sedimentation stability offering new opportunities for storage and transport of such slurries.

Atomization of the stabilized slurries was investigated using an external mixing atomizer varying gas-to-liquid ratio (GLR) between 0.5 and 1.5 at a constant liquid mass flow of 10 kg h^{-1}. Sauter mean diameter (SMD) of the created droplets decreases substantially with increasing secondary fluid content, especially at low GLR. SMD reduction is more pronounced for wheat straw than for beech wood coke slurries. These findings are attributed to the reduction of surface tension induced by the added octanol. Furthermore, the spray angle decreases with increasing octanol content at low GLR. The reported

results provide valuable insight for suitable design of the gasification process.

3.2 Introduction

Biomass is the only renewable carbon source and is supposed to become a major raw material for organic chemistry. Beside this, biomass can be used as fuel in common power plants by torrefaction pretreatment [Basu, 2013], to receive bio-gas (mixture of CH_4 and CO_2) from fermentation [Wellinger et al., 2013] or for synthesis gas production (mixture of CO, CO_2, H_2 and H_2O) via gasification [Bridgwater, 2001]. The synthesis gas can subsequently serve as fuel for a gas turbine, e.g. in an IGCC (Integrated Gasification Combined Cycle) to produce heat and power or chemicals through synthesis steps [Iglesias Gonzalez et al., 2011]. The bioliq®-process, developed at the Karlsruhe Institute of Technology, provides a new way to use residual biomass (e.g. wheat straw or beech wood). This is done in a two-step procedure. In a first step the biomass is converted by pyrolysis into a high energy density biogenic fluid that is subsequently used as fuel for a high pressure entrained flow gasifier (EFG) [Higman and Burgt, 2003]. The obtained synthesis gas can be converted by gas cleaning into high value products, such as methanol, liquefied petroleum gas (LPG) or synthetic natural gas (SNG) [Dahmen et al., 2012]. Flow behavior of the pyrolysis products is utterly important for almost all process steps. While storage stability (e.g. against sedimentation) is controlled by the viscosity at low shear rates, the intermediate shear rate regime is relevant for unit operations like pumping and mixing, finally the flow behavior at high shear rates is decisive for the atomization in the entrained flow gasifier. Rheology of coal water slurries and its effect on their stability and atomization behavior has been investigated previously. Strong non-Newtonian flow behavior at high particle loading was observed and the dependency of viscosity on particle volume fraction for different types of coal was described [Turian et al., 2002].

Mansour and Chigier showed experimentally that spray quality is mostly determined by the high shear limiting value of the apparent viscosity [Mansour and Chigier, 1995]. Working with an internal mixing twin-fluid jet atomizer Tsai and Vu confirmed that slurry viscosity has a strong impact on airblast atomization quality but also emphasize the relevance of particle size distribution [Tsai and Vu, 1986]. Zhao et al. investigated break-up regimes and jet break-up length in highly viscous coal water slurries. Rayleigh type break-up is dominant for these systems and jet break-up length as well as droplet size increase with increasing viscosity [Zhao et al., 2012]. Furthermore, slurry viscoelasticity can also have an impact on the spray structures. Shear wave structure is common

for low viscoelasticity while jet oscillation is pre-dominant for high viscoelasticity and additionally the occurrence of periodic spray structures depending on slurry viscosity is reported [Zhao et al., 2014]. Atomization at increased reactor pressure was also examined using an external mixing twin-fluid atomizer because most EFG operate at increased ambient pressure to account for the demand of subsequent process steps. At constant aerodynamic We number an increase of droplet size with increasing ambient pressure was observed [Jakobs et al., 2015].

Preventing particle sedimentation in coal water slurries generally requires high energy input (e.g. permanent stirring of storage tanks) and accordingly significant operating costs. Turian et al. investigated the sedimentation of coal particles in water regarding particle size and sphericity. They report a delayed settling rate for smaller and non-spherical particles [Turian et al., 1992]. Particle settling can be reduced increasing the continuous phase viscosity e.g. using polymeric thickeners (e.g. CMC, rhamsan gum or polymethacrylate) [Dinçer et al., 2003, Usui et al., 1997]. Low molecular weight amphiphilic additives can be used to control the flocculation and network structure of coal water slurries. Tudor et al. discuss how the settling rate, as well as concentration profile and compression strength of the sediment can be controlled changing the coverage of the particle surface with non-ionic surfactant and upon addition of non-adsorbing polymer to the continuous phase [Tudor et al., 1996].

The addition of an immiscible secondary fluid can have a strong impact on the flow behavior of suspensions. Under certain conditions adding the secondary fluid can result in a viscosity reduction [Xu et al., 2013b, Zhang et al., 2015a]. In this work a novel stabilization concept for coke water slurries based on the capillary suspension phenomenon [Koos and Willenbacher, 2011] is presented. Adding a small amount ($\sim 1-3$ vol.%) of a second immiscible fluid to a suspension results in a sample-spanning and stable particle network controlled by capillary forces. This results in a drastic increase in low shear viscosity and pronounced shear thinning. Two different types of capillary suspensions are observed depending on the three-phase wetting angle $\theta_{(S,B)}$ the secondary fluid forms against the particle surface surrounded by the primary or bulk fluid.

In the pendular state the secondary fluid preferentially wets the particles ($\theta_{(S,B)} < 90°$) and forms pendular bridges connecting the particles finally resulting in a percolating network. In the so-called capillary state ($\theta_{(S,B)} > 90°$) clusters of particles are formed around small droplets of secondary fluid and these clusters are the building blocks of the sample-spanning network [Bossler and Koos, 2016]. According to this structure formation capillary suspensions are highly resistant to sedimentation and exhibit unique flow properties. Their flow behavior can be easily adjusted to the demands of different

manufacturing or application processes in a wide range [Koos et al., 2012] selecting the appropriate type and amount of secondary fluid.
The capillary suspension concept has been established as a generic formulation platform for a broad range of innovative materials including novel food formulations [Koos and Willenbacher, 2011], capillary suspension based foams [Zhang et al., 2014, Zhang et al., 2015b] or pastes for printed electronics providing unique shape accuracy and surface uniformity [Bitsch et al., 2014]. Capillary suspensions are even used as precursors for highly porous, high mechanical strength membranes [Dittmann et al., 2013, Dittmann et al., 2016]. The concept has also been used to control structure formation in particle-laden polymer blends [Domenech and Velankar, 2014] or to assemble metals and nanoparticles into novel nanocomposites superstructures [Xu et al., 2013a].
Here we describe the application of the capillary suspension concept to coke water slurries and we thoroughly discuss its impact on flow behavior, sedimentation stability, i.e. storage and transport, as well as atomization in entrained flow gasification.

3.3 Materials and methods

3.3.1 Materials

Coke particles from beech wood and wheat straw were used in this study. Equivalent sphere particle size distribution was determined by Fraunhofer diffraction (HELOS H0309, sympatec GmbH, Clausthal-Zellerfeld, Germany) using an ultrasonic wet dispersing unit (QUIXEL, sympatec GmbH) for dispersing the particles in deionized water. Density was determined using a pycnometer after Gay-Lussac (Carl-Roth GmbH, Karlsruhe, Germany). Porosity was measured with mercury intrusion porosimetry (AutoPore IV, micromeritics, Norcross, USA). Furthermore, ash content, carbon content and higher heating value have been determined according to DIN 51719, DIN 51732 and DIN 51900, respectively. Corresponding results are summarized in Table 3.1, equivalent sphere particle size distributions and respective scanning electron microscopy (SEM) images are shown in Figure 3.1.

The SEM images indicate a rough but fairly isometric particle shape with visible pores. The coke was stored under N_2 atmosphere in barrels to minimize surface oxidation. Deionized water was used as the bulk phase for the slurries and acted as a model fluid for the aqueous pyrolysis condensate. Octanol-1 (Alfa Aesar, Karlsruhe, Germany) with a density of 0.83 g cm^{-3} and a dynamic viscosity of 9 mPas was used as secondary phase for the formation of capillary suspensions. Both coke sorts are highly hydrophobic. The three-phase contact angle for beech wood coke in water with added octanol is $\theta_{(S,B)} = 67$

Table 3.1: Characteristic physico-chemical specifications of investigated coal particles.

	Wheat straw coke	**Beech wood coke**
Volumetric mean equivalent sphere diameter	20 μm	12 μm
Particle density	1.85 g cm^{-3}	1.53 g cm^{-3}
Particle porosity	73 %	57 %
Ash content (DIN 51719)	29.2 %	4.5 %
Carbon content (DIN 51732)	49.5 %	78.5 %
Higher heating value (DIN 51900)	20 MJ kg^{-1}	30 MJ kg^{-1}

$\pm$ 6° and for the wheat straw coke with the same conditions it is $\theta_{(S,B)} = 64 \pm 12°$, i.e. both coke types have similar wetting behavior and both systems are supposed to form pendular state capillary suspensions when octanol is added to the aqueous coal slurry.

3.3.2 Sample preparation

The coke particles were slowly mixed into the bulk fluid using a turbulent beater blade until a homogeneous, air bubble free slurry was achieved. An increase of the angular mixing speed from 400 to 1000 rpm during an additional stirring period of 20 min was performed after all particles had been added to the sample to break remaining agglomerates. Then the secondary fluid was added to the suspension and thoroughly mixed again using a dispensing stirrer at $\sim$ 1000 rpm for 10 min. This procedure worked for the lab scale samples with a volume of ca. 50 ml and also for the bigger volume of 40 l needed for the atomization experiments. All rheological measurements were performed right after sample preparation unless otherwise stated.

3.3.3 Rheological characterization

The rheological properties of the basic fluids and coke water slurries were characterized through the shear rate dependent viscosity (η) as well as the storage (G') and loss (G'') modulus as a function of the angular velocity (ω). Measurements were performed using a rotational rheometer (Physica MCR501, Anton Paar GmbH, Graz, Austria) with a plate-plate geometry (diameter 50 mm, gap height 1 mm) for the lower shear rates ($\dot{\gamma} <$ 1 s^{-1}) and a coaxial cylinder geometry (inner diameter 26.66 mm, outer diameter 28.92 mm) for higher shear rates ($\dot{\gamma} >$ 1 s^{-1}). Those measurements were conducted using a shear rate ramp (initial shear rate 0.001 s^{-1}, final shear rate 1000 s^{-1}), holding the shear rate for 30 s before recording the shear stress and calculating the corresponding viscosity.

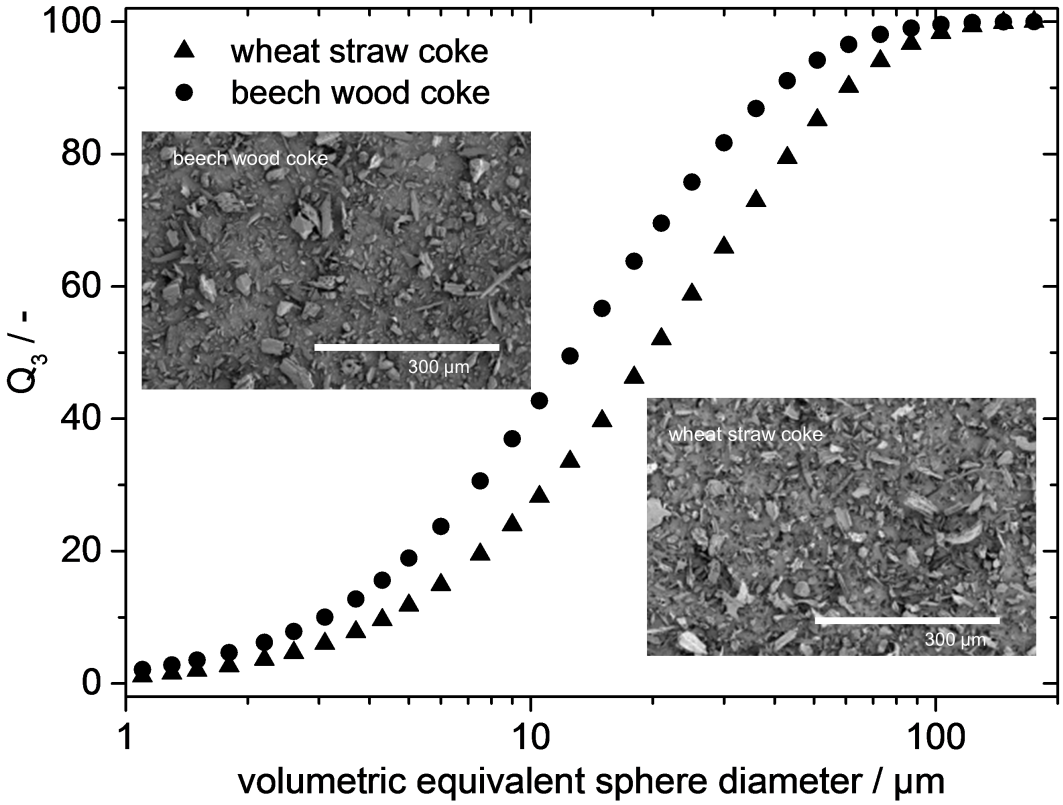

Figure 3.1: Volumetric equivalent sphere particle size distributions and SEM images of the investigated wheat straw and beech wood coke particles. Q_3 is the cumulated particle size distribution determined by Fraunhofer diffraction.

Oscillatory measurements were performed using a coaxial cylinder geometry as described above. Frequency sweeps were done at a constant stress amplitude $\sigma_0 = 0.5$ Pa. For the capillary suspensions this corresponds to the linear viscoelastic response regime, the pure coke water slurries do not exhibit linear response for $\sigma_0 \geq 0.5$ Pa, but lower stress amplitudes did not reveal reasonable modulus data due to a high noise-to-signal ratio. The temperature for all rheological measurements was 20 °C.

3.3.4 Sedimentation stability

The sedimentation stability was examined by filling graduated measuring glass cylinders of 500 ml volume with stabilized and non-stabilized slurries at a temperature of 20 °C. After waiting times of several days those filled glass cylinders were investigated optically. A supernatant formed when the coke particles sedimented. To prevent evaporation or

other environmental influences these containers were sealed on top. For evaluation of the optical tests each time 20 g of the freshly prepared slurries were put into a centrifuge (Universal 320, Hettich GmbH, Tuttlingen, Germany) at 800 rpm for 6 min. After centrifugation the supernatant of those slurries was scaled and compared to the original mass value. All measurements were performed at least four times.
Magnetic resonance imaging (MRI) experiments were performed on a 200 MHz tomograph (Bruker Avance 200 SWB, Bruker BioSpin GmbH, Rheinstetten, Germany). The superconducting magnet with a 150 mm vertical bore has a magnetic-flux density B_0 of 4.7 T. The Bruker gradient system micro2.5 was used with a ^{1}H-NMR linear bird-cage (10 mm inner diameter). The 90° radiofrequency block pulse was 7.5 μm at 0 dB. A sinc-pulse of 1 ms excited the magnetization (30 dB attenuation). For refocusing, a bandwidth matched sinc-pulse of 0.749 ms (21 dB attenuation) was applied. From the pool of imaging pulse sequences provided by Bruker within Paravision® 4.0 (Bruker BioSpin GmbH), the ″Rapid Acquisition with Relaxation Enhancement″ (RARE) sequence was selected due to the good signal to noise ratio for the chosen experimental time period and the transverse relaxation differences in the sample. Gradient echo sequences were shown not to provide suitable image quality due to the samples specific magnetic susceptibility differences. The cylindrical sample tubes were placed into the sample holder with the symmetry axis along $B_0 \parallel z$. The measured axial slices with a slice thickness of 0.5 mm ($n = 27$) and an interslice center distance of 0.7 mm were orientated in the xy-plane and measured from bottom to top, while the sagittal slices were oriented in the yz-plane. Data was processed within ParaVision® 4.0 and via self-written scripts in Matlab® (version R2012a, The MathWorks Inc., Natick, Massachusetts, USA).

3.3.5 Atomization

Atomization experiments were performed at the atmospheric test rig (ATMO) applying an external mixing twin-fluid atomizer as described in [Sänger et al., 2014]. For a better understanding of the atomization process a simple nozzle geometry (air and liquid are parallel discharged in axial direction) was chosen. The liquid mass flow can be controlled almost pulsation-free in a range of 5 - 50 kg h^{-1} with an eccentric screw pump (Nemo, Netzsch GmbH, Waldkraiburg, Germany) and is measured by an inductive flow meter (Proline Promass 83A, Endress+Hauser AG, Reinach, Swiss). The air mass flow can be varied between 1 and 20 kg h^{-1} and was measured with hot-wire anemometry (F-206AI, Bronkhorst GmbH, Kamen, Germany). The Sauter Mean Diameter (SMD) of the droplets was obtained with a Malvern Spraytec drop size detector (Malvern Instruments Ltd., Worcestershire, United Kingdom) mounted 200 mm below the nozzle, as also shown

in Figure 3.2 (b). This device is equipped with a He-Ne-laser with a wavelength of 632.8 nm and a beam diameter of 10 mm. Based on laser diffraction spectroscopy an integral volumetric drop size distribution is measured in the intersection volume of the spray cone and the laser beam line. An evaluation of the measured data was made with the Mie-theory [Hergert and Wriedt, 2012]. The schematic set-up of ATMO is shown in Figure 3.2 (a) with a more detailed sketch of the twin-fluid nozzle in Figure 3.2 (b). A high speed camera Photron Fastcam SA-Z (Photron Ltd., Buckinghamshire, United Kingdom) was mounted at two different positions, in the near nozzle region and 200 mm away from the nozzle to proof the sphericity of the droplets, since the Mie-theory is only feasible for round droplets [Pollack and Cuzzi, 1980]. Further information about the setup can be found in [Sänger et al., 2014]. All measurements were performed at an ambient temperature of 20 °C. The fluid temperature was set to 20 °C using a double pipe heat exchanger.

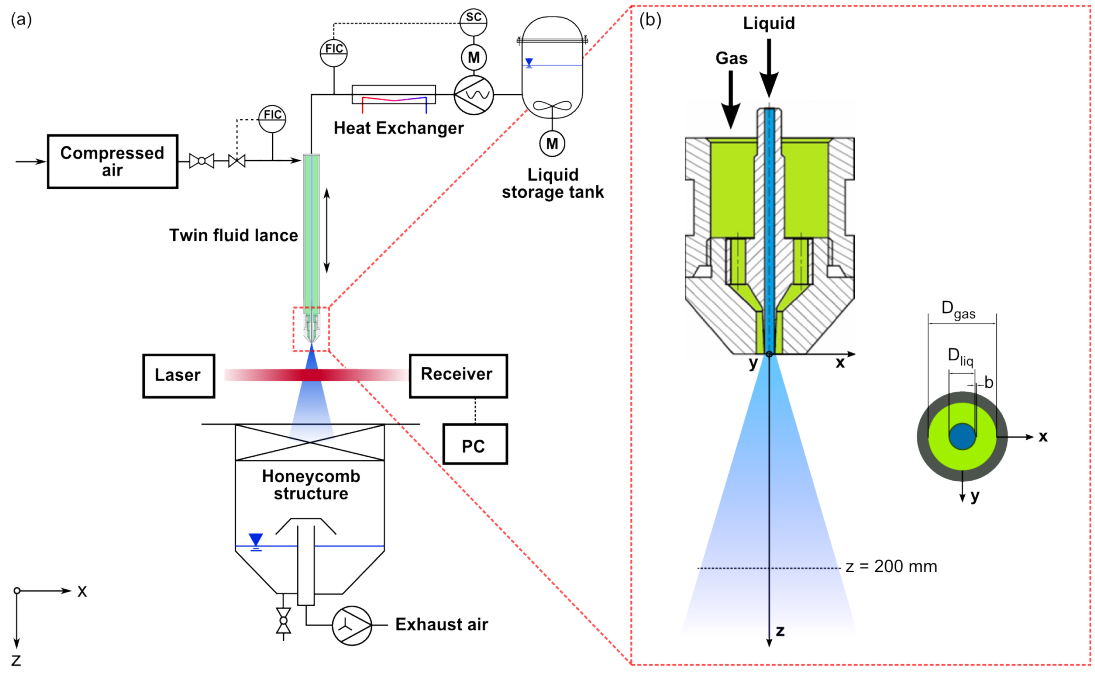

Figure 3.2: (a) Schematic set-up of the ATMO with (b) the used external mixing twin-fluid nozzle [Sänger et al., 2014]

3.4 Results and discussion

3.4.1 Rheological characterization

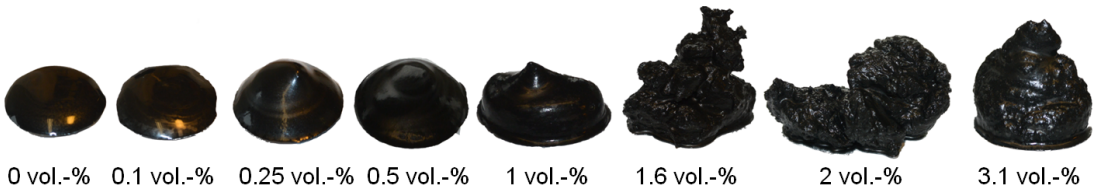

Figure 3.3: Characteristic texture of beech wood coke slurries with increasing content of octanol as second fluid (ϕ_{sf}).

As shown in Figure 3.3 the structure of the beech wood coke slurry changes significantly with increasing secondary fluid content. Suspensions without and with a very small amount (0 vol.% and 0.1 vol.%) of octanol spread as expected for low viscosity suspensions. Further addition of secondary fluid (0.25 vol.% and 0.5 vol.%) results in a more paste-like texture and flow behavior due to a sample spanning network induced by capillary bridges between the particles. With further addition of secondary fluid the slurry becomes stiffer resulting in an improved sedimentation stability, as will be shown later. Figure 3.4 shows the viscosity as a function of shear rate for wheat straw coke and beech wood coke slurries at different octanol content. The pure suspensions are shear thinning and both slurries exhibit similar absolute viscosity values at low shear rates, more than three orders of magnitude higher than the viscosity of the continuous phase. This viscosity level is determined by attractive van-der-Waals interactions among particles. A high shear limiting viscosity value is obtained in both cases and according to the higher volumetric particle loading of the wheat straw coke its limiting high shear viscosity is about three times higher than that of the beech wood coke. However, these slurries without a secondary fluid are not stable regarding to sedimentation. Addition of a small amount of octanol changes the flow behavior dramatically. The low shear viscosity increases by orders of magnitude even at an octanol content as low as 1.6 vol.%. In contrast the high shear viscosity is unaffected by the added octanol. The viscosity curves for the pure and capillary suspensions superimpose for $\dot{\gamma} > 300$ s^{-1}. Obviously, high shear forces destroy the capillary network and it cannot contribute to the viscosity at high shear rates. Similar results have been obtained for other capillary suspension systems [Koos et al., 2012, Bitsch et al., 2014].

The dependence of the low shear viscosity (here measured at $\dot{\gamma} = 0.01$ s^{-1}) on secondary fluid content is displayed in Figure 3.5 (a) for both types of coke slurry. For both

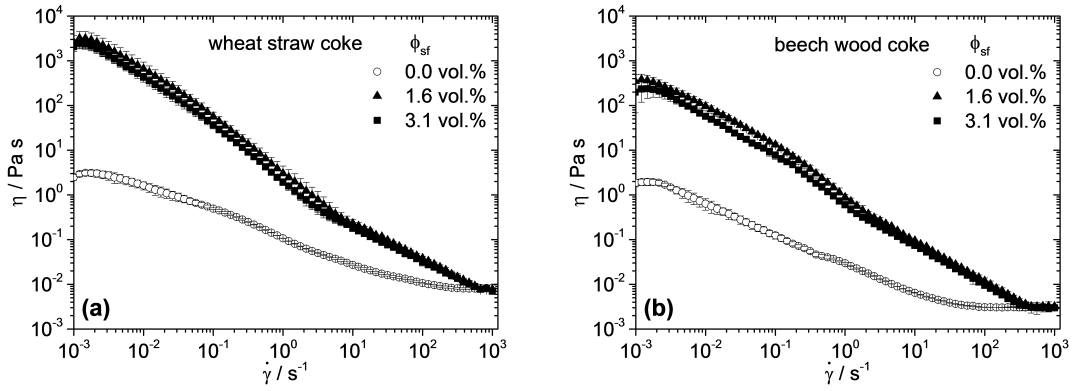

Figure 3.4: Viscosity vs. shear rate for slurries of (a) wheat straw coke(ϕ_m = 20 %, ϕ_V = 44 %) and (b) beech wood coke (ϕ_m = 20 %, ϕ_V = 33 %).

systems η increases drastically with increasing secondary fluid content and a plateau of the viscosity is reached at $\phi_{sf} \approx 1.5$ %. The absolute value of this plateau is higher for the wheat straw coke slurry than for the beech wood coke system and this is attributed to the higher volumetric particle volume fraction of the former system.
The dramatic change of suspension structure and flow behavior is also directly visible from the shear modulus data shown in Figure 3.5 (b). For the pure suspension modulus values are low, G'' increases linearly with angular frequency and G' is immeasurably small typical for fluid-like systems. However, the suspension including octanol exhibits orders of magnitude higher G', G'' values, G' is essentially independent of frequency and much larger than G'' characteristic for gel-like systems. Data shown in Figure 3.5 (b) are for wheat straw coke suspensions but similar results confirming the formation of capillary suspensions have been obtained for the beech wood coke slurry, too.

3.4.2 Sedimentation stability

Samples with 20 wt.% coke were prepared which resulted in ϕ_V = 44 % for the wheat straw coke and ϕ_V = 33 % for the beech wood coke slurry. After sample preparation the fresh slurry appeared homogeneous as shown in Figure 3.6 (a). However, particles in the slurry with 0 vol.% octanol settled within a few hours but the supernatant remained strongly opaque, after 8 days the supernatant got transparent as shown in Figure 3.6 (b). In contrast the slurry with an octanol content of 3.1 vol.% remained as manufactured even after 8 days storage (Figure 3.6 (c)). This result of visual inspection was further confirmed by centrifugation experiments, applying a relative centrifugal force (RCF) of

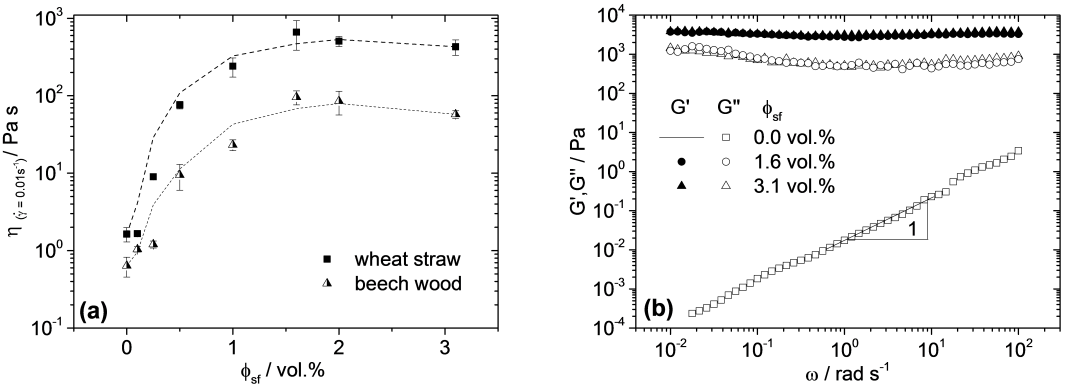

Figure 3.5: (a) Low shear viscosity for slurries of beech wood coke and wheat straw coke, both with 20 wt.% particles, at $\dot{\gamma} = 0.01$ s^{-1} as function of the second fluid volume. (b) Storage (G') and loss (G'') modulus vs. angular velocity ω for a wheat straw coke slurry with $\phi_m = 20$ % at an octanol content of 0 vol.% and 3.1 vol.%, respectively.

71. The dimensionless RCF is given as a multiple of the acceleration of gravity.

$$RCF = \frac{4\pi^2}{g} r n^2 \tag{3.1}$$

Where r is the radius of the rotor, which is 99 mm for our setup, g is the constant of gravitation and n are the revolutions per second. This allows a comparison of stabilized and non-stabilized slurries within minutes.

After procuring this RCF for 6 minutes the supernatant of the slurries was weighted. The results of those measurements are illustrated in Figure 3.6 (d). For the wheat straw suspension with 0 vol.% octanol the supernatant weight was $\sim$ 12 % referred to the total sample mass after that procedure and $\sim$ 16 % for the beech wood suspension with 0 vol.% octanol. With an octanol content of 1.6 vol.% for the stabilized suspensions the supernatant content was reduced to about 5 % after centrifugation for both slurries. No further reduction of supernatant weight was achieved for the slurries including 3.1 vol.% octanol as expected since the slurries with 1.6 and 3.1 vol.% of secondary fluid exhibit similar low shear viscosity (shown in Figure 3.4). The samples are in a low shear viscosity stable plateau. These results clearly demonstrate an increased slurry stability due to the added secondary fluid. This phenomenon was further investigated using magnetic resonance imaging (MRI).

Stable and non-stable slurries were screened by MRI, corresponding images are shown

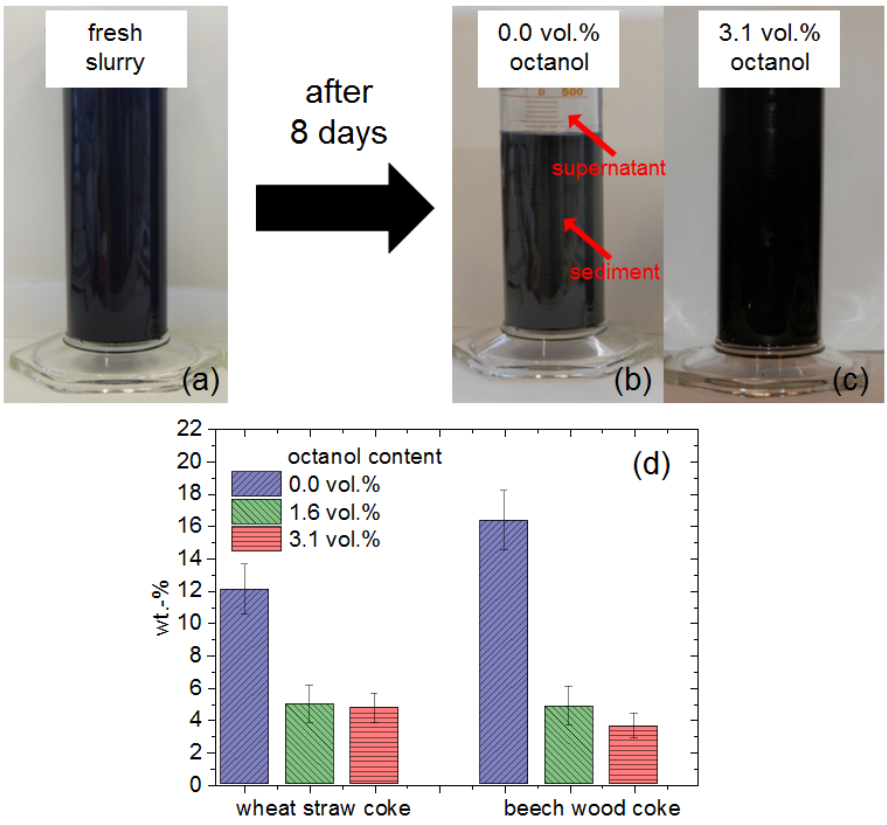

Figure 3.6: Beech wood coke slurry (a) freshly prepared and after a storage time of 8 days with (b) an octanol amount of 0 vol.% and (c) 3.1 vol.%. (d) shows supernatant weight relative to the total sample mass of wheat straw and beech wood coke suspensions with $\phi_m = 20$ % for octanol contents of 0 vol.% (blue), 1.6 vol.% (green) and 3.1 vol.% (red) after centrifugation for 6 min at 800 rpm.

in Figure 3.7. The normalized signal intensity is color-coded displayed by the color bar, blue indicates low intensity (close to noise level), which corresponds to the solid material in the sample tube, highlighted by the white lines. Higher signal intensity is represented by colors according to the color bar on the right of each image and indicates the presence of water. A homogenous distribution of coke particles in the sample tubes for the slurries of wheat straw and beech wood with 3.1 vol.% octanol is directly visible in these NMR images. In contrast the samples without a secondary fluid show a pronounced settling of the coke particles for both coke types. Scans in the cross section (axial slice) were also performed confirming the above results. No water could be detected at the tube bottom, as shown in Figure 3.7 (c), for the samples with 0 vol.% octanol due to the

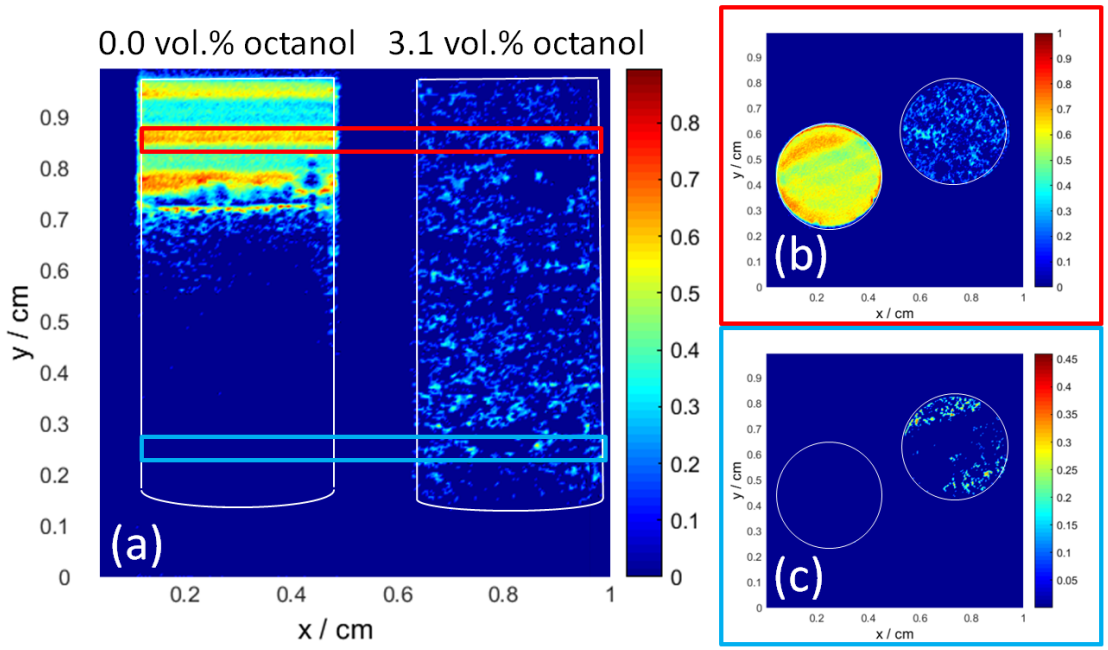

Figure 3.7: (a) MRI sagittal images of a wheat straw coke with ϕ_m = 20 % and an octanol content of 0 vol.% (left side) and 3.1 vol.% (right side). Additionally, axial slices are shown, which are measured at (b) top and (c) bottom of the samples. The positions are indicated by the rectangles in (a).

high amount of the settled coke particles. The samples with 3.1 vol.% octanol show a homogenous mixture of a coke water slurry, indicating that capillary bridges between the particles are present and stabilize the sample. No change in composition was found in the cross section scans for the upper part, as indicated in Figure 3.7 (b), of the samples containing 3.1 vol.% octanol, while only water was detected in the upper part for the slurries with 0 vol.% octanol. Those results are in agreement with the results of the oscillatory measurements as shown in Figure 3.5 (b). While the viscous properties predominate for the slurries without octanol, the elastic properties are dominant for those with added octanol.

This improved static stability is required for storage and transportation of coke water slurries as intended in the bioliq®-process and is achieved without further mechanical homogenization treatment. The unique homogeneity of the slurries is also a great benefit for gasification.

3.4.3 Atomization

The wheat straw and beech wood coke slurries with particle mass fraction of 20 % and octanol content of 0, 1.6 and 3.1 vol.% were atomized. The gas-liquid ratio (GLR= $\dot{m}_{gas}/\dot{m}_{liquid}$) was varied according to the values 0.50, 0.75, 1.00 and 1.50 while the liquid mass flow was kept constant at 10 kg h^{-1}. In Figure 3.8 the integral Sauter Mean Diameter (SMD) data detected at 200 mm distance from the nozzle exit are shown as a function of GLR. For measurements without secondary fluid the wheat straw coke slurry has larger SMD than the beech wood coke slurry, since the same mass fraction corresponds to a higher volume fraction and hence higher viscosity of the wheat straw coke slurry. This phenomenon has already been ascertained by Rizkalla and Lefebvre [Rizkalla and Lefebvre, 1975]. For increasing GLR both slurries show a strong decrease in droplet size due to the increasing energy input and at a GLR of 1.50 a SMD around 20 μm is found for both slurries.
Beyond that, adding octanol as a secondary fluid results in a SMD reduction, especially at low GLR. At an octanol content of 1.6 vol.% and a GLR of 0.5 the SMD is reduced by 12 % (from 120 μm to 106 μm) for the beech wood coke slurry and by 20 % (from 176 μm to 139 μm) for the wheat straw coke slurry. Only a minor decrease of the SMD is observed with a further increase of secondary fluid fraction to 3.1 vol.%. In this case beech wood coke slurry exhibit a SMD reduction of 2 % (from 106 μm to 104 μm) and the wheat straw coke slurry of 4 % (139 μm to 133 μm) compared to the suspension with 1.6 vol.%. The effect of secondary fluid on the SMD decreases with increasing GLR and no significant reduction is found for GLR 1.50.

The results suggest that atomization can be performed at a lower energy input when octanol is added to the slurry thus increasing the efficiency of the process. When oxygen is used as gasification agent and atomization agent at the same time, GLR is directly proportional to the stoichiometric ratio applied in an entrained flow gasifier [Sänger et al., 2014]. The necessary mean droplet size could be achieved with lower GLR, which increases the synthesis gas quality (i.e. cold gas efficiency). The trace amount of octanol is not supposed to have a detrimental effect on the quality of the resulting synthesis gas. As proposed by Mansour and Chigier [Mansour and Chigier, 1995], the atomized fluids, using gas-assisted nozzles, are subjected to high shear rates ($\dot{\gamma} > 1000$ s^{-1}). Therefore, the observed reduction in SMD is probably not a viscosity controlled phenomenon since the added secondary fluid does not affect the viscosity at $\dot{\gamma} > 300$ s^{-1}. The physical explanation for the observed phenomenon could be the change in surface tension induced by the added secondary fluid. The SMD obtained in a spraying process is related to the dimensionless Weber number (Eq. 2), which describes the ratio of aerodynamic forces to

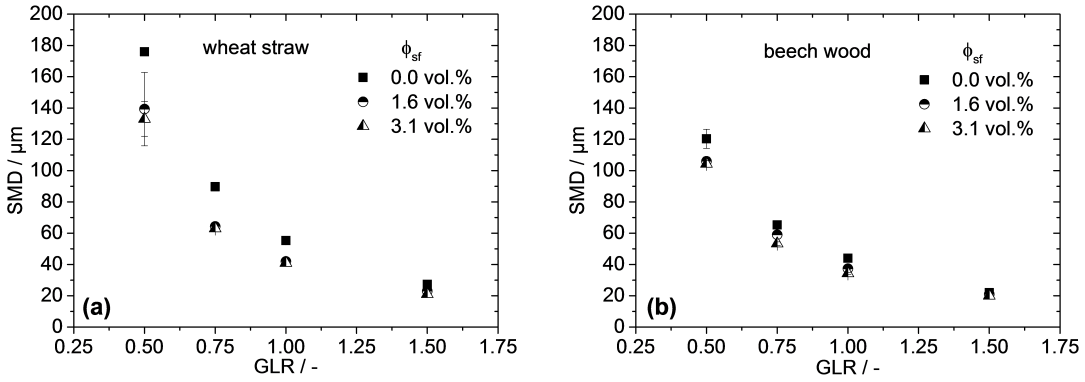

Figure 3.8: Integral SMD vs. GLR for (a) wheat straw coke (ϕ_m = 20 %, ϕ_V = 44 %) and (b) beech wood coke (ϕ_m = 20 %, ϕ_V = 33 %) slurry with increasing octanol content ϕ_{sf}.

surface tension forces. Depending on definition of L_C, the Weber number(We_i) describes jet break-up ($i = aero$, $L_C = D_{liq}$) or single droplet disintegration ($i = dr$, $L_C = D_{dr}$), where D_{liq} defines the diameter of the undisturbed liquid jet and D_{dr} the diameter of a single drop. Further v_{rel} defines the relative velocity between gas v_{gas} and liquid phase v_{liq}, ρ_{gas} the density of the gas and Γ is the surface tension of the atomized liquid.

$$We_i = \frac{v_{rel}^2 \rho_{gas} L_C}{\Gamma} \tag{3.2}$$

The higher the Weber number the finer the SMD should be [Bayvel and Orzechowski, 1993]. In this equation the numerator remains constant and only the surface tension may vary upon addition of octanol. Surface tension Γ of the systems investigated here was measured using the pendant drop method [Song and Springer, 1996] and corresponding data are shown in Table 3.2. In agreement with the results of Rizkalla and Lefebvre [Rizkalla and Lefebvre, 1975], the addition of octanol to aqueous coke suspensions decreases the surface tension substantially and thus induces the observed SMD reduction. The more distinctive SMD reduction observed for the wheat straw coke than for the beech wood coke slurries is in line with the higher decrease in surface tension found for the former system. The minor decrease of the SMD with increasing secondary fluid content (1.6 vol.% to 3.1 vol.%) can be attributed to the nearly constant surface tension value of those slurries.

Besides drop size distribution, the spray angle $\overline{\alpha}_{sp}$ was investigated as another important parameter which affects the entrained flow gasification process. Spray angle

Table 3.2: Surface tension values of wheat straw and beech wood coke slurries at different octanol contents.

Octanol content	**Wheat straw**	**Beech wood**
0 vol.%	72.0 ± 0.6 mN m^{-1}	71.7 ± 0.7 mN m^{-1}
1.6 vol.%	26.1 ± 4.5 mN m^{-1}	35.4 ± 1.1 mN m^{-1}
3.1 vol.%	27.6 ± 3.7 mN m^{-1}	34.6 ± 1.3 mN m^{-1}

particularly influences local stoichiometry (ratio of fuel to gasification agent O_2) and probably determines flame expansion in the reactor. From a matrix of high-speed images the influence of GLR and amount of secondary fluid (ϕ_{sf}) on time averaged spray angle $\overline{\alpha}_{sp}$ can be seen qualitatively. In Figure 3.9 the jet disintegration of beech wood coke slurry without and with ϕ_{sf} = 3.1 vol.% secondary fluid octanol is shown for two different gas-to-liquid ratios GLR = 0.5 and 1.5. The gas-to-liquid ratio increases from left to right and the amount of octanol increases from up to down. Comparing Figure 3.9 (a) with (c) reveals a significant decrease of $\overline{\alpha}_{sp}$ with increasing amount of octanol at low GLR of 0.5. Certainly, this decrease of spray angle can be referred to two different mainly observed primary instabilities of the liquid jet in the near nozzle region. In case of 0 vol.% octanol, as shown in Figure 3.9 (a), jet disintegration originates predominantly from a primary so-called flapping instability. This phenomenon, which was intensively investigated by Matas et al. [Matas and Cartellier, 2013], is characterized as a non-axisymmetric oscillatory instability. In contrast, the pulsating instability which can be seen in Figure 3.9 (c) is characterized by the formation of longitudinal waves at the interface between gas and liquid. As investigated and proposed by several authors (e.g. [Villermaux, 1998], [Raynal et al., 1997]), this instability can be classified as a shear induced phenomenon analogous to Kelvin-Helmholtz instability. Consequently, in case of the flapping instability, the ligaments and droplets disintegrating from the intact liquid jet are hurled to left and right, resulting in a large spray angle. In contrast the pulsating instability results in smaller trajectory angles of the droplets that shear off the liquid jet. The reason for this change in primary instability from flapping to pulsating by adding octanol as secondary may be rationalized as follows: As shown by Sänger et al. [Sänger et al., 2014] the occurring primary instability (flapping or pulsating) depends on both aerodynamic forces and dynamic viscosity. Atomization of Newtonian liquids covering a wide range of dynamic viscosities using an external mixing twin-fluid atomizer revealed that for low GLR a decrease of liquid viscosity results in a transition from flapping to pulsating mode. Since both liquid viscosity and surface tension stabilize the liquid jet it is assumed, that decreasing surface tension has the same influence as low-

ering the liquid viscosity. Amplitude height and wave length of the occurring flapping instability decrease with increasing amount of secondary fluid until the dominating flapping instability transforms into mainly occurring pulsating mode. The stabilizing effect of surface tension is reduced with decreasing surface tension as confirmed by measuring the frequency of the occurring primary instability using proper orthogonal decomposition technique [Arienti and Soteriou, 2009]. As known from literature [Lin, 2003] increase of destabilizing aerodynamic forces result in increased instability frequency. Therefore a decrease of surface tension should result in an increase in primary instability frequency at constant aerodynamic forces as well. Accordingly, for GLR of 0.5 our analysis revealed that primary instability frequency increases from f_{prim} = 616 s^{-1} at 71.7 mN m^{-1} (ϕ_{sf} = 0 vol.%) to f_{prim} = 938 s^{-1} at 35.4 mN m^{-1} (ϕ_{sf} = 3.1 vol.%).

At high GLR the spray angle remains almost constant (see Figure 3.9 (b) and (d)) since the pulsating mode is already reached here in both cases (0 and 3.1 vol.% octanol). This is in accordance with a previous study [Sänger et al., 2014] revealing that pulsating instability dominates at high aerodynamic forces. In addition to the influence of octanol, the influence of pure aerodynamic forces can be observed from high-speed images as well. In both cases, ϕ_{sf} = 0 vol.% (see Figure 3.9 (a) and (b)) and ϕ_{sf} = 3.1 vol.% (see Figure 3.9 (c) and (d)), an increase of GLR results in decrease of spray angle $\overline{\alpha}_{sp}$.

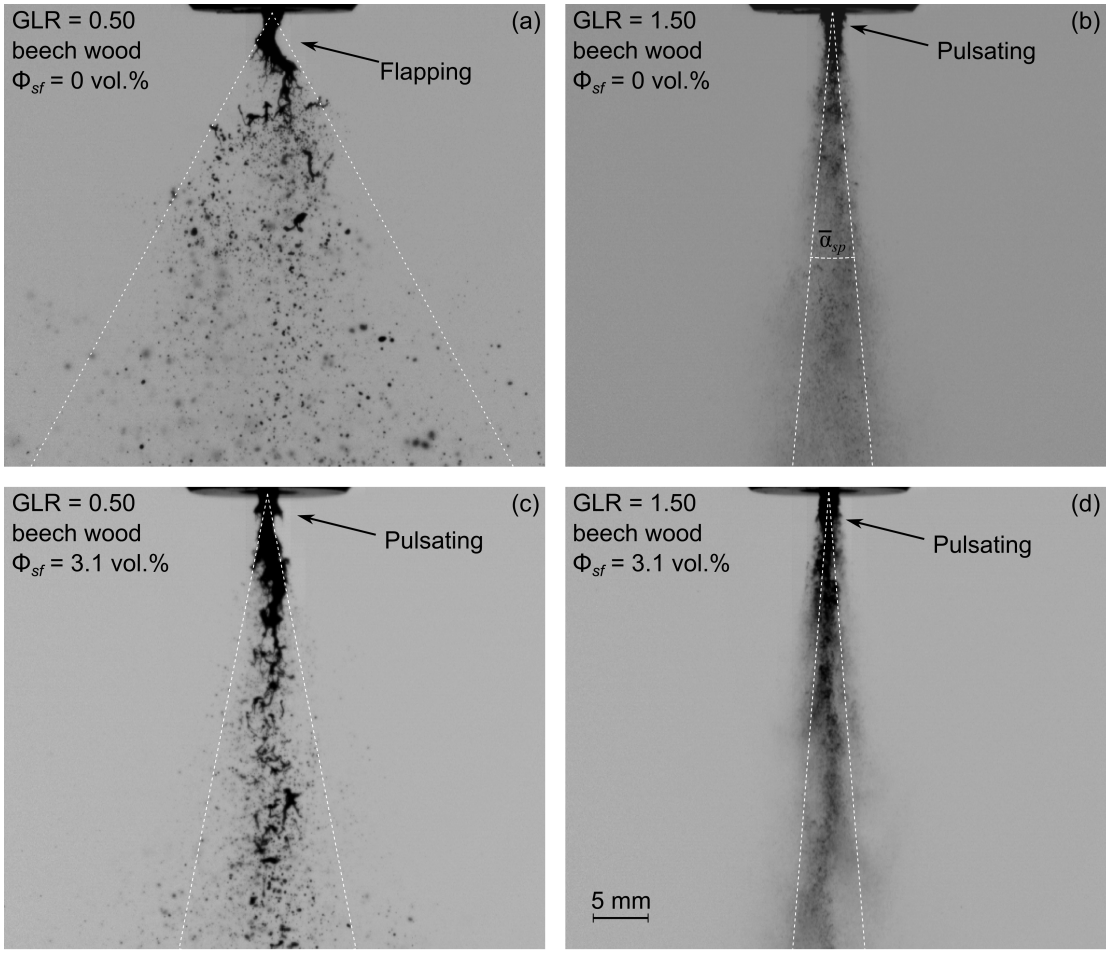

Figure 3.9: High-speed visualization of beech wood coke slurry with different amounts of secondary fluid at two different GLR (0.5 and 1.5). The white dashed lines indicate the spray angle $\overline{\alpha}_{sp}$ determined using a threshold value $\mathrm{Th}_{sp} = 0.9$, as explained in the text.

In addition to the qualitative results presented above, the spray angle $\overline{\alpha}_{sp}$ was determined quantitatively using a set of high-speed images. Time series of images were analyzed using an in-house Matlab® Code (SprayCat). The different steps of the spray angle detection procedure are described in the following: The first step consists in image pre-processing. Homogenization of the slightly inhomogeneous illuminated raw image background was performed using a reference image taken prior to the recording of images with spray. This step enhances image segmentation. (see Figure 3.10 (a))
To separate the liquid (liquid jet, ligaments and droplets) from the image background each spray image was converted into a binary image (BW image) using the threshold detection algorithm for image segmentation proposed by Kapur et al. [Kapur et al.,

1985]. The value 1 (white) belongs to background and 0 (black) to the fluid. For each image this threshold was determined individually to account for possible time dependent variation of image illumination. (see Figure 3.10 (b)) Within a next step all binary images for a given set were superimposed to get a matrix containing information about the successive positions of jet and spray. Dividing each element of this matrix by the number of images given for one set (N_{pic}) results in a matrix containing values between 0 and 1. These values describe the time-integrated probability of finding fluid at a given position (pixel) within the image. When a cell is always filled with fluid the value of this element is 0 and it is 1 when the fluid never passes a given cell. This enables the definition of contour lines with constant values (isoline). Using the coordinates of the contour line with a fixed threshold value $Th_{sp} \in [01]$ on both sides of the spray cone, the edge of the spray can be calculated by means of linear interpolation. (see Figure 3.10 (c)) Finally, the spray angle is calculated from the slope m of both lines using trigonometry $\overline{\alpha}_{sp}/2 = \tan^{-1}(m)$.

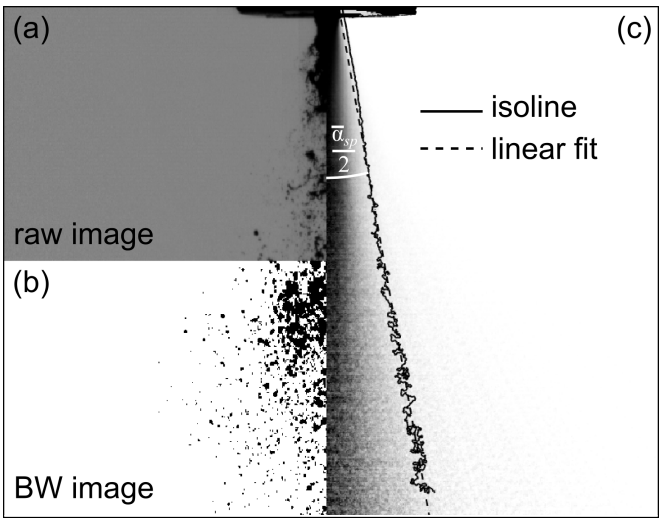

Figure 3.10: Schema for determination of the spray angle $\overline{\alpha}_{sp}$ with (a) the raw image, (b) the binary image and (c) the analyzed image, while the solid line indicates the isoline and the dashed line the corresponding linear fit.

For each operational point three data sets with each $N_{pic} = 500$ images were analyzed. In all cases the threshold for determination of the time averaged spray edge was set to a constant value of $Th_{sp} = 0.9$.

For beech wood coke slurry the determined values of the time averaged spray angles $\overline{\alpha}_{sp}$ confirm the qualitative observations. As shown in Figure 11, $\overline{\alpha}_{sp}$ decreases with increasing amount of octanol. This effect is more pronounced for low GLR than for high

GLR. In addition, the spray angle decreases systematically with increasing GLR for all considered slurries (0, 1.6 and 3.1 vol.% octanol) which can be reasoned as follows: The atomization air emerging from the nozzle orifice into the ambient air typically propagates as a free jet. Due to large velocity gradients between the high-speed gas jet and the still ambient air (mixing layer) a distinct amount of ambient air $\dot{m}_s$ is drawn into the free jet. The momentum of this gas flow affects the trajectories of the droplets within the two-phase free jet in a manner counteracting the radial momentum of the droplets. Since the mass flow of suction air is linear proportional to the mass flow directly at the nozzle exit $\dot{m}_{gas}$ [Günther, 1984], we assume that an increase in GLR results in higher momentum and therefore in a decreasing propagation angle of the droplets within the two-phase free jet.

Finally, it should be noted that a similar decrease in spray angle with increasing amount of secondary fluid as well as increasing GLR was also found for the wheat straw coke system. However, the dependencies were less pronounced than for the beech wood coke system.

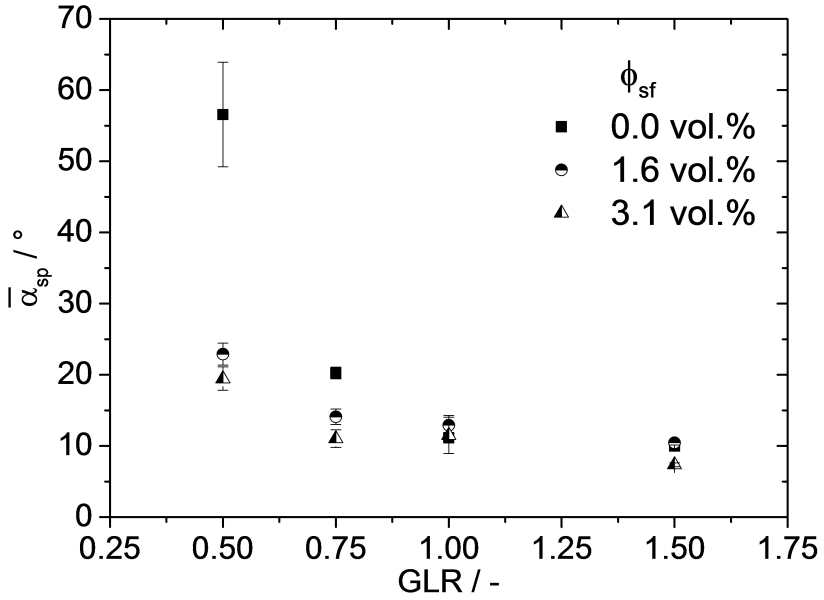

Figure 3.11: Spray angle $\overline{\alpha}_{sp}$ of beech wood coke slurry for varying GLR at different secondary fluid volume content ϕ_{sf}.

3.5 Conclusion

In this work we have introduced a new concept to improve sedimentation stability and atomization of coke water slurries used for biomass energy conversion, e.g. in the bioliq®-process. This concept is based on the capillary suspension phenomenon: a small amount of an immiscible, secondary fluid is added to the suspension resulting in the formation of a sample spanning particle network controlled by capillary forces. This transition from a fluid-like state to a gel-structure is accompanied by a strong increase in low shear viscosity controlling sedimentation whereas the high shear viscosity relevant for atomization is unaffected. Aqueous wheat straw and beech wood coke slurries ($\phi_m = 20$ %) have been used as model systems and octanol-1 was added as secondary fluid ($\phi_{sf} = 0$ - 3.1 vol.%) to demonstrate the concept. Visual inspection, centrifugation experiments as well as magnetic resonance imaging confirm the drastically increased sedimentation stability, even after several days of storage no sedimentation could be detected. This offers new opportunities for storage and transport of such systems, e.g. storage and transport times can be increased, stirring of storage tanks is rendered unnecessary, clogging of pipes and nozzles is avoided, i.e. process down times may be reduced and process efficiency increases. The effect of secondary fluid on atomization was investigated using an external mixing twin-fluid atomizer varying gas-liquid ratio (GLR) between 0.5 and 1.5 at a constant mass liquid flow of 10 kg h^{-1}. Capillary suspensions were firstly prepared at pilot scale level with batch volumes of 40 l to perform these experiments. The utilized secondary fluid does not affect the higher heating value, for the entrained flow gasification in the bioliq®-process but it has a strong impact on the Sauter mean diameter (SMD) of the produced droplets and the resulting spray angle. Both quantities decrease by adding secondary fluid content. Qualitatively, the observed changes in atomization may be attributed to the remarkable reduction in surface tension induced by the added secondary fluid used here. The SMD reduction is stronger for wheat straw coke than for the beech wood coke and especially pronounced at low GLR suggesting that atomization is enabled at lower energy input (i.e. increased cold gas efficiency). The spray angle decrease observed for both systems has to be taken into account by determining the reactor design. The findings suggest that the capillary suspension concept enhances gasification and may lead to higher process variability and efficiency.

3.6 Acknowledgement

The Authors like to thank the Helmholtz Association of German Research Centers (HGF) for funding. Thanks to Mark Eberhard for providing the coke. Further we would like greatly to acknowledge K. Becker, T. Körber, C. Hotz and Dr. S. Fleck for experimental support.

4 Influence of particle shape on the rheology of high solids coke water slurries

Full title	Coke slurries with improved higher heating value and good processability via particle shape design
Authors	Leon Jampolski, Tobias Jakobs, Thomas Kolb, Norbert Willenbacher
Status	accepted
Bibliographic data	Chemical Engineering & Technology DOI: 10.1002/ceat.201700061

4.1 Abstract

Coke water slurries can be used as biogenic intermediates in conversion of residual biomass into high value fuels such as LPG or SNG. The effect of particle size and shape on the flow behavior of slurries including coke particles obtained from fast pyrolysis was investigated. Particles were shaped in a planetary ball mill and equivalent sphere diameter and circularity were used to characterize size and shape. An increased circularity resulted in a strong decrease in slurry viscosity. Accordingly, a higher mass fraction of particles can be mixed into the slurry thus increasing the higher heating value while still preserving good processing properties.

4.2 Introduction

Coal water slurries play an important role in classical energy conversion processes. As the conventional crude oil resources are running low, new opportunities have to be found for producing carbon based fuels and chemicals. One such possibility could be the bioliq®-process, developed at the Karlsruhe Institute of Technology. Residual biomass (e.g. wheat straw or beech wood) is converted to synthesis gas in a two-step procedure. The first step consists of a fast pyrolysis of the biomass, which is converted into a high energy density biogenic intermediate fuel that serves in the second step as feed for high

pressure entrained flow gasification (EFG) to produce synthesis gas [Higman and Burgt, 2003]. This synthesis gas is treated in a subsequent gas cleaning to obtain high value products, such as methanol, liquefied petroleum gas (LPG) or synthetic natural gas (SNG) [Dahmen et al., 2012]. The solid product of the pyrolysis is coke, which is used in suspensions in subsequent processing steps. The flow behavior of those suspensions has to be controlled carefully for successful and efficient processing. This requires thorough understanding of the effect of particle size (distribution) and shape on suspension rheology. Slurries with carbonaceous solids should have a certain higher heating value (HHV), e.g. to increase the energy output by enhancing the input. Using an aqueous continuous phase, the required HHV can only be reached suspending a high mass and therefore volume fraction of coke in such slurries. The particle packing plays an important role to accomplish this challenge.

For spherical particles it is well known that the maximum packing fraction $\phi_{V_{max}}$ at which viscosity diverges can be increased using bi- or multimodal particle size distributions. Freely flowing suspensions with $\phi_V > 80$ % can be achieved as the finer particles fill the voids between the coarser ones [Farris, 1968]. For bimodal systems at a given total solids content viscosity reaches a minimum for a fine particle fraction of about 30 %. The maximum packing fraction of anisotropic particles is higher than for spheres [Weitz, 2004] but little is known about the variation of $\phi_{V_{max}}$ with size distribution and its effect on flow behavior.

Consequently, starting in the early days of rheology numerous investigations have been performed regarding the effect of anisotropic, non-Brownian particles on the flow behavior of suspensions, including experimental, theoretical and numerical investigations [Jeffery, 1922, Taylor, 1932, Rallison, 1978, Haber and Brenner, 1984, Brenner, 1974, Santamaría-Holek and Mendoza, 2010, Giesekus, 1983, Brown et al., 2000, Yamamoto and Matsuoka, 1999, Pabst et al., 2006]. In general, at a given particle loading, low shear viscosity increases with increasing particle anisotropy.

Prior work with carbonaceous solids suspended in fluids mainly focused on the flow behavior of coal slurries with water or oil as continuous phase. Those kind of fuels were of particular interest as substitute for fuel oil during the Oil Crisis in the 1970s [Hashimoto, 1999]. The packing of nonporous spherical coal particles in aqueous slurries has been investigated. Based on data for suspensions including coal particles of distinctly different sizes in various mixing ratios, the so-called reachable concentration, i.e. the particle concentration at which an upper viscosity limit acceptable for coal slurry processing is reached, could be increased by about 3%. Particularly low viscosities could be achieved for mixtures with large size ratio (≈1:10) [Tu et al., 2015, Yang et al., 2016].

Papachristodoulou and Trass discussed the rheology of coal oil slurries covering a broad coal range. Flow behavior is Newtonian up to mass fractions of $\phi_m = 30$ % and beyond this point it can be described with the Bingham plastic model due to the emerging yield stress. This flow characteristic is a consequence of dominating attractive Vander-Waals (vdW) interactions among particles. A decrease of the viscosity and yield stress with increasing mean particle size was observed, especially for high solid concentrations as a consequence of the d^{-1} scaling of the stress related to the vdW attraction [Papachristodoulou and Trass, 1984]. Similar trends for yield stress and viscosity were found by Shivaram et al., though biochar was used instead of coal. Lower viscosities at similar solids loading were achieved using polymeric additives (carboxymethylcellulose sodium salt and poly(budadiene-maleic acid) sodium salt), which may be adsorbed on the particle surface thus decreasing attractive vdW interactions [Shivaram et al., 2013]. Several investigations have shown that coal water slurries exhibit shear thinning flow behavior. Viscosity could be reduced using a certain amount of fine particle content. For further viscosity reduction different surface active additives were used as dispersing or wetting agents, thus an agglomeration of particles could be prevented and an increase of solids loading of the slurry could be achieved due to reduced attractive interactions among particles [Roh et al., 1995, Aktas and Woodburn, 2000, Tiwari et al., 2004, Chen et al., 2011a, Pawlik et al., 1997, Pawlik, 2005, Xu et al., 2009b].
The effect of particle porosity and shape were not taken into account in those investigations. However, Zhang et al. investigated the influence of pores in coal particles on the viscosity of coal water slurries. Dry coal particles (lignite) absorbed water from air filling the pores partially, resulting in sealed pores. The effective particle porosity is reduced through this phenomenon, which results in a lower viscosity at a given solids content. This effect was not observed for activated carbon or coke particles, since the whole pore volumes were filled with the absorbed water [Zhang et al., 2016]. The effect of particle size distribution (PSD) and porosity on flow behavior at different volume fractions, was investigated by Boylu et al. Here the porosity remained constant during treatment in a laboratory scale ball mill. A viscosity decrease at constant volume fraction and PSD was observed for coal from lower to higher rank. The dependency of coal water slurry viscosity on particle shape was hypothesized and the sphericity was suggested as shape parameter but no systematic data were presented [Boylu et al., 2004]. He et al. showed that milling of petroleum coke for petroleum coke-oil slurries resulted in an increased viscosity and they attribute this to the decreasing width of the PSD [He et al., 2011]. Particle size was decreased and more isometric particles were obtained by dispersing raw Indian coal in ionic liquids, microscopic images of the raw coal indicate irregular

shapes and rough surfaces but the shape was not analyzed quantitatively [Bhoi et al., 2016]. However, it is well known that particle shape has a significant influence on the flow behavior of suspensions including nonspherical particles.
As the information about the influence of particle shape on flow behavior is rare for coal respectively coke water slurries, this work focuses on manipulation of particle shape and its impact on the viscosity in dependency of shear rate. Therefore, two coke types with different milling properties were systematically studied.

4.3 Materials and methods

4.3.1 Materials

Coke particles from wheat straw and beech wood were used in this study. Water was used as bulk phase, acting as a model fluid for the aqueous pyrolysis condensate. The volumetric equivalent sphere diameter, as a parameter for the particle size, was determined through Fraunhofer diffraction (HELOS H0309, sympatec GmbH, Clausthal-Zellerfeld, Germany). An ultrasonic wet dispersing unit (QUIXEL, sympatec) was used for dispersing the particles in water. Porosity ε was measured with mercury intrusion porosimetry (AutoPore IV, micromeritics, Norcross, USA) using a powder sample. The characteristic sharp bend in the intrusion curve separates the regime of inter and intra particle pores [Lowell and Shields, 1991]. Density ρ determination was done using a pycnometer after Gay-Lussac (Carl-Roth GmbH, Karlsruhe, Germany). The mass fraction of the dispersed solid particles ϕ_m is calculated from the mass of the solid m_{solid} and the mass of the liquid phase m_{liquid}:

$$\phi_m = \frac{m_{solid}}{m_{solid} + m_{liquid}} \tag{4.1}$$

Then the density of the solid particles ρ_{solid} can be calculated from ϕ_m and the measured densities of the suspension ρ_{susp} and the liquid phase ρ_{liquid}.

$$\rho_{solid} = \frac{\phi_m}{\frac{1}{\rho_{susp}} - \frac{1-\phi_m}{\rho_{liquid}}} \tag{4.2}$$

Volume fraction ϕ_V of the coke water slurries was calculated using Eq. 4.3, where V_{solid} is the volume of the solid, V_{liquid} the volume of the liquid andV_{pore} the particle pore volume.

$$\phi_V = \frac{V_{solid} + V_{pore}}{V_{solid} + V_{liquid}} \tag{4.3}$$

V_{pore} is defined through Eq. 4.4:

$$\varepsilon = \frac{V_{pore}}{V_{solid} + V_{pore}} \tag{4.4}$$

Substituting of Eq. 4.4 and Eq. 4.1 into Eq. 4.3 results in the final equation for calculating ϕ_V:

$$\phi_V = \frac{\frac{1}{\rho_{solid}}(1 + \frac{\varepsilon}{1-\varepsilon})}{\frac{1}{\rho_{solid}} + \frac{1-\phi_m}{\phi_m \rho_{liquid}}} \tag{4.5}$$

With ρ_{solid} as the density of the solid and ρ_{liquid} as the liquid density assuming that all pores are filled with the liquid.

4.3.2 Particle size and shape design

A planetary ball mill (PM200, Retsch GmbH, Haan, Germany) was used for manipulation of particle size and shape. Coke water suspensions with $\phi_m = 25$ % particles were mixed 1:1 (mass ratio) with zirconium oxide balls (diameters 5 mm) in two grinding jars with a volume of 125 ml each. The sun wheel speed was set to 600 min^{-1} and the milling time was varied between 0 to 15 min in 5 min steps. After the milling process and extraction of the milling balls the suspensions with the milled particles were centrifuged (Universal 320, Hettich GmbH, Tuttlingen, Germany) at 9000 rpm for 15 min and the remaining particles were dried at 105°C for 24 h. A change of physico-chemical properties was not observed through this particle treatment.

4.3.3 Particle shape determination

Microscopic images for particle shape determination were taken with an inverse light microscope (Axio Observer D1, Carl Zeiss GmbH, Jena, Germany), equipped with a A-Plan 40x, N.A. 0.65 lens combined with a 1x optovar magnification changer. Images were taken using a sCMOS camera Zyla X (Andor Technology Ltd., Belfast, United Kingdom) with a 21.8 mm diagonal sCMOS sensor size resulting in a maximal size of 2560x2160 pixel. The dimensions of the taken images were 2048x2048 pixel with a resolution of 0.155 μm per pixel for this setup resulting in a side length of 317 μm. A small amount of particles was dispersed in ethanol using a turbulent beater blade. Afterwards the suspension was dripped onto a microscope slide. Microscopic images were taken after the ethanol evaporated and the particles were uniformly distributed on the slide. Image analysis was performed using an in-house developed image analyzing tool based on

MatlabÂ® (version R2015a, The Mathworks Inc., Natick, Massachusetts, USA) scripts. Filter for particle size separation were applied for the detection of agglomerates or too small particles, which appear almost round due to the resolution limits of the taken images. Particles touching the image edges were also eliminated. An example image is shown in Figure 4.1. A light microscopic image of standardized, well-characterized spherical silica particles (Kromasil 100-7-SIL, batch no. 11937, Akzo Nobel, Bohus, Sweden; purchased from MZ-Analysentechnik GmbH, Mainz, Germany) with a nearly monomodal PSD (d_{50} = 6.1 μm) is shown in Figure 4.1 (a) and a typical filtered and contrast enhanced image is displayed in Figure 4.1 (b). Several agglomerates were purposely left in the image to demonstrate that the applied filters successfully excluded such agglomerates and only single particles were analyzed. Circularity was chosen as the particle shape parameter since it could be detected with a higher accuracy and reproducibility than the aspect ratio of the coke particles. Circularity not only characterizes overall particle shape but also accounts for their roughness [Olson, 2011].
Generally, a change in aspect ratio also results in a change in circularity. The definition of the circularity C is given in Eq. 4.6, where A is the detected particle area and P the perimeter of this area. For the spherical silica particles our image analysis strategy provided a monomodal circularity distribution with C $\approx$ 1.

$$C = \frac{4\pi A}{P^2} \tag{4.6}$$

A detailed insight into the irregular shape, roughness and porosity of the coke particles investigated here is provided by SEM images as exemplarily shown in Figure 4.1 (c).

4.3.4 Sample preparation

Coke particles were slowly mixed into the water using a turbulent beater blade at an angular mixing speed of 200 rpm. An additional stirring period at 400 to 700 rpm (depending on solids content) of 20 min was performed after all particles had been added to the sample to break remaining agglomerates. All rheological measurements were performed right after sample preparation.

4.3.5 Rheological characterization

Shear rate dependent viscosity $\eta(\dot{\gamma})$ measurements were performed using a strain rate controlled rotational rheometer (MARS II, Thermo Fisher Scientific, Karlsruhe, Germany) equipped with a coaxial cylinder geometry (inner diameter 20 mm, outer diameter 21.7 mm) in controlled strain mode. These measurements were conducted using a

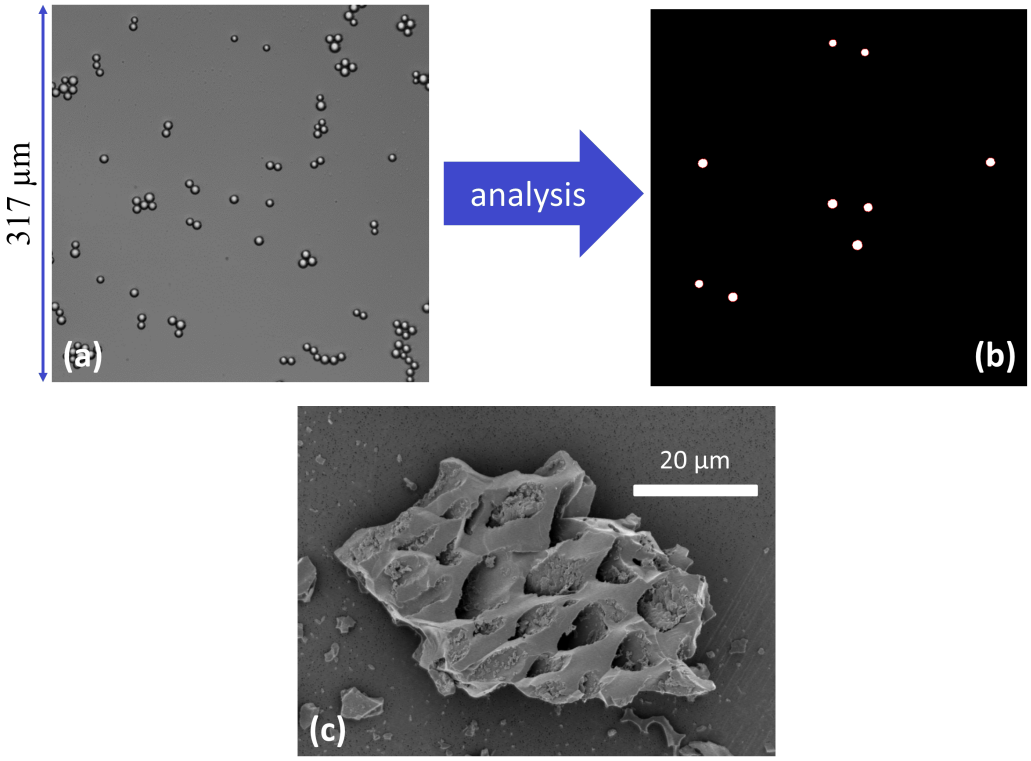

Figure 4.1: Particle shape analysis. (a) light microscopy image of SiO_2 particles and (b) image processed using the in-house Matlab scripts. (c) SEM image of a single coke particle.

shear rate ramp (initial shear rate: $\dot{\gamma} = 1\ s^{-1}$, final shear rate: $\dot{\gamma} = 1000\ s^{-1}$), holding the shear rate for 30 s or until the measured stress reached a steady state $(\Delta\sigma/\sigma)/\Delta t < 0.01\ \%\ s^{-1}$ before recording the shear stress and the corresponding viscosity. Preliminary experiments showed that no hysteresis occurred for a shear rate ramp with interchanged initial and final shear rates. All measurements were performed at least 3 times at a temperature of 20 ± 0.1 °C.

4.3.6 Intrinsic viscosity

Determination of the intrinsic viscosity was performed using an Ubbelohde viscometer type I (Schott AG, Mainz, Germany) with an inner capillary diameter of 0.63 mm and a device constant of 0.009869 $mm^2\ s^{-2}$. The measurements were conducted in a dilute regime where the relative viscosity η_{rel} (Eq. 4.7), which is the ratio of the suspension

viscosity η to the viscosity of the matrix fluid η_{fluid} and depends linearly on ϕ_V ($\phi_V \leq 0.01$). Intrinsic viscosity was determined from an extrapolation of $(\eta_{rel}\text{-}1)\phi_V^{-1}$to $\phi_V = 0$. Standard deviations were calculated from the results of five repeated measurements of each sample. All experiments were performed at 20 ± 0.1 °C.

$$\eta_{rel} = \frac{\eta}{\eta_{fluid}} \tag{4.7}$$

4.4 Results and discussion

4.4.1 Milling influence

Figure 4.2 (a) and (c) show a sample image of wheat straw coke particles at $t_{mill} = 0$ min and 15 min, respectively. Comparison indicates the decrease in particle size, also the shape of the milled particles seems smoother than that of the untreated ones. Corresponding images for beech wood coke particles are displayed in Figure 4.2 (b) and (d). While a decrease of particle size is clearly visible, shape change like for the wheat straw coke particles is not obvious from visual inspection. Deeper insight into the effect of milling on the shape of the coke particles is revealed by quantitative image analysis.

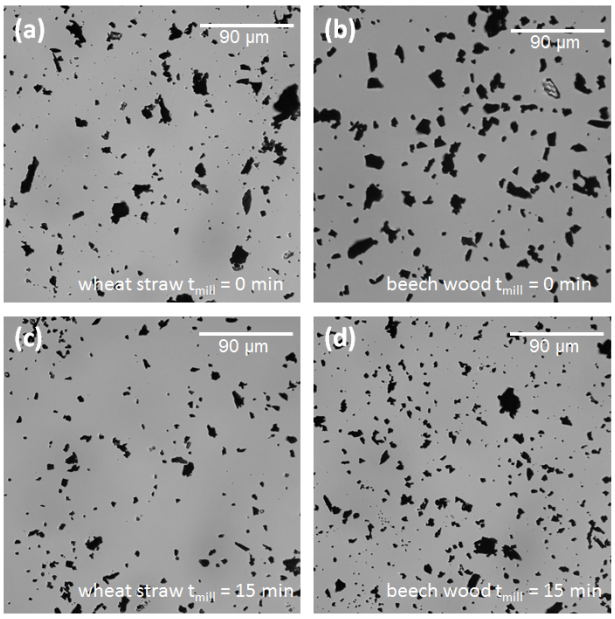

Figure 4.2: Raw images of wheat straw coke particle at $t_{mill} = 0$ min (a) and 15 min (c) as well as beech wood coke particles at $t_{mill} = 0$ min (b) and 15 min (d), qualitatively indicating particle shape and size.

After the described milling procedure the volumetric equivalent sphere diameter was measured for both coke sorts using Fraunhofer diffraction. Figure 4.3 (a) shows the differential and cumulated particle size distributions q_3 and Q_3, respectively, as a function of the particle diameter $d_{particle}$ for wheat straw coke particles. A monotonic decrease of the particle size with increasing milling time is observed and a similar trend is found for beech wood coke particles, as seen in Figure 4.3 (b).
Both initial samples exhibit a broad PSD but the beech wood powder exhibits a distinct bimodality. This feature vanishes upon milling and for both coke types milling results in a narrower PSD. Table 4.1 summarizes the characteristic particle sizes d_{16}, d_{50} and d_{84}, PSD width σ_{PSD}, porosity ε and density ρ_{solid} data together with the corresponding milling times t_{mill}. The median particle diameters of the unmilled coke types were essentially equal ($d_{50} \approx 20$ μm). After similar milling time the equivalent sphere diameters of both coke types were still in the same range, e.g. with a milling time of 15 min the median diameter d_{50} of both samples decreased to 7 μm. Moreover, the d_{16} and d_{84} values are also in the same range. Mercury intrusion porosimetry measurements reveal that the particle porosity is not affected by the grinding procedure even after extended milling. The same is true for the density. Manipulation of particle size in a planetary ball mill provides reproducible results regarding the PSD for both coke feedstocks.

Table 4.1: Characteristic particle sizes at a cumulated PSD of 16 % d_{16}, 50 % d_{50}, 84 % d_{84}, PSD width $\sigma_{PSD} = ln(d_{84}/d_{16})$, porosity ε and particle density ρ_{solid} at different milling times for wheat straw and beech wood coke

	$\mathbf{t_{mill}}$ / **min**	$\mathbf{d_{16}}$ / μ**m**	$\mathbf{d_{50}}$ / μ**m**	$\mathbf{d_{84}}$ / μ**m**	σ_{PSD} / **-**	ε / **%**	ρ_{solid} / **g cm^{-1}**
Wheat straw	0	6.4	20.0	49.4	2.04	73	1.85
	5	3.9	11.3	31.0	2.07	73	1.85
	10	3.2	8.7	24.1	2.02	73	1.85
	15	2.6	7.0	18.8	1.98	73	1.85
Beech wood	0	5.6	20.8	60.0	2.37	58	1.53
	5	3.7	11.0	32.7	2.18	58	1.53
	10	3.0	8.6	24.2	2.09	58	1.53
	15	2.6	7.0	18.0	1.93	58	1.53

The shape of the particles was analyzed with the method described above using the circularity as characteristic feature. At least 5000 individual particles were analyzed for every particle batch. In Figure 4.4 the corresponding differential circularity distributions are shown. The dashed lines indicate the basis splines between the measured points,

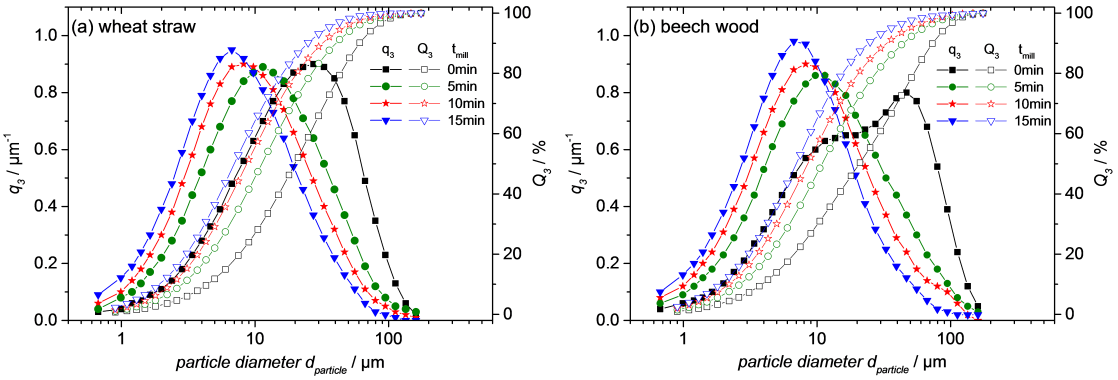

Figure 4.3: Differential PSD q_3 and cumulated PSD Q_3 as functions of the particle diameter $d_{particle}$ for (a) wheat straw coke and (b) beech wood coke after different milling times in a planetary ball mill.

which fit to the measured data sets. Figure 4.4 (a) shows the circularity distribution of the wheat straw coke particles. A transition from lower to higher circularity with increasing milling time is clearly observed, suggesting a change to a more spherical and smoother particle shape. Figure 4.4 (b) displays the circularity distributions for beech wood coke particles after different milling times. Those curves exhibit no significant change with increasing milling time, indicating that the particle shape remains the same within experimental uncertainty. Comparing the distributions of both coke types at t_{mill} = 0 min shows that the beech wood coke particles are rounder than the wheat straw coke particles in their original state.

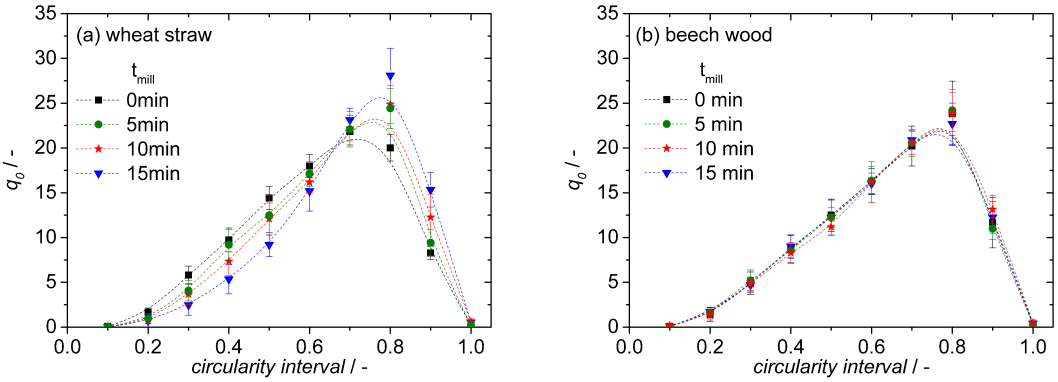

Figure 4.4: Differential distribution q_0 of circularity after different milling times for (a) wheat straw and (b) beech wood coke. The dashed lines indicate the basis splines between the measured points.

4.4.2 Influence of mass and volume fraction on flow behavior

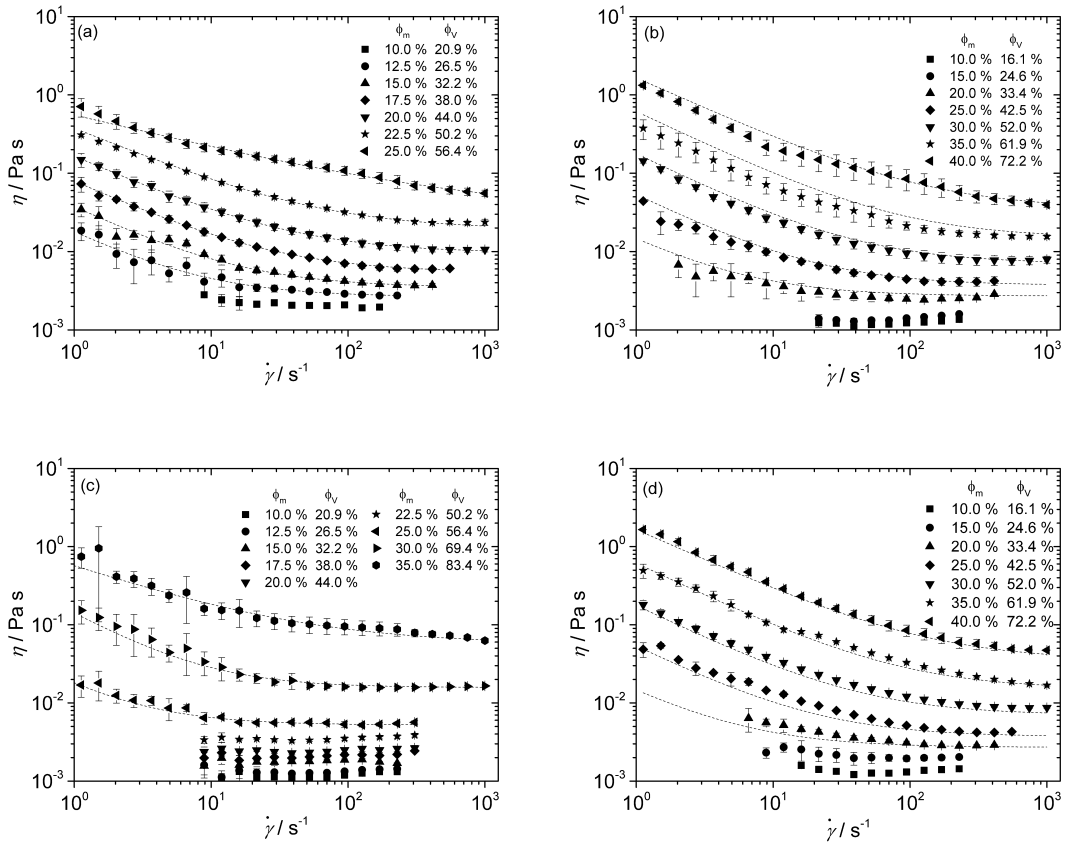

Figure 4.5: Viscosity η versus shear rate $\dot{\gamma}$ for (a) wheat straw coke slurries (WSCS), (b) beech wood coke slurries (BWCS), both at $t_{mill} = 0$ min and (c) WSCS, (d) BWCS at $t_{mill} = 15$ min with different mass and volume fractions. Points are measured values while the dashed lines refer to the fits of the Sisko model to the respective data.

In Figure 4.5 (a) the viscosity functions for a wheat straw coke slurry (WSCS) with non-milled particles ($t_{mill} = 0$ min) at different mass, respectively volume fractions (ϕ_m = 10 - 25 % or ϕ_V = 20.9 - 56.4 %) are depicted. At low mass fractions the slurries exhibit Newtonian flow behavior, i.e. the viscosity is constant over the whole shear rate range. This constant value is assumed also to be valid for shear rates which could not be measured here. Note, the shear rate range was limited due to the sensitivity of the experimental setup at low shear rates and due to the onset of secondary flows at high shear rates. This Newtonian behavior is common for dilute suspensions of spheri-

cal particles (ϕ_V *leq* 30 %) without thermodynamic interactions [Metzner, 1985]. With increasing particle loading the flow behavior gets more and more non-Newtonian. A plateau for the zero shear viscosity is not detectable in the investigated shear rate range. Shear thinning behavior is observed for slurries with mass fractions $\phi_m \geq 12.5$ % ($\phi_V \geq 26.5$ %). The high viscosities at low shear rates are due to interparticle forces like e.g. vdW forces but with increasing shear rate hydrodynamic forces dominate those particle-particle interactions and a viscosity decrease occurs, also particle orientation in the flow has to be considered. This non-Newtonian flow behavior can be described with the three parameter Sisko-Model [Sisko, 1958]. Here η is the viscosity, K_S the consistency index, $\dot{\gamma}$ the shear rate, m the flow index and η_∞ the infinite shear rate viscosity.

$$\eta = K_S \dot{\gamma}^{m-1} + \eta_\infty \tag{4.8}$$

The Sisko-Model was already successfully applied to coal water slurries, although this model does not include a yield stress parameter. Nevertheless, it describes the flow curves over a wide shear rate range very well [Turian et al., 2002].
It has to be mentioned that this model does not preclude the presence of a yield stress but just does not cover this aspect of flow behavior. In the case investigated here, a potential yield stress can be estimated to be well below 1 Pa and thus is not relevant for technical processing. Resulting m, K_S and η_∞ values are summarized in Table 4.2 for the four highest volume fractions measured for both slurries at t_{mill} = 0 min and 15 min. The viscosity functions fitted with this model are indicated by the dashed lines through the symbols in all graphs of Figure 4.5 for the non-Newtonian flow curves.

In Figure 4.5 (b) the viscosity functions for a beech wood coke slurry (BWCS) with non-milled particles (t_{mill} = 0 min) at different mass or volume fractions (ϕ_m = 10 - 40 % or ϕ_V = 16.1 - 72.2 %), respectively are shown. Viscosity values are quite similar to those obtained for WSCS and non-Newtonian flow behavior sets in at mass fractions $\phi_m \geq 20$ % and data for $\phi_m > 20$ % can also be fitted with the three parameter Sisko model. For both slurries non-Newtonian behavior sets in at $\phi_V \approx 25$ - 30 %, i.e. at slightly lower ϕ_V values than expected for ideal spherical particles and this is presumably due to the irregular particle shape. A comparison of WSCS and BWCS with same mass fractions (from Figure 4.5 (a) and (b)) reveals that the WSCS has a higher viscosity, especially at high shear rates, than BWCS due to the higher porosity of the wheat straw particles resulting in a higher particle volume fraction for the WSCS at a given mass fraction. The

Table 4.2: Fitting values n, K_S and η_∞ of the Sisko-Model for WSCS and BWCS at t_{mill} = 0 min and 15 min

Slurry	ϕ_V / **%**	ϕ_m / **%**	**m -**	K_S / **Pa s**$^{m-1}$	η_∞ / **mPa s**
WSCS, 0 min	38.0	17.5	0.186	0.074	5.4
	44.0	20.0	0.280	0.142	8.9
	50.2	22.5	0.263	0.357	19
	56.4	25.0	0.312	0.788	55.6
WSCS, 15 min	50.2	22.5	-	-	3.6
	56.4	25.0	0.000	0.014	5.2
	69.4	30.0	0.001	0.196	16.2
	83.4	35.0	0.385	0.524	56.6
BWCS, 0 min	42.5	25.0	0.127	0.058	3.8
	52.0	30.0	0.150	0.177	7.4
	61.9	35.0	0.165	0.623	15.4
	72.2	40.0	0.212	1.621	37.3
BWCS, 15 min	42.5	25.0	0.122	0.060	3.6
	52.0	30.0	0.140	0.173	7.7
	61.9	35.0	0.162	0.636	17.1
	72.2	40.0	0.216	1.624	36

high shear limiting viscosity η_∞ is independent of thermodynamic particle interactions and solely determined by particle shape and volume fraction.

The viscosity curves at different mass fractions of milled wheat straw particles (t_{mill} = 15 min) are shown in Figure 4.5 (c). For every mass fraction a significant reduction of the viscosity compared to the corresponding suspension of unmilled particles is observed. This also shows up in the η_∞ data summarized in Table 4.2. We attribute this phenomenon to the increased circularity of the milled wheat straw particles, as the density and porosity remain constant. The influence of the particle shape is discussed in more detail later. Remarkably, using the milled particles it was possible to prepare a suspension with ϕ_m = 35 % with essentially the same viscosity function as the suspension of unmilled particles with ϕ_m = 25 %. The milling step thus turns out to be a valuable tool to increase the energy density of the slurry.

Figure 4.5 (d) exhibits the corresponding viscosity curves of milled beech wood coke (t_{mill} = 15 min) with increasing mass content. In contrast to the WSCS the BWCS shows minor changes in the viscosity function upon milling comparing Figure 4.5 (b) with Figure 4.5 (d) or the corresponding K_S and η_∞ values in Table 4.2. Minor differences between viscosity functions at the same ϕ_m are presumably due to the differences in the PSD, the suspensions of milled particles with narrower PSD exhibit slightly lower viscosity

than suspensions of unmilled particles. The high volume fractions of WSCS with milled particles (up to $\phi_V = 83.4$ %) and BWCS (up to $\phi_V = 72.2$ %) are enabled by the broad PSD. For mono-modal suspensions of spherical particles viscosity diverges at a volume fraction $\phi_{V_{max}} = 74$ % assuming face centered cubic packing. Farris showed that the volumetric maximum packing fraction $\phi_{V_{max}}$ is strongly dependent on the PSD and $\phi_{V_{max}}$ > 90 % can be reached for multi-modal of very broad PSDs, since the small particles fill the interstitial volume between the bigger particles efficiently [Farris, 1968, Servais et al., 2002].

At constant mass fractions the WSCS still show a higher infinite shear rate viscosity than BWCS with particles which were treated 15 min in the planetary ball mill. However, the flow behavior of WSCS is almost Newtonian for mass fractions up to $\phi_m = 22.5$ %, whereas BWCS exhibit a shear thinning flow behavior starting at mass fraction of $\phi_m = 20$ %. It has to be mentioned that the second Newtonian plateau adjusts faster for the WSCS with milled particles than for the BWCS. As shown above an impact of the particle shape on flow behavior occurs for the WSCS due to milling. In contrast, the flow behavior of BWCS remains constant upon milling since this processing step affects only the particle size but not their shape. This is in common with the findings of Thomas, who investigated suspensions with different particle size and also the matrix fluid viscosity had been varied substantially. No effect of particle size or fluid viscosity on the relative suspension viscosity could be observed [Thomas, 1965]. The relative viscosity η_{rel} (Eq. 4.7) has to be considered as a function of the volume fraction ϕ_V.

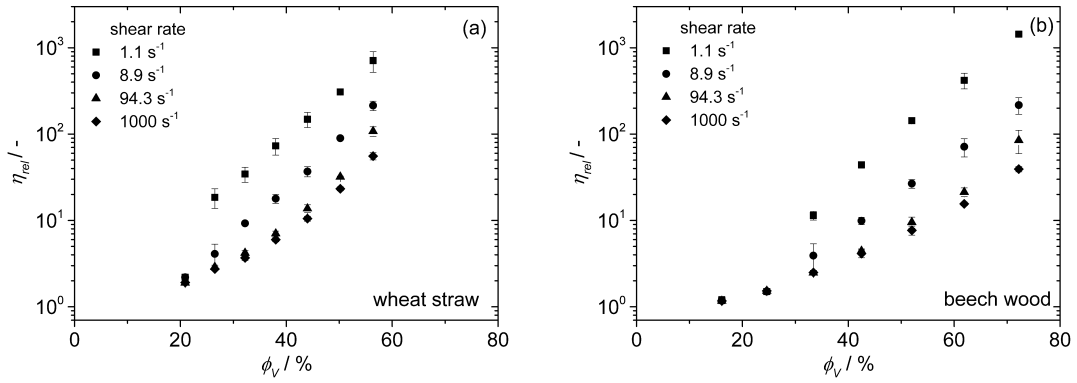

Figure 4.6: Relative viscosity η_{rel} versus volume fraction ϕ_v at shear rates $\dot{\gamma}$ of 1.1 s^{-1} (square), 8.9 s^{-1} (circle), 94.3 s^{-1} (triangle) and 1000 s^{-1} (diamond) for (a) WSCS and (b) BWCS with untreated particles (t_{mill} = 0 min).

Figure 4.6 indicates the relative viscosities of untreated WSCS (a) and BWCS (b) suspensions versus volume fraction at various shear rates between 1.1 s^{-1} and 1000 s^{-1}, η values are taken from Figure 4.5 and η_{fluid} = 1 mPa s. With increasing shear rate η_{rel} reduces due to decreasing relevance of thermodynamic particle interactions compared to hydrodynamic forces and due to an alignment of particles in the flow field. The effect of flow alignment on particle packing and flow resistance has been thoroughly discussed by Donev et al [Donev et al., 2004]. Newtonian flow behavior for the dilute suspensions (ϕ_V < 25 %) implies that the respective η_{rel} data lie in a narrow range. For higher volume fractions the η_{rel} versus ϕ_V curves obtained at different shear rates diverge reflecting the shear thinning behavior. Note, for volume fractions ϕ_V > 44 % even the η_{rel} versus ϕ_V curves for the two highest shear rates (94.3 s^{-1} and 1000 s^{-1}) diverge since the second Newtonian plateau is attained at higher shear rates as ϕ_V increases. Observations, made for WSCS and BWCS, are very similar. However, the non-Newtonian flow behavior starts at higher volume fraction for BWCS than for WSCS, and the same applies for the second Newtonian plateau. For further investigations regarding the influence of the particle shape on flow behavior, the relative viscosity, taken at shear rates of $\dot{\gamma}_{low}$ = 1.1 s^{-1} and $\dot{\gamma}_{high}$ = 1000 s^{-1}, will be discussed.

4.4.3 Influence of particle shape on viscosity in the low and high shear regime

Figure 4.7 displays the relative viscosity as a function of volume fraction for coke slurries with particles, which were milled for different periods of time. For WSCS (Figure 4.7 (a)), a monotonic decrease of the relative viscosity with increasing milling time of the particles is observed in the low shear regime as well as in the high shear regime. Nicoleit et al. made similar observations regarding a decrease of η_{rel} with milled particles, but received a reduced porosity of the wheat straw coke particles due to their grinding setup and therefore attributed this decrease in relative viscosity at constant mass fraction to the porosity decrease. However, the particle shape was not taken into account [Nicoleit et al., 2016]. Here we can exclude a change in porosity due to milling and hence the decrease of viscosity is ascribed to the increase in circularity of the particles, as shown in Figure 4.4 (a). From a milling time of 0 min to 5 min η_{rel} at $\dot{\gamma}_{low}$ = 1.1 s^{-1} drops from 710 to 30 at ϕ_V = 56.4 % which is a reduction by a factor of almost 25. Similar relative viscosity values are found for milling times of 5 min and 10 min as expected since the circularity distribution is essentially the same. A further increase in circularity was achieved for t_{mill} = 15 min, resulting in a further drop of low shear viscosity to η_{rel} = 17. At a high shear rate of 1000 s^{-1} the relative viscosity reduces from η_{rel} = 55 to

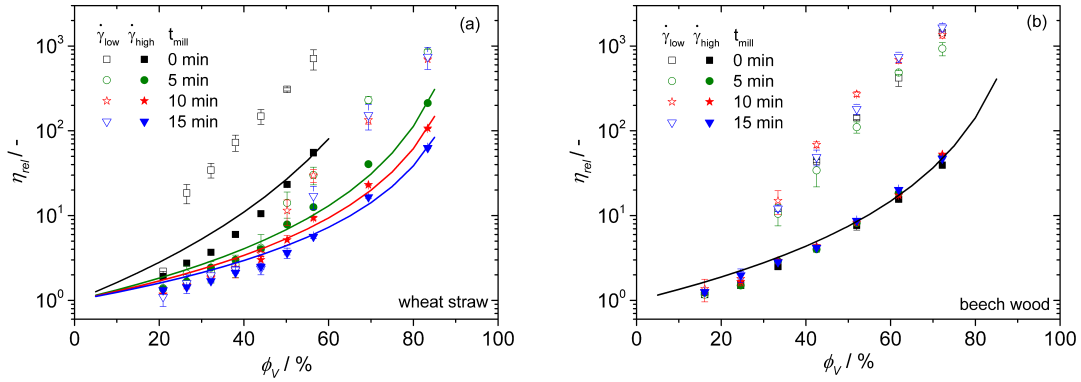

Figure 4.7: Relative viscosity Î·rel versus volume fraction ϕ_V at $\dot{\gamma}_{low}$ = 1.1 s^{-1} and $\dot{\gamma}_{high}$ = 1000 s^{-1} for (a) WSCS and (b) BWCS made from coke particles milled for different periods of time. The lines indicate fits of the model suggested by Santamaria-Holek and Mendoza keeping the parameter $\phi_{V_{max}}$ constant at $\phi_{V_{max}}$ = 96 % and using $[\eta]$ as the only free fit parameter characterizing the change in particle shape upon milling [Santamaría-Holek and Mendoza, 2010].

η_{rel} = 5.6 for a milling time of 15 min. The model of Santamaria-Holek and Mendoza was used to describe the dependence of η_{rel} and ϕ_V quantitatively. This model is a modification of the Krieger-Dougherty approach [Krieger and Dougherty, 1959] taking the effect of particle shape on intrinsic viscosity $[\eta]$ and maximum packing fraction $\phi_{V_{max}}$ into account [Santamaría-Holek and Mendoza, 2010]. Their expression for the relative viscosity is given in Eq. 4.9. Here c is a constant calculated according to in Eq. 4.10.

$$\eta_{rel} = (1 - \frac{\phi_V}{1 - c\phi_V})^{[\eta]} \tag{4.9}$$

$$c = \frac{1 - \phi_{V_{max}}}{\phi_{V_{max}}} \tag{4.10}$$

This model includes two parameters, namely the maximum packing fraction $\phi_{V_{max}}$ and the intrinsic viscosity $[\eta]$. The former depends on the particle size distribution as well as on particle shape, whereas the latter is solely determined by particle shape. Both parameters are strongly correlated and cannot be fitted simultaneously. Thus we held the maximum packing fraction constant and determined the intrinsic viscosity $[\eta]$. A value $\phi_{V_{max}}$ = 96 % was selected here considering the very broad PSDs for all used coke fractions and assuming that the change of shape relevant here is of minor impact. This

assumption seems to be reasonable especially in the high shear regime where particle alignment is supposed to occur and only those η_{rel}-ϕ_V data sets were fitted. The intrinsic viscosity is therefore the only fitting parameter. The resulting values for the averaged intrinsic viscosity values for WSCS are 4.6 ± 0.07, 2.7 ± 0.01, 2.3 ± 0.01 and 2.1 ± 0.01 at milling times of 0, 5, 10 and 15 min. This decrease is consistent with the increasing circularity, i.e. increasing roundness and decreasing roughness. The limiting $[\eta]$-value for spheres is 2.5 but for anisotropic particles aligned in strong flow fields even lower values are possible.

In conclusion, the milling step enabled us to increase the particle mass fraction and hence the HHV of WSCS without increasing the viscosity level thus guaranteeing good pumpability and gasification.

In Figure 4.7 (b) the relative viscosity versus ϕ_V data for BWCS are shown. In contrast to WSCS no significant change of the η_{rel} versus ϕ_V curves could be achieved by the milling procedure irrespective of milling time. Neither at low nor at high shear rates a measurable effect could be detected as expected, since circularity distribution does not change during milling time of the beech wood coke particles (Figure 4.4 (b)). The porosity and density of the particles also remain constant, and obviously the flow behavior of BWCS does not depend on particle size in the investigated range. Again setting $\phi_{V_{max}}$ = 96 % as for the WSCS an intrinsic viscosity $[\eta] = 2.8 \pm 0.04$ was obtained from fitting the relative viscosities at $\dot{\gamma}_{low} = 1000\ s^{-1}$ independent of milling time. This is in the same range as the value for $[\eta]$ for WSCS at a milling time of 5 min. Finally, it should be noted that the intrinsic viscosity data obtained from viscosity measurements according to the fitting procedure described above are in excellent agreement with direct determinations of this quantity from dilute suspension viscosity, see Table 4.3. These consistent results including three independent sets of experimental data justify to neglect the effect of circularity on $\phi_{V_{max}}$ allowing for a robust fit of the model described by Eq. 4.9 to our experimental data. Note, the intrinsic viscosity values below the rigid sphere limit of 2.5 can be rationalized keeping in mind the high porosity of the particles allowing for a fluid flow inside the particles [Nawab and Mason, 1958].

4.5 Conclusion

We have investigated the influence of particle volume fraction, size and shape on flow behavior of coke water slurries. Two different coke feedstocks (wheat straw and beech wood) with similar initial mean particle diameter have been treated in a planetary ball mill. Both coke sorts exhibit an equal decrease in particle size with increasing milling

Table 4.3: Values of the intrinsic viscosity $[\eta]$ obtained with an Ubbelohde viscometer from plots of $(\eta_{rel} - 1)\ \phi_V^{-1}$ against $\phi_V = 0$

	$\mathbf{t}_{mill}$ **/ min**	$[\eta]$ / −
Wheat straw	0	4.38 ± 0.02
	15	2.24 ± 0.05
Beech wood	0	2.74 ± 0.10
	15	2.83 ± 0.07

time. Additionally, the wheat straw coke particles change their shape with increasing milling time, quantitatively evaluated by an increasing circularity. In contrast, the shape of the beech wood coke particles does not change. In both cases the particle porosity remains constant irrespective of milling time.

Slurries including those coke particles were prepared and rheologically characterized. For low mass, respectively volume fractions ($\phi_V \leq 20$ %), the suspensions behave like Newtonian fluids, while for higher particle loadings shear thinning behavior occurs. The shape of the corresponding viscosity over shear rate curves is mathematically well described by the Sisko model. For WSCS the viscosity at constant mass fraction decreases with increasing milling time of particles, which is attributed to the increased circularity. Accordingly, higher mass fraction of particles could be mixed into the slurry, at a selected viscosity level providing good processability. This corresponds to an increased energy density and thus HHV of the slurry. In contrast, the BWCS exhibit similar viscosity functions independent of the milling time as their circularity distribution remains unaltered. Porosity and density of both coke feedstocks stay constant during milling and the particle size decreases in the same manner. Obviously, particle shape is the relevant parameter controlling the change in flow behavior observed for WSCS.

The effect of particle shape on coke slurry viscosity was captured quantitatively using the model of Santamaria-Holek and Mendoza describing the dependence of relative viscosity on particle volume fraction. This model includes two parameters, namely the maximum packing fraction and the intrinsic viscosity. The former depends on the particle size distribution as well as on particle shape, whereas the latter is solely determined by particle shape. Accordingly, both parameters are strongly correlated and cannot be fitted simultaneously. Thus we held the maximum packing fraction constant and determined the intrinsic viscosity $[\eta]$ from fitting the well-established phenomenological model to our experimental data. The intrinsic viscosity values obtained that way remained unchanged upon milling for beech wood coke while they decreased for wheat straw coke. This is in line with image analysis results revealing a constant circularity for beech wood coke

and an increase of this shape parameter upon milling for wheat straw coke. Moreover, we found excellent agreement of absolute intrinsic viscosity values obtained from modelling the viscosity of concentrated suspensions and those directly obtained from dilute suspension viscometry. This consistent data analysis including three independent measurements justifies this simplified but robust approach suggested here for quantitatively modelling coke slurry viscosity.

Our investigations finally provide evidence that the flow behavior of coke water slurries can be tailored by changing particle shape. A viscosity reduction can be achieved by milling of wheat straw coke particles enabling a substantially increased particle loading, i.e. HHV at a viscosity level still providing good transport and gasification properties.

4.6 Acknowledgement

The authors like to thank the Helmholtz Association of German Research Centers (HGF) for partial funding of the work. Thanks to Mark Eberhard for providing the coke. Furthermore, we gratefully acknowledge experimental support by Rafael Mayorga Gonzalez and Astrid Huber.

5 Flow Behavior and Aging of Pyrolysis Oils from Different Feedstocks

Full title	Flow Behavior and Aging of Pyrolysis Oils from Different Feedstocks
Authors	Leon Jampolski, Marco Tomasi Morgano, Helmut Seifert, Thomas Kolb, Norbert Willenbacher
Status	published
Bibliographic data	Energy & Fuels 31 (5), 5165-5173, 2017 DOI: 10.1021/acs.energyfuels.7b00196

5.1 Abstract

This work focuses on the flow behavior and accelerated aging of pyrolysis oils produced in a screw reactor from different feedstocks. Beech wood, wheat straw, chicken manure, and sewage sludge were pyrolyzed at 350, 400, 450, and 500 °C, and the viscosity of the corresponding oils was measured at four different temperatures between 20 and 80 °C, with values up to 1 Pa s at 20 °C. Newtonian flow behavior was observed, except for wheat straw pyrolysis oils at temperatures below 50 °C. Absolute viscosity values as well as flow activation energies (E_A), covering a range from 38 to 57 kJ mol^{-1}, turned out to be independent of the pyrolysis temperature, except for beech wood oil. In this latter case, a peak in viscosity and activation energy was found at a pyrolysis temperature of 450 °C and is attributed to the low water content of the oil obtained at this temperature. Accelerated aging experiments were conducted for 24 h at 40 and 80 °C. For the latter temperature, the effect of a free surface and an inert gas atmosphere on aging was examined. This enabled us to separate the effect of polymerization and evaporation of volatiles on the change in viscosity. In both cases, beech wood pyrolysis oil showed the strongest aging (~20-fold increase in viscosity). The lowest aging was found for wheat straw pyrolysis oil in a free surface sample cell, while almost no aging occurred under an inert gas atmosphere. Therefore, we conclude that aging of beech wood oil is mostly due to polymerization, whereas aging of wheat straw oil is essentially due to

evaporation of volatiles. For chicken manure and sewage sludge oils, both polymerization and evaporation contribute almost equally to the increase of viscosity when an open sample cell is used. For beech wood pyrolysis oil, size-exclusion chromatography revealed a change in molecular weight upon aging from $M_W = 190$ to 240 Da. A slight increase in M_W could be detected for chicken manure and sewage sludge, but no indication for polymerization was found for wheat straw. Gas chromatography coupled with mass spectrometry was used to determine the concentration of characteristic oil components quantitatively, confirming the conclusions from viscosity measurements regarding aging mechanisms.

5.2 Introduction

Biomass pyrolysis is defined as a thermochemical process performed in the absence of oxygen at typical temperatures of 350-550 °C, where the lignocellulosic biomass is converted into solids (char/coke), gases, and liquids [Bridgwater, 1999, Bridgwater and Peacocke, 2000]. One of the obtained liquids is called pyrolysis oil or bio-oil. It has a dark brown color and a pronounced smoky odor and consists of a large number of organic compounds [Ortega et al., 2011]. Those oils can be used as an alternative carbonaceous fuel in the future as well as a replacement or blending agent of abating fossil fuels in the field of transportation and gasification [Alonso et al., 2010, Higman and Burgt, 2003, Jiang and Ellis, 2010]. Pyrolyzed biomass used as feed for gasification can be reformed into synthesis gas, with a subsequent gas cleaning using the Fischer-Tropsch process to produce synthetic fuels or hydrocarbons [Dahmen et al., 2012, Wright et al., 2008]. Because many pyrolysis oils tend to become unstable or exhibit phase separation during storage [Oasmaa, A., Kuoppala, 2003], a lot of effort has been spent to upgrade and stabilize pyrolysis oils through catalysis [Zhang et al., 2006, Fisk et al., 2009, Widayatno et al., 2016, Koike et al., 2016, Xu et al., 2009b, Oh et al., 2016]. This catalytic treatment mostly improves the properties of the pyrolysis oils, but it is sophisticated, time-consuming, and, therefore, expensive. Whether such a catalytic stabilization is necessary has to be examined for each oil individually. The flow behavior of pyrolysis oils is a key parameter for handling and processing [Yang et al., 2015] and has motivated this broadly based study on viscosity of such oils, including the effect of aging.
Previously, Chaala et al. performed thermal stability tests measuring the variation in viscosity, molecular weight distribution, and water content of different wood-based pyrolysis oils at increased temperatures for certain time periods with a spindle in cup viscometer. An increase of the viscosity was accompanied by a decrease of low-molecular-weight

compounds, while the amount of high-molecular-weight compounds increased, indicating polymerization [Chaala et al., 2004]. Similar observations were reported by others, and polymerization turned out to be more pronounced at an increased aging temperature [Diebold and Czernik, 1997, Junming et al., 2008, Alsbou and Helleur, 2014].

In all of the above mentioned investigations, the viscosity was determined at only one shear rate and one temperature. Nolte and Liberatore [Nolte and Liberatore, 2010] investigated the viscosity of oils from different feedstocks as a function of the shear rate at various temperatures. Viscosity values in the range of 15-400 mPa s were obtained at 25 °C; viscosity values in the range of 10-130 mPa s were obtained at 40 °C; and viscosity values in the range of 5-50 mPa s were obtained at 55 °C, always determined at a shear rate of 100 s^{-1} [Nolte and Liberatore, 2010]. A correlation between viscosity and feedstock origin was not discussed. The covered viscosity range decreased with an increasing temperature, confirmed in an earlier work [Diebold and Czernik, 1997]. Wood-based oils were found to be non-Newtonian at low temperatures, and oils from switch grass and wheat straw turned out to be biphasic and shear thinning in the whole investigated temperature range. Zhang et al. showed that biochar acts as a catalyst and boosts reactions within the pyrolysis oil, resulting in an increased water content and, thus, a decreased viscosity in the examined shear rate range from 100 to 500 s^{-1} [Zhang et al., 2013]. Furthermore, investigations of the flow behavior of blends of pyrolysis oil, char, and additives were performed, showing a viscosity reduction as a result of those additives [Gao et al., 2016].

In contrast to previous studies, Nolte and Liberatore used a sealed pressure cell in a rheometer for the *in situ* measurements of the viscosity during accelerated aging and confirmed that this procedure yields similar results as common aging experiments, where viscosity measurements are performed after different storage times [Nolte and Liberatore, 2011]. The treatment of a pyrolysis oil sample at 80 °C for 24 h in an tightly sealed container was found to be equivalent to an aging of the oil for approximately 1 year at room temperature in a sealed reservoir [Trinh et al., 2013].

This work focuses on the flow properties of oils from four different feedstocks (beech wood, wheat straw, sewage sludge and chicken manure) pyrolyzed at 350, 400, 450, and 500 °C, and their aging behavior. Rotational rheometer measurements were conducted at different temperatures. The effect of polymerization and evaporation of volatiles on the aging of pyrolysis oils from different feedstocks was examined. Aging experiments were performed using an open sample cell as well as a sealed pressure cell similar to the cell used by Nolte and Liberatore, providing an inert gas atmosphere. In contrast, we used a double-wall concentric cylinder system instead of a regular couette cell, providing

higher torque sensitivity. Viscosity measurements characterizing aging were complemented by size-exclusion chromatography (SEC) and gas chromatography coupled with mass spectroscopy (GC-MS) to disclose the dominating aging mechanisms.

5.3 Materials and methods

5.3.1 Materials

Pyrolysis oils were produced using an intermediate pyrolysis trough screw reactor called STYX, which integrates hot gas filtration within the reactor vessel as a vapor precondition step that is known to have a stabilizing effect on the oil [Case et al., 2014, Chen et al., 2011b, Baldwin and Feik, 2013]. This reactor measures approximately 2 m in heated length, has a diameter of 0.15 m, and is divided into seven segments. The feed has a well-defined residence time in the reactor by adjusting the rotational speed of the screw. Temperatures between 350 and 550 °C can be regulated with external independent electrical heaters. A particle and ash-free oil is obtained by recovering desired substances at different positions along the reactor [Tomasi Morgano et al., 2015]. Four different feedstocks were pyrolyzed at 350, 400, 450, and 500 °C at mass flows between 2 and 4 kg h^{-1}. Beech wood (BW) and wheat straw (WS) were included in this study as lignocellulosic biomass as well as sewage sludge (SS) and chicken manure (CM) as the biogenic residues from zoomass. The density ρ of the obtained oils was measured using a pycnometer after Gay-Lussac with a volume of 10.210 ml (Carl Roth GmbH, Karlsruhe, Germany), and the surface tension Γ was obtained using a customized setup based on the pendant drop principle [Song and Springer, 1996] with a needle diameter of 1.65 mm. These values are summarized in Table 5.1.

5.3.2 Rheological measurements

Shear-rate-dependent viscosity

The rheological properties of the pyrolysis oils were characterized through the shear-rate-dependent viscosity η. Measurements were performed using a rotational rheometer (Physica MCR501, Anton Paar GmbH, Graz, Austria) equipped with a coaxial cylinder geometry (inner diameter, 26.66 mm; outer diameter, 28.92 mm). These measurement were conducted using a shear rate ramp (initial shear rate, 0.1 s^{-1}; final shear rate, 1000 s^{-1}), holding the shear rate for 20 s before recording the shear stress and calculating the corresponding viscosity. Preliminary experiments on WS pyrolysis oil revealed that this was sufficient to reach the steady state for each measuring point. The shear rate

Table 5.1: Pyrolysis oil feedstocks, corresponding pyrolysis temperature, density, surface tension, and mass flow.

feedstock	**pyrolysis temperature T_{pyro} (°C)**	**density ρ (g cm^{-3})**	**surface tension Γ (mN m^{-1})**	**mass flow (kg h^{-1})**
beech wood	350	1.155 ± 0.001	35.1 ± 0.1	2
(BW)	400	1.163 ± 0.003	35.5 ± 0.1	2
	450	1.179 ± 0.003	36.1 ± 0.1	2
	500	1.156 ± 0.001	35.6 ± 0.1	2
wheat straw	350	1.092 ± 0.001	28.8 ± 1.0	3
(WS)	400	1.098 ± 0.001	26.6 ± 2.2	3
	450	1.108 ± 0.003	25.7 ± 0.8	3
	500	1.069 ± 0.004	22.6 ± 1.1	3
chicken manure	350	1.043 ± 0.001	31.7 ± 1.3	4
(CM)	400	1.039 ± 0.003	29.1 ± 0.7	4
	450	1.044 ± 0.006	32.4 ± 0.1	4
	500	1.050 ± 0.001	32.5 ± 0.1	4
sewage sludge	350	1.000 ± 0.001	28.5 ± 0.1	4
(SS)	400	1.004 ± 0.002	28.5 ± 0.1	4
	450	0.998 ± 0.001	28.4 ± 0.1	4
	500	1.026 ± 0.002	28.6 ± 0.2	4

ramp was carried out at temperatures of 20, 40, 60, and 80 °C, and the WS produced at T_{pyro} = 450 °C was additionally measured at 50 °C. Viscosity measurements at high temperatures and low shear rates were limited by the torque resolution of the rheometer. Data access at high shear rates and low viscosity was limited presumably as a result of the formation of Taylor vortices indicated by an unexpected increase of viscosity at high shear rates.

The Arrhenius equation (Eq. 5.1) was used to calculate the flow activation energy E_A

$$\frac{\eta(T)}{\eta(T_0)} = exp\frac{E_A}{R}(\frac{1}{T} - \frac{1}{T_0}) \tag{5.1}$$

where R is the ideal gas constant, $\eta(T)$ is the viscosity at the temperature T, and $\eta(T_0)$ is the viscosity at a reference temperature T_0.

Aging under shear

When pyrolysis oil shows an increase in viscosity after or during heating over time, this phenomenon is termed ”aging” [Ortega et al., 2011, Diebold and Czernik, 1997, Alsbou and Helleur, 2014, Nolte and Liberatore, 2011, Yu et al., 2007, Oasmaa and Peacocke,

2001]. To obtain insight into the aging behavior of the pyrolysis oil, samples were continuously sheared at a constant shear rate for 24 h at process relevant temperature of 40 and 80 °C. Viscosity was recorded every 60 s. A coaxial cylinder sample cell geometry with a surface open to the atmosphere was used for these experiments, and a shear rate of 10 s^{-1} was selected to mimic a pumping process. Secondary flows could be neglected at this intermediate shear rate. The torque was sufficient, even for the sample with the lowest viscosity, to receive a stress signal from the rheometer. Measurements of the shear-rate-dependent viscosity after the aging procedure were performed as described in section 5.3.2.

A pressure cell from Anton Paar, shown in Figure 5.1, was used to perform viscosity measurements under an inert gas atmosphere (N_2 with 99.999% purity, Air Liquide SA, Paris, France). This avoids evaporation of volatiles, and the viscosity increase observed in these experiments can be attributed to polymerization reactions. This hermetically sealed concentric double-wall cylinder geometry (with a gap width of 0.6 mm for both gaps) is specified for pressures up to 400 bar and temperatures up to 200 °C. Measurements were conducted at a shear rate of 10 s^{-1}, a temperature of 80 °C, and a constant pressure of 10 bar procured by a N_2 atmosphere. These real time viscosity measurements are similar to those described by Nolte and Liberatore [Nolte and Liberatore, 2011].

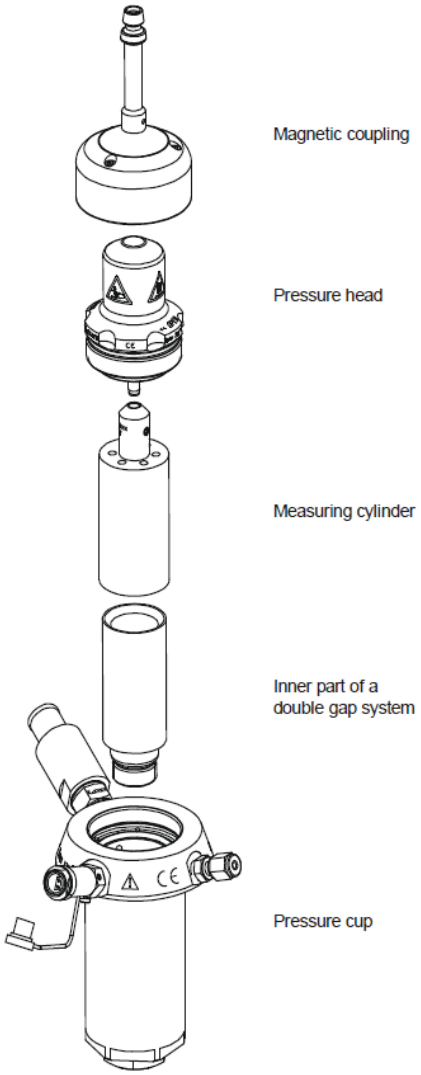

Figure 5.1: Scheme of the pressure cell setup (courtesy of Anton Paar).

5.3.3 Instrumental analysis

The fresh pyrolysis oils were analyzed by means of elemental analysis as well as ash and water content according to the respective DIN standards. CHNO were determined using the German standard DIN EN 51732, where O was calculated by difference. Sulfur and chlorine were determined according to DIN EN 14582. The heating values were measured under the standard DIN 51900. Finally, the ash and water contents were determined according to DIN 51719 and DIN EN 14346, respectively (see Tables 5.2 - 5.5).

Table 5.2: Elemental composition of BW oil obtained at different pyrolysis temperatures (T_{pyro}), including the ash and water contents.

$\mathbf{T}_{pyro}$	**350 °C**	**400 °C**	**450 °C**	**500 °C**
C (%)	49	51	54	55
H (%)	5	6	6	6
N (%)	0	0	0	0
O (%)	30	29	29	25
S (%)	0	0	0	0
water (%)	16	14	11	14
LHV (MJ kg^{-1})	21.0	21.1	22.3	22.6

Table 5.3: Elemental composition of WS oil obtained at different pyrolysis temperatures (T_{pyro}), including the ash and water contents.

$\mathbf{T}_{pyro}$	**350 °C**	**400 °C**	**450 °C**	**500 °C**
C (%)	50	58	53	56
H (%)	6	6	6	6
N (%)	1	1	1	1
O (%)	23	16	21	16
S (%)	0	0	0	0
water (%)	20	19	19	20
LHV (MJ kg^{-1})	20.8	23.3	22.3	23.4

GC-MS was employed to identify the most relevant substances in the pyrolysis oils. The samples were shaken strongly and homogenized in an ultrasonic bath for about 10-15 min. Afterward, 10 ml of tetrahydrofuran (THF, SEC grade, Scharlau, Scharlab S.L., Barcelona, Spain) was used to dilute 1 g of pyrolysis oil. In the case of fresh and aged pyrolysis oils from lignocellulosic feedstocks, i.e., beech wood and wheat straw, isotope-marked internal standards of furfural, phenol, and guaiacol were added to each solution for a quantitative evaluation of these selected markers. The analysis were carried out adopting HP 6890 MSD; the column is a splitless Agilent CP-Wax 52 CB 60 m/0.32 m inner diameter/0.25 μm film (Agilent Technologies, Santa Clara, CA, U.S.A.). Helium is used as the carrier gas. The profile of the oven temperature was the following: hold of 3 min at 45 °C, followed by a ramp of 3 °C min^{-1} up to 180 °C. Then, the rate was increased to 7.5 °C min^{-1} until 240 °C was reached.
The ash content was below the detection limit for BW, CM, and SS oils. Only for WS oil could an ash content of 0.1% be detected.

Table 5.4: Elemental composition of CM oil obtained at different pyrolysis temperatures (T_{pyro}), including the ash and water contents.

$\mathbf{T}_{pyro}$	**350 °C**	**400 °C**	**450 °C**	**500 °C**
C (%)	67	53	61	54
H (%)	8	7	7	7
N (%)	5	6	7	9
O (%)	9	14	9	12
S (%)	0	1	1	1
water (%)	11	19	15	17
LHV (MJ kg^{-1})	31.4	22.3	27.9	26.5

Table 5.5: Elemental composition of SS oil obtained at different pyrolysis temperatures (T_{pyro}), including the ash and water contents.

$\mathbf{T}_{pyro}$	**350 °C**	**400 °C**	**450 °C**	**500 °C**
C (%)	57	65	64	65
H (%)	8	8	8	8
N (%)	6	7	8	8
O (%)	9	4	6	5
S (%)	1	1	1	1
water (%)	19	15	13	13
LHV (MJ kg^{-1})	28.0	28.9	28.3	30.2

5.3.4 SEC

High-performance liquid chromatography (HPLC) was used to evaluate the occurrence of polymerization under accelerated aging conditions. Therefore, the pyrolysis oil was dissolved in THF with a concentration of 3 mg ml^{-1} and filtrated through 0.2 μm polytetrafluoroethylene (PTFE) membrane filters. SEC was performed on HPLC (Agilent 1200 series, Agilent Technlogies, Santa Clara, CA, U.S.A.) equipped with three polystyrene-divinylbenzene copolymer gel-packed columns (SDV LUX, 5 μm beads in a 5 x 50 mm column and two 8 x 300 mm columns) with a nominal pore diameters of 10^3, 10^3, and 10^5 $\mathring{A}$ (PSS Polymer Standards Service GmbH, Mainz, Germany). The THF flow rate was 1.0 ml min^{-1}, and the total injection volume was 100 μl. A calibration curve using polystyrene standards was applied to convert retention time into molecular weight. The molecular weight was calculated using the software provided by the manufacturer Agilent. These measurements were performed at the Institute for Chemical Technology and Polymer Chemistry at the Karlsruhe Institute of Technology (KIT).

5.4 Results and discussion

5.4.1 Flow behavior

Viscosity data for oils from different feedstocks pyrolyzed at T_{pyro} = 450 °C were determined with rotational rheometry. At this pyrolysis temperature, the mass yield of oil from lignocellulosic feedstocks was largest compared to the other pyrolysis products (e.g., coke and aqueous condensate) [Oasmaa et al., 2016]. The viscosity of the BW, CM, and SS pyrolysis oils turned out to be independent of the shear rate at all investigated temperatures between 20 and 80 °C. Viscosity values for Newtonian oils (produced at T_{pyro} = 450 °C) are displayed in Table 5.6, with corresponding flow curves shown in the supporting information.

Table 5.6: Newtonian viscosity values of BW, WS, CM, and SS produced at T_{pyro} at temperatures between 20 and 80 °C.

feedstock	**measuring temperature (°C)**	**viscosity (mPa s)**
beech wood (BW)	20	187
	40	44
	60	16
	80	7.5
wheat straw (WS)	60	13
	80	7
chicken manure (CM)	20	760
	40	161
	60	54
	80	22
sewage sludge (SS)	20	141
	40	40
	60	16
	80	8

The viscosity of BW oil decreases from 187 mPa s at 20 °C to 7.5 mPa s at 80 °C. For CM, the viscosity decreases from 760 mPa s at 20 °C to 22 mPa s at 80 °C. SS oil viscosity varies between 141 mPa s at 20 °C and 8 mPa s at 80 °C. Flow curves for WS pyrolysis oil are shown in Figure 5.2.

Non-Newtonian flow behavior is observed at temperatures up to 50 °C. This might be caused by the high amount of lignin-derivated substances, such as phenol and guaiacol, present in this oil, as shown in Figure 5.7. These substances melt around 50 °C, and at $T \leq 50$ °C, probably a sample-spanning network exists formed of small crystals, resulting finally in the observed strong shear thinning. Moreover, phase separation was

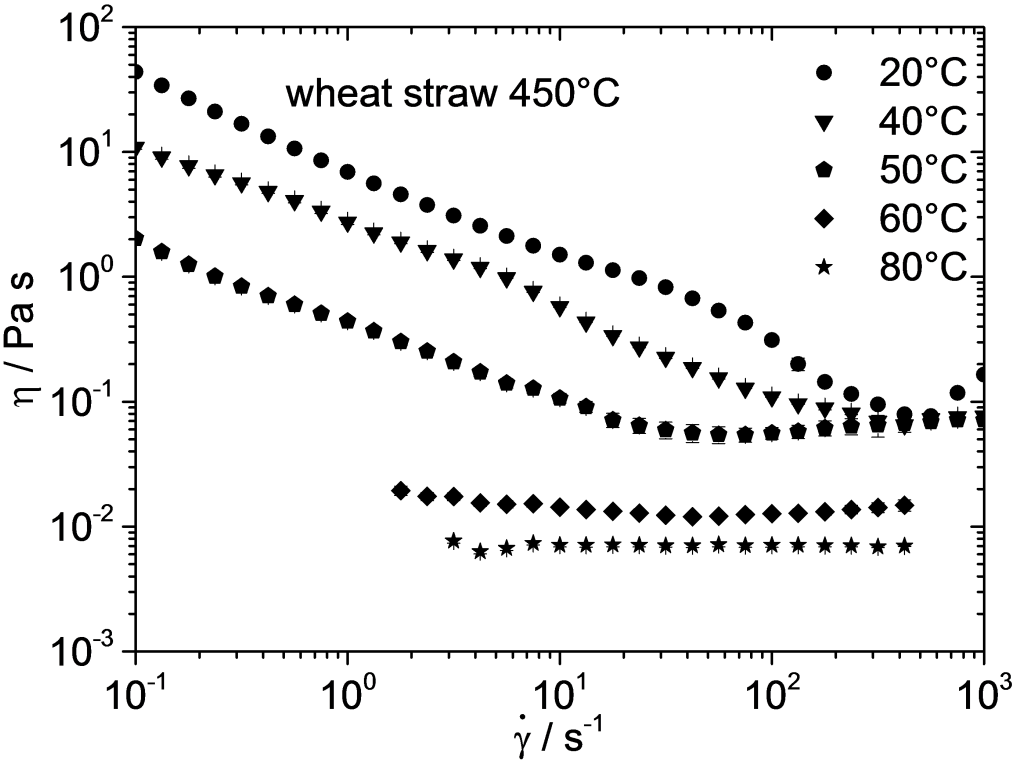

Figure 5.2: Flow curves of WS pyrolysis oil at 20 °C (circle), 40 °C (triangle), 50 °C (pentagon), 60 °C (diamond), and 80 °C (star) pyrolyzed at a temperature of 450 °C.

observed for shear rates above 100 s^{-1}. However, Newtonian flow behavior adjusts for temperatures above 50 °C for this sample, and the viscosity drops to 7 mPa s at 80 °C, similar to that for BW oil. In summary, independent of the feedstock, Newtonian flow behavior is found at temperatures $\geq$ 60 °C and the absolute viscosity values at those temperatures are quite similar, except for the CM pyrolysis oil, which exhibits a ~ 3 times higher viscosity than the other oils investigated here.

5.4.2 Temperature dependency

The viscosity at a shear rate of $\dot{\gamma} = 100\ s^{-1}$ was considered for determination of the flow activation energy E_A because the WS oil exhibits shear thinning behavior at lower shear rates for T < 50 °C. The effect of the pyrolysis temperature (T_{pyro}) on the viscosity of the resulting oils is shown in Figure 5.3. To determine E_A, viscosity values for the different

pyrolysis oils at 20, 40, 60, and 80 °C at $\dot{\gamma} = 100\ s^{-1}$ are plotted over reciprocal absolute temperature, multiplied by 1000, and E_A is calculated according to Eq. 5.1, as described in section 5.3.2. E_A characterizes the dependency of viscosity on the temperature and can be related to the energy of vaporization [Glasstone et al., 1941]. Figure 5.3 (a) clearly shows that BW oil obtained at $T_{pyro} = 450$ °C exhibits a maximum viscosity as well as activation energy. This may be due to the water content, which is at a minimum fr the oil obtained at this pyrolysis temperature (see Table 5.2). Similar findings have been reported for oak pyrolysis oil [Nolte and Liberatore, 2010]. The reason for this variation in the water content is attributed to the thermal degradation of the essentially ash-free woo. Dehydration takes place for $T_{pyro} \leq 450$ °C, resulting in a decrease of the water content with increasing T_{pyro} up to 450 °C. This is followed by active and passive pyrolysis for higher temperatures [Slopiecka et al., 2012], and secondary gasphase reactions become predominant in this temperature range, where an enhanced cracking of large compounds is also promoted by hot-gas filtration at such high temperatures. In combination with the further heterogeneous cracking at the surface of the filter, the presence of species with a higher molecular weight is reduced and the water content increases again, finally resulting in a maximum of viscosity and activation energy at $T_{pyro} = 450$ °C.

The water content of the second lignocellulosic pyrolysis product, namely, the WS oil, is independent of the pyrolysis temperature and slightly higher than that for the BW oil. In this case, non-Newtonian flow behavior is observed at low measuring temperatures, indicating a heterogeneous composition, and the simple Arrhenius-type temperature dependence of viscosity may not hold. We observe a large scatter in viscosity data (see Figure 5.3 (b)) and no systematic trend with the pyrolysis temperature. Nevertheless, the whole set of $\eta(T)$ data was used to determine an apparent activation energy E_A. Obviously, no systematic variation of absolute viscosity value or activation energy occurs for the oils from the zoomass feedstocks (see panels (c) and (d) of Figure 5.3). These results seem surprising because a variation in the water content is found similar to that for the BW oil. However, the oils from zoomass feedstocks include much more nitrogen than the lignocellulosic oils, providing the capability to bind water by hydrogen bridging. The pyrolysis oil from CM not only exhibits the highest absolute viscosity values but also the strongest temperature dependence, resulting in $E_A = 57 \pm 2$ kJ mol^{-1}. The lowest temperature dependence is found for WS pyrolysis oil, with $E_A = 38 \pm$ kJ mol^{-1}, and the values found for SS and BW oils are in between.

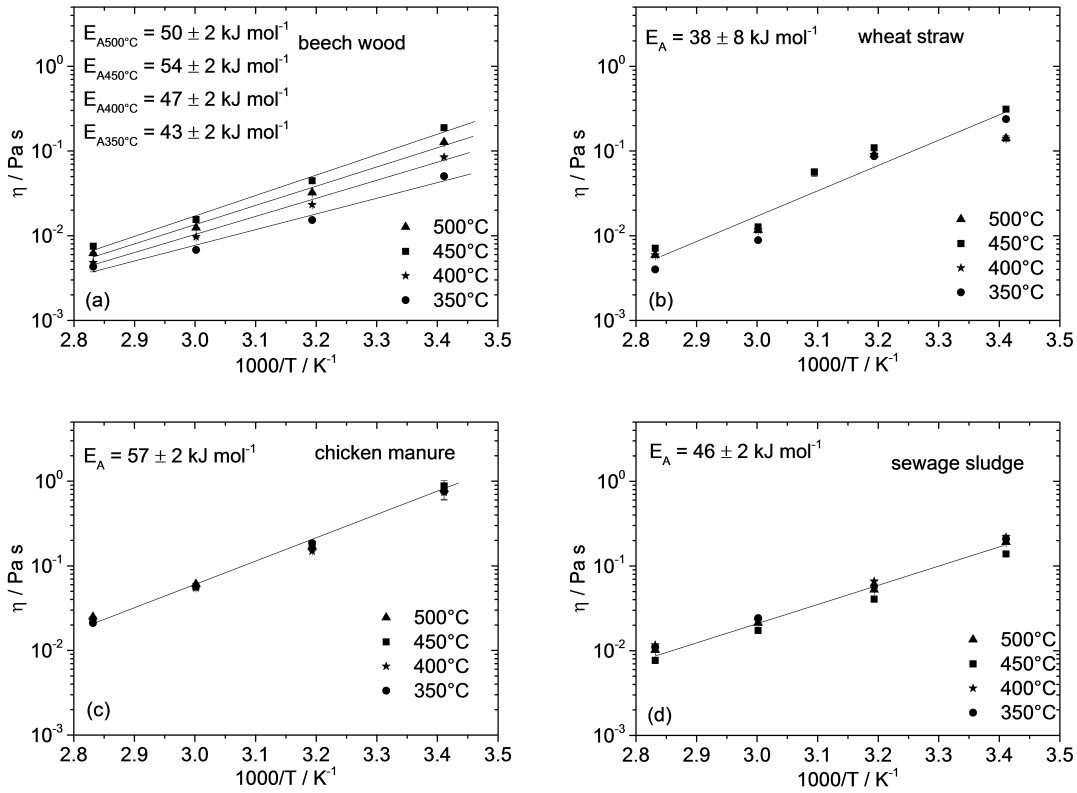

Figure 5.3: Viscosity at a shear rate of 100 s^{-1} over the reciprocal measuring temperature for oils obtained at different pyrolysis temperatures of 350 °C (circle), 400 °C (star), 450 °C (square), and 500 °C (triangle) of the following feedstocks: (a) BW, (b) WS, (c) CM, and (d) SS.

5.4.3 Aging under a free surface

Viscosity is a key parameter for evaluation of processability and fuel quality. It affects fuel-pumping and combustion operations. Stability tests are usually performed at 80 °C for 24 h, measuring the absolute viscosity change over time. Such tests are called accelerated aging experiments [Yang et al., 2015]. The change of viscosity is mainly associated with an increase in the molecular weight as a result of (phenolic) polymerization reactions, which are hastened at those conditions [Diebold and Czernik, 1997]. Aging, however, can also be caused by evaporation of organic volatiles or water [Oh et al., 2016, Diebold and Czernik, 1997]. Aging experiments have been performed under quiescent conditions as well as under shear [Nolte and Liberatore, 2011]. In this work, we carried out aging experiments under shear, simulating a pumping process ($\dot{\gamma}$ = 10

s^{-1}) at 40 and 80 °C using a sample cell with a free surface as well as in a hermetically sealed pressure cell with an inert gas atmosphere at 80 °C. This allows for a distinction between polymerization- and evaporation-controlled aging phenomena.

Figure 5.4: Viscosity data normalized to the respective initial value prior to aging $\eta(t = 0)$ for BW, WS, CM, and SS at 10 h (diagonal pattern) and 24 h (no pattern) for 40 °C (red) and 80 °C (blue) with a constant shear rate of $\dot{\gamma} = 10\ s^{-1}$.

Figure 5.4 shows the viscosity increase after 10 and 24 h obtained from the sample cell with the free surface exemplary for samples produced at $T_{pyro} = 450$ °C. Data are normalized to the initial viscosity value for both temperatures. The first set of bars in Figure 5.4 displays the aging behavior of BW pyrolysis oil. The viscosity at 40 °C was ~1.4 and ~2.4 times higher than initially after 10 and 24 h of aging, respectively. An even more significant increase in viscosity by about a factor of 7 and 20 was observed at 80 °C for both time intervals. The second set of bar in Figure 5.4 shows the aging behavior of WS pyrolysis oil. At 40 °C, almost no rise in viscosity occurs for the whole time range, but at 80 °C, viscosity increases by a factor of ~1.7 after 10 h and then by ~2.7 after

24 h of aging. The viscosity values for CM are shown in the third set of bars in Figure 5.4. In this case, no significant aging is observed at 40 °C; similar to wheat straw, the viscosity rises ~1.1-fold at the end of the experiment. At 80 °C, a more distinct aging effect occurs with viscosity values ~2 and ~3.3 times that of the native oil for both time intervals. The last bar set of Figure 5.4 comprises the aging behavior of SS. $\eta/\eta(t=0)$ goes up to ~1.6 at 40 °C, and a value of ~4.9 is reached at 80 °C after 24 h of aging. Obviously, BW oil has the most significant increase in viscosity in this accelerated aging experiment, followed by SS and CM, while WS is most stabled under those aging conditions. For none of the examined particle-free pyrolysis oils did phase separation occur during the aging procedure. On the basis of Karl Fischer titration experiments, a water content below 1% is detected in the aged samples similar to that shown in previous studies [Diebold and Czernik, 1997]. Additional weight measurements performed before and after aging revealed that the total loss of matter was in the range of the initial water content of the samples. Gravimetric measurements are not sensitive and accurate enough to detect the additional loss of apparently small fractions of organic volatiles.

Flow curve measurements (see section 5.4.1) performed for all investigated oils before and after aging confirmed that the flow behavior remains Newtonian, similar to that reported earlier [Nolte and Liberatore, 2011]. The absolute increase in viscosity for BW oil is shown in Figure 5.5(a), and corresponding data for WS oil are displayed in Figure 5.5(b). Similar results were obtained for CM (Figure 5.5(c)) and SS (Figure 5.5(d)) oil. In all cases, flow behavior remains Newtonian even after accelerated aging. Note that the viscosity ratio $\eta(t = 24h)/\eta(t = 0)$ obtained in these experiments is in excellent agreement with the results shown in Figure 5.4. The deviation between these viscosity ratio values shown in Figures 5.4 and 5.5 is 2% for BW, CM, and SS oils but 10% for the WS oil.

5.4.4 Aging under an inert gas atmosphere

A pressure cell similar to the cell used by Nolte and Liberatore [Nolte and Liberatore, 2011] was used to avoid evaporation of volatiles. The setup is described in section 5.3.2. Aging was performed at T = 80 °C for 24 h, and viscosit was continuously recorded at a shear rate of $\dot{\gamma} = 10\ s^{-1}$. Figure 5.6 displays corresponding results compared to those obtained using an open surface sample cell. For all investigated pyrolysis oils, the increase in viscosity under an inert gas atmosphere is significantly lower than with the free surface geometry, thus indicating that there is a contribution of volatile components to the observed viscosity increase for the free surface setup. The remaining increase in viscosity under an inert gas atmosphere is attributed to polymerization (or other

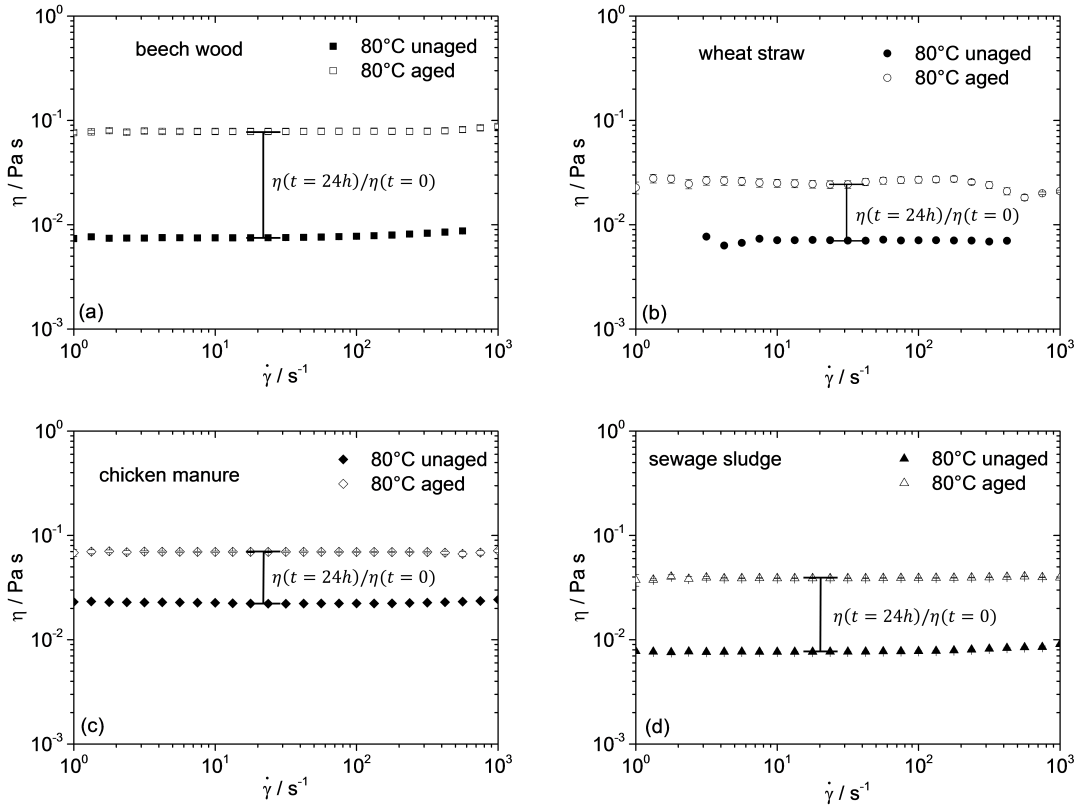

Figure 5.5: Flow curves of (a) BW, (b) WS, (c) CM, and (d) SS oils at 80 °C for the unaged (closed symbols) and aged (open symbols) samples. $\eta(t = 24h)/\eta(t = 0)$ is the viscosity increase during the accelerated aging experiment with a free surface sample cell.

chemicals reactions) [Diebold, 2000]. As seen from the first set of bars in Figure 5.6, this polymerization is the major contributino to aging of BW oil.

In contrast, polymerization is insignificant, and the viscosity increase observed with the free surface system is solely due to evaporation of volatile compounds for the WS oil (second bar set in Figure 5.6), with the total increase in viscosity lowest in this case. Finally, for the CM and SS oils, evaporation and polymerization contribute equally to the viscosity increase observed using the free surface sample cell. Data documenting the full time evolution of viscosity during aging with an open surface as well as an inert gas atmosphere can be found in the supporting information.

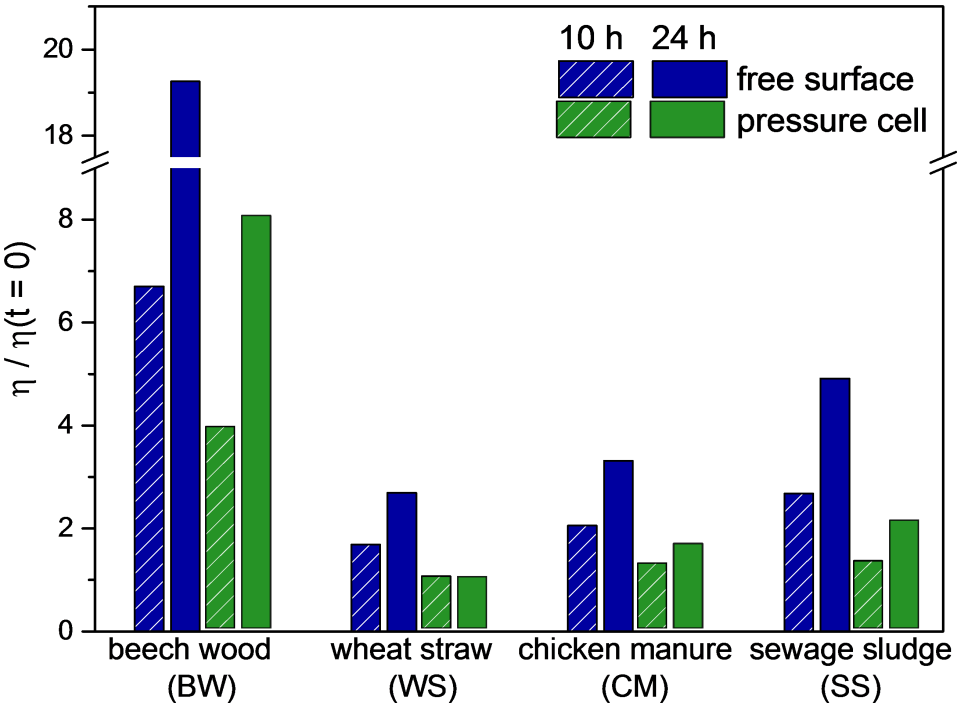

Figure 5.6: Viscosity data normalized to the respective initial value prior to aging $\eta(t = 0)$ for BW, WS, CM, and SS at 10 h (diagonal pattern) and 24 h (no pattern) for an open surface (blue) and pressure cell (green) at 80 °C with a constant shear rate of $\dot{\gamma} = 10\ s^{-1}$.

5.4.5 GC-MS and SEC analyses

Native and differently aged oils were analyzed with respect to their chemical composition using GC-MS and their molecular weight via SEC. A first qualitative analysis of the GC-MS results reveals an increase of the number and intensity of the peaks at the tail, above 50 min of retention time, comparing the aged samples to the native samples. Furfural, phenol, and guaiacol were measured quantitatively as markers of potentially ongoing reactions, with corresponding results shown in Figure 5.7.

The amount of phenol and guaiacol is much higher in the WS oil than in the BW oil. However, the furfural content in the BW oil is ~4 times that in the WS oil, but only a very small furfural content was detectable for the CM and SS oils as a result of their alkaline nature. The fraction of guaiacol in the oils from zoomass is substantially lower than in the oils from lignocellulosic feedstocks.

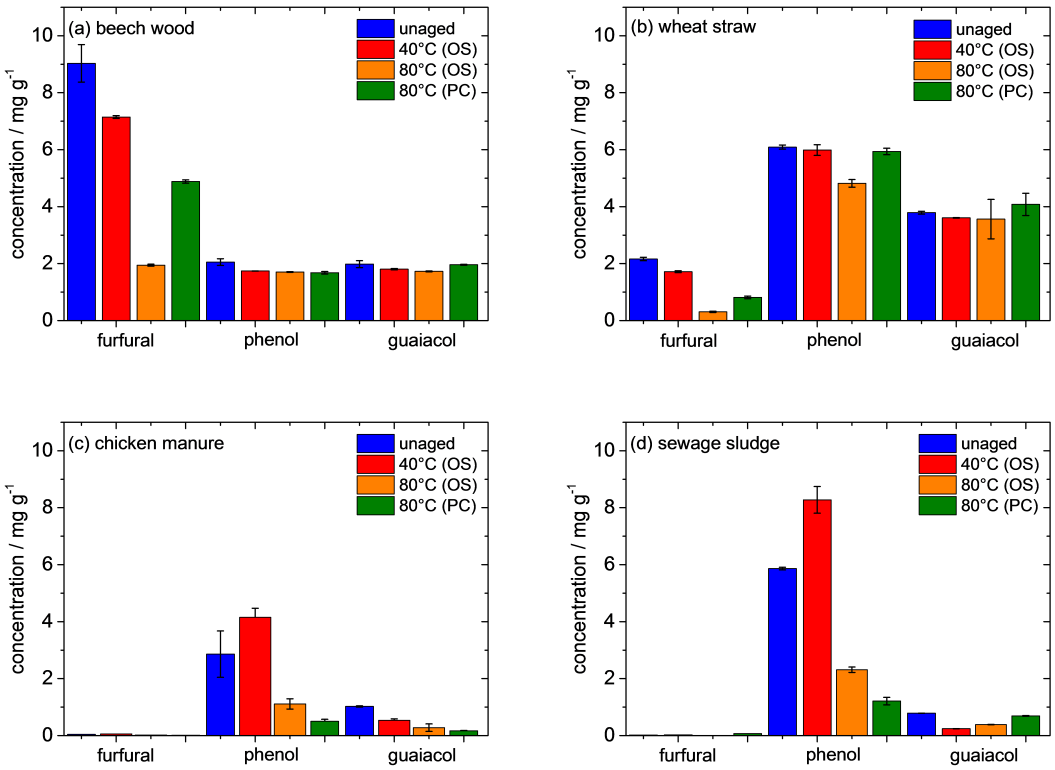

Figure 5.7: Concentration of furfural, phenol, and guaiacol in unaged (blue), open surface (OS) aged at 40 °C (red), OS aged at 80 °C (orange), and pressure cell (PC) aged at 80 °C (green) conditions of (a) BW, (b) WS, (c) CM, and (d) SS oils.

Aging at 40 °C has essentially no effect on the concentration of all three species in WS oil but leads to a slight reduction of these markers in BW oil. For the latter, aging at 80 °C results in a drastic drop of the concentration for furfural but onl in a slight decrease of phenol and guaiacol contents, regardless of whether an open surface or a sealed sample cell was used. Similarly, the concentration of these substances in WS oil drops when aged 80 °C in an open surface sample cell. However, the concentration of phenol and guaiacol in WS oil remains constant upon aging at 80 °C in the pressure cell; only the furfural conent semms to decrease under these conditions. This might be due to the systematic error resulting from the evaporation of the highly volatile substance during transfer of the sample from the pressure cell to the GC-MS device.
For the CM and SS oils, a rise of the phenol content during aging at 40 °C and a decrease during aging at 80 °C is found, which is more pronounced under an inert gas atmosphere

than for the open surface conditions. The origin of this phenomenon remains unresolved because the chemistry in the presence of nitrogen (ions) is complex [Diebold, 2000]. The guaiacol content of CM and SS oils is so small that a change of the relative content cannot be clarified considering the experimental uncertainty given here.

To confirm whether polymerization takes place during aging of these pyrolysis oils or not, SEC measurements were performed. An increase in the average molecular weight M_W from 190 to 240 Da is found for BW oil, indicating that the viscosity increase described above is partly due to polymerization, whereas no change in M_W is found for WS oil, which is in line with the viscosity data discussed above. For CM and SS oils, a weak increase in M_W (from 210 to 220 Da and from 190 to 200 Da, respectively) was found, indicating that polymerization may contribute to aging in these oils but to a lower extent than that in the BW oil.

Polymerization of BW oil may be due to furfural, which is presen in the sample (see Figure 5.7) and has a strong tendency to polymerize as a result of its carbonyl group [Hu et al., 2013]. Polymerization or self-condensation could also be induced by olefin side groups of all lignin compounds in the oil [Kim et al., 2012]. The increase in M_W for BW oil is in the same range as found for oak wood pyrolysis oil aged at 90 °C for 24 h [Nolte and Liberatore, 2011].

In summary, these results suggest that polymerization-induced aging occurs in CM and SS oils but is most pronounced in BW oil. No indication for polymerization contribution to aging is found for WS oil. However, evaporation contributes to the viscosity increase during aging for all investigated oils.

5.5 Conclusion

We have investigated the flow behavior of pyrolysis oils from four different feedstocks (BW, WS, SS, and CM) pyrolyzed at 350, 400, 450, and 500 °C using coaxial cylinder rotational rheometry. Additionally, aging experiments were conducted with a free surface sample cell at 40 and 80 °C as well as in a hermetically sealed pressure cell with an inert gas atmosphere at 80 °C; in all cases, a shear rate of $\dot{\gamma} = 10\ \mathrm{s}^{-1}$ was applied. With this setup, it was possible to distinguish between the influence of evaporation of organic volatiles or water and polymerization reactions on the viscosity increase during aging.

All investigated pyrolysis oils exhibit Newtonian flow behavior in the whole investigated temperature range between 20 and 80 °C, except for oil from WS, which exhibits strong shear thinning at temperatures of $T \leq 50$ °C. This latter behavior may be attributed to residual phenolic crystals or aggregates forming a sample-spanning network structure.

Oil from CM exhibits 3 times higher viscosity compared to the oils from BW, WS, and SS at temperatures of T > 50 °C.

The pyrolysis temperature has essentially no effect on viscosity and its temperature dependence, except for BW oil. The temperature dependence of viscosity follows Arrhenius' law and is solely determined by the flow activation energy E_A. This quantity is highest for CM oil and lowest for WS oil. When BW is used as feedstock, absolute viscosity and E_A values are highest if pyrolysis is performed at $T_{pyro} = 450$ °C, and this is presumably due to the low water content of the oil obtained at this temperature.

A substantial viscosity increase is observed during so-called accelerated aging experiments performed at 80 °C for BW and SS oil aging; i.e., an increase in viscosity is observed even during storage at 40 °C. This viscosity increase is most pronounced for BW oil and least for WS oil, and the viscosity increase for CM and SS oils is intermediate.

From a comparison of viscosity measurements performed using an open sample cell and a pressure cell providing an inert gas atmosphere, we conclude that aging of BW oil is mostly due to polymerization, whereas aging of WS oil is solely due to evaporation of volatiles. This is corroborated by GC-MS and SEC measurements. For CM and SS oils, both polymerization and evaporation contribute almost equally to the increase of viscosity when an open sample cell is used.

5.6 Supporting information

Flow curves of pyrolysis oils pyrolyzed at 450 °C

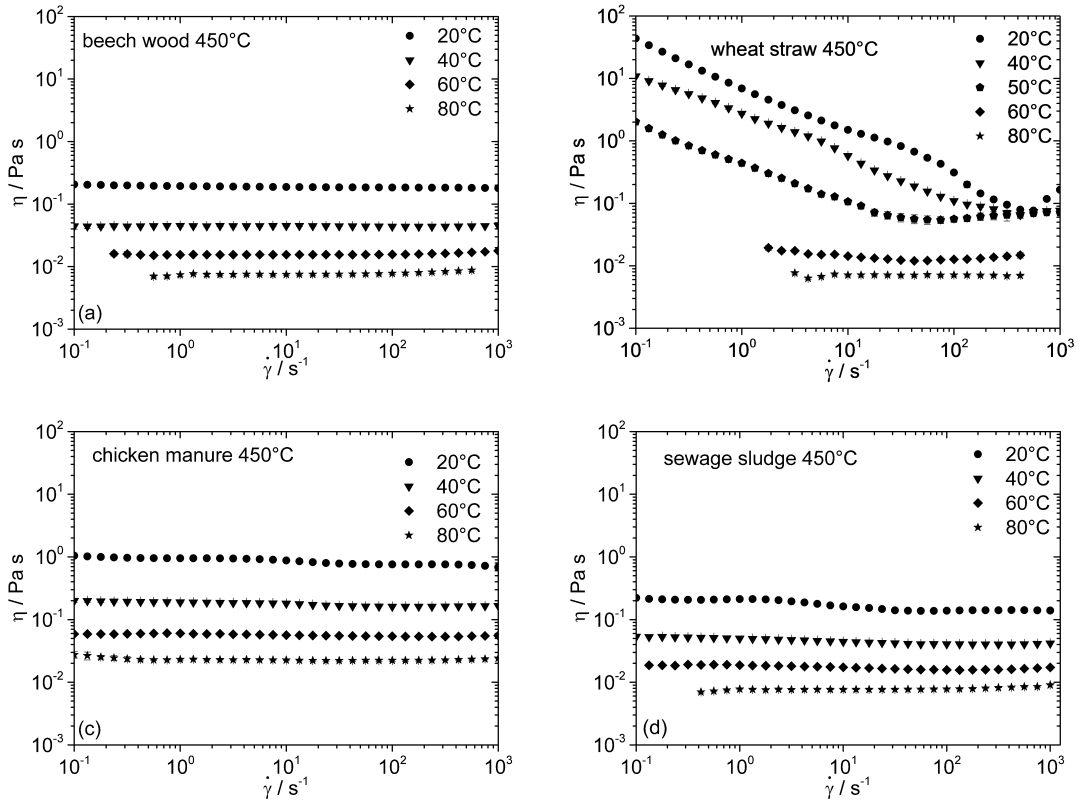

Figure 5.8: Flow curves of pyrolysis oils at 20 °C (circle), 40 °C (triangle), 60 °C (diamond) and 80 °C (star) of (a) beech wood (BW), (b) wheat straw (WS), (c) chicken manure (CM) and (d) sewage sludge (SS) pyrolyzed at a temperature of 450 °C. For WS an additional measurement at a temperature of 50 °C (pentagon) was performed.

Influence of pyrolysis properties on atomization

The aerodynamic Weber number (Eq. 5.2) is an important parameter in atomization relating surface and the inertia forces:

$$We_{aero} = exp\frac{\rho_{gas} v_{rel}^2 D_{liq}}{\Gamma} \tag{5.2}$$

Here ρ_{gas} represents the density of the gas, v_{rel} the relative velocity and D_{liq} the diameter of the undisturbed jet [Lefebvre, 1990]. The data presented above suggest the following conclusions: In twin-fluid atomization the spray droplet size is known to

decrease with decreasing viscosity [Ghezelchi et al., 2015] and accordingly the CM oil should yield the largest droplet size in this combustion process. The other oils exhibit very similar viscosities at T > 50 °C in these cases we expect smallest droplet size for the WS oil since it shows the lowest surface tension Γ (see Table 5.1) and hence the highest We-number.

Continuous viscosity measurements during aging

Open surface

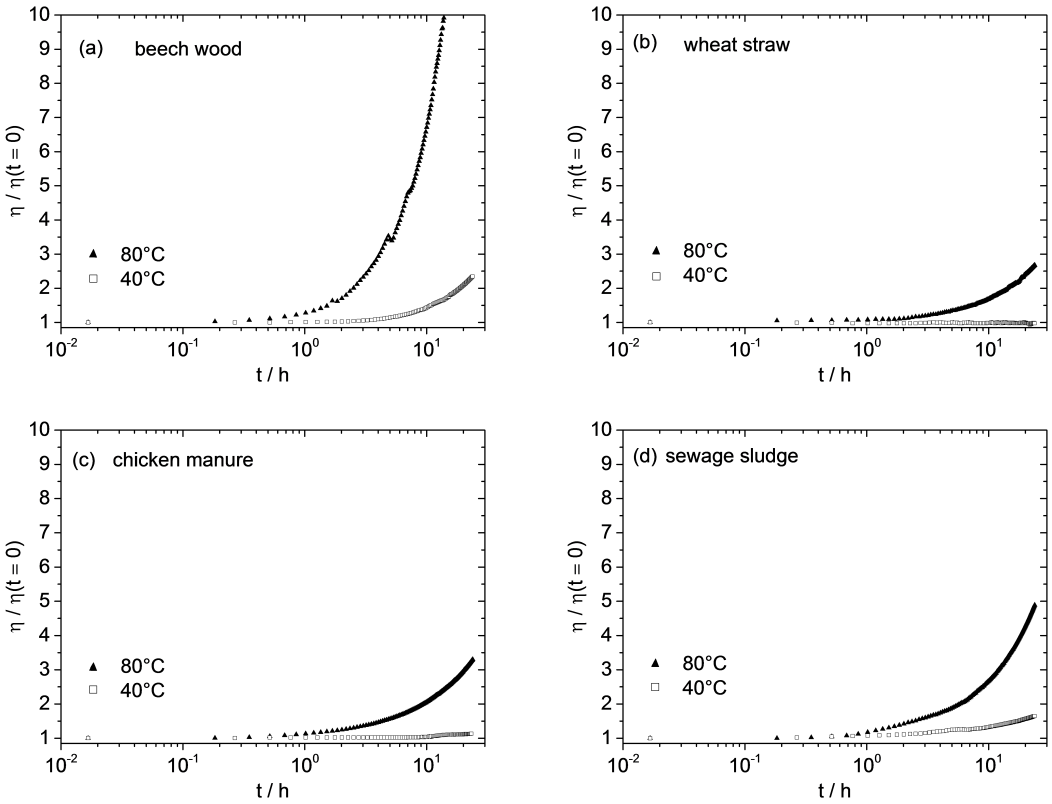

Figure 5.9: Viscosity as a function of time during aging at 40 °C (open square) and 80 °C (black triangle) for pyrolysis oils from: (a) BW, (b) WS, (c) CM and (d) SS, shear rate $\dot{\gamma} = 10\ s^{-1}$. Viscosity data are normalized to the respective initial value prior to aging $\eta(t = 0)$.

Inert gas atmosphere

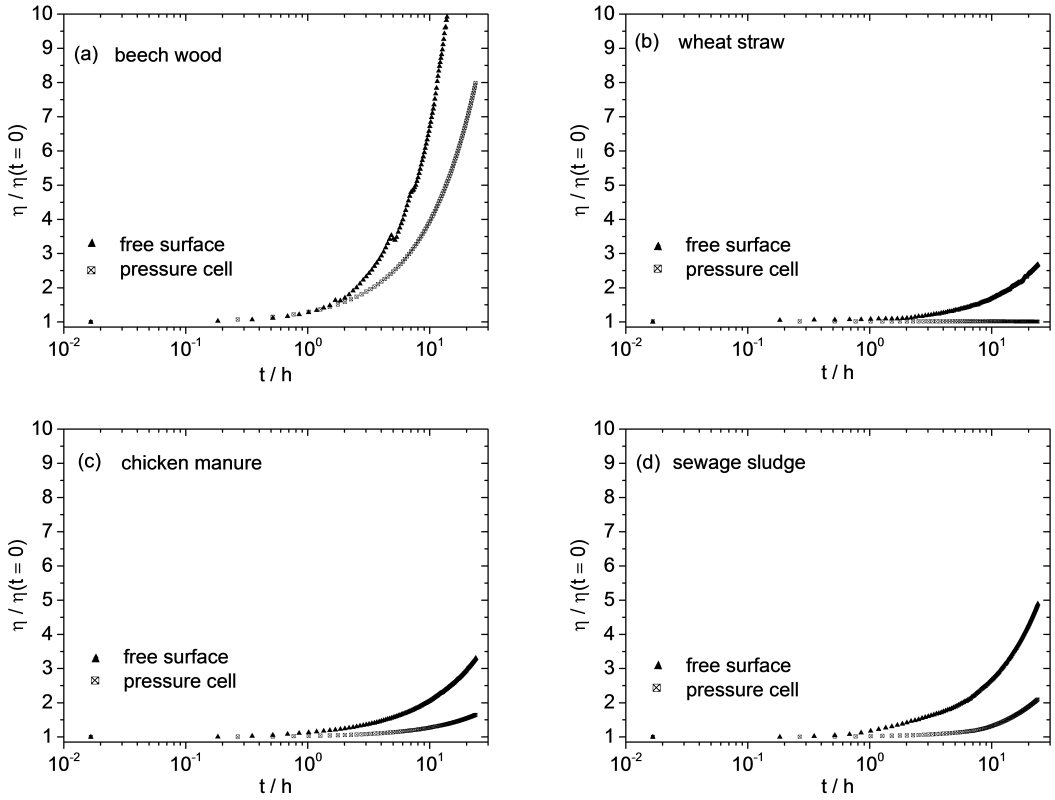

Figure 5.10: Normalized viscosity $\eta/\eta(t=0)$ measured at $\dot{\gamma} = 10\ s^{-1}$ and T = 80 °C as a function of time for (a) BW, (b) WS, (c) CM and (d) SS oil. The black triangle symbols correspond to the aging process with a free surface, while the open square symbols refer to the aging under inert gas (N_2) atmosphere (10 bar) in the pressure cell.

5.7 Acknowledgments

The authors thank the Helmholtz Association of German Research Centers (HGF) for partial funding of the work. Furthermore, the authors gratefully acknowledge Christoph Pfeifer from the Institute for Chemical Technology and Polymer Chemistry for performing the SEC measurements and Karim Abdel Aal for experimental support with rotational rheometry measurements. Additionally, the authors thank Tobias Jakobs for fruitful discussions.

6 Summary

This thesis used experimental studies on the flow and processing behavior of pyrolysis products within the so called bioliq®-process. New ways of characterizing and improving the processability have been demonstrated regarding the process relevant shear rates. The results are related to three topics:

1. Improvement of sedimentation stability and atomization properties of coke slurries made from wheat straw and beech wood while maintaining the pumpability.
2. Phenomenological description of flow behavior of coke water slurries in dependency of particle loading and shape.
3. Rheological characterization of flow behavior and aging of pyrolysis oils made from different feedstocks (beech wood, wheat straw, chicken manure and sewage sludge) produced at various temperatures (350, 400, 450 and 500°C).

A new concept to improve sedimentation stability and atomization of coke slurries used for biomass energy conversion was introduced. Water is used as a surrogate bulk-liquid for the coke slurries. This concept is based on the capillary suspension phenomenon: a small amount of an immiscible, secondary fluid is added to the suspension resulting in the formation of a sample spanning particle network controlled by capillary forces. This transition from a fluid-like state to a gel-structure is accompanied by a strong increase in low shear viscosity controlling sedimentation whereas the high shear viscosity, relevant for atomization, is nearly unaffected. Aqueous wheat straw and beech wood coke slurries (ϕ_m = 20 %) have been used as model systems and octanol-1 was added as secondary fluid (ϕ_{sf} = 0 - 3.1 vol.%) to demonstrate the concept. Visual inspection, centrifugation experiments as well as magnetic resonance imaging confirmed the drastically increased sedimentation stability, even after several days of storage no sedimentation could be detected. This offers new opportunities for storage and transport of such systems, e.g. storage and transport times can be increased, stirring of storage tanks is rendered unnecessary, i.e. process down times may be reduced and process efficiency increases. The effect of secondary fluid on atomization was investigated using an external mixing twin-fluid atomizer varying gas-liquid ratio (GLR) between 0.5 and 1.5 at a constant

mass liquid flow of 10 kg h^{-1}. Capillary suspensions were firstly prepared at pilot scale level with batch volumes of 40 l to perform these experiments. The utilized secondary fluid does not affect the higher heating value, for the entrained flow gasification in the bioliq®-process but it has a strong impact on the Sauter mean diameter (SMD) of the produced droplets and the resulting spray angle. Both quantities decrease by adding secondary fluid content. Qualitatively, the observed changes in atomization may be attributed to the remarkable reduction in surface tension induced by the added secondary fluid used here. The SMD reduction is stronger for wheat straw coke than for the beech wood coke and especially pronounced at low GLR. The spray angle decrease observed for both systems has to be taken into account by determining the reactor design. The findings suggest that the capillary suspension concept improves the gasifier performance and may lead to higher process variability and efficiency.

As it is possible to stabilize aqueous coke slurries and tailor the rheology in the low shear rate regime the influence of particle volume fraction, size distribution and shape on flow behavior of coke water slurries was investigated to tailor the viscosity in a large shear rate range. Therefore, two different coke feedstocks (wheat straw and beech wood) with similar initial mean particle diameter have been treated in a planetary ball mill. Both coke sorts exhibit an equal decrease in particle size with increasing milling time. Additionally, the wheat straw coke particles change their shape with increasing milling time, quantitatively evaluated by an increasing circularity. In contrast, the shape of the beech wood coke particles does not change. In both cases the particle porosity remains constant irrespective of milling time.
Slurries including those coke particles were prepared and rheologically characterized. For low mass, respectively volume fractions ($\phi_V \leq 20$ %), the suspensions behave like Newtonian fluids, while for higher particle loadings shear thinning behavior occurs. The shape of the corresponding viscosity over shear rate curves is mathematically well described by the Sisko model. For wheat straw coke slurries (WSCS) the viscosity at constant mass fraction decreases with increasing milling time of particles, which is attributed to the increased circularity. Accordingly, higher mass fraction of particles could be mixed into the slurry, at a selected viscosity level providing good processability. This corresponds to an increased energy density and thus HHV of the slurry. In contrast, the beech wood coke slurries (BWCS) exhibit similar viscosity functions independent of the milling time as their circularity distribution remains unaltered. Porosity and density of both coke feedstocks stay constant during milling and the particle size decreased in the same manner. Obviously, particle shape is the relevant parameter controlling the change in flow

behavior observed for WSCS.
The effect of particle shape on coke slurry viscosity was captured quantitatively using the model of Santamaria-Holek and Mendoza describing the dependence of relative viscosity on particle volume fraction. This model includes two parameters, namely the maximum packing fraction and the intrinsic viscosity. The former depends on the particle size distribution as well as on particle shape, whereas the latter is solely determined by particle shape. Accordingly, both parameters are strongly correlated and cannot be fitted simultaneously. Thus the maximum packing fraction was held constant and the intrinsic viscosity $[\eta]$ was determined from fitting the well-established phenomenological model to the experimental data. The intrinsic viscosity values obtained that way remained unchanged upon milling for beech wood coke while they decreased for wheat straw coke. This is in line with image analysis results revealing a constant circularity for beech wood coke and an increase of this shape parameter upon milling for wheat straw coke. Moreover, excellent agreement of absolute intrinsic viscosity values obtained from modelling the viscosity of concentrated suspensions and those directly obtained from dilute suspension viscometry was found. This consistent data analysis including three independent measurements justifies this simplified but robust approach suggested here for quantitatively modelling coke slurry viscosity.

Those investigations finally provide evidence that the flow behavior of coke water slurries can be tailored by changing particle shape. A viscosity reduction can be achieved by milling of wheat straw coke particles enabling a substantially increased particle loading, i.e. HHV at a viscosity level still providing good transport and gasification properties.

The third part of this thesis deals with the flow behavior of pyrolysis oils from four different feedstocks: Beech wood (BW), wheat straw (WS), chicken manure (CM) and sewage sludge (SS), pyrolyzed at 350, 400, 450 and 500°C. A rotational rheometer equipped with a coaxial cylinder geometry was used to characterize those oils rheologically. Additionally, aging experiments were conducted with a free surface sample cell at 40 and 80 °C as well as in a hermetically sealed pressure cell with an inert gas atmosphere at 80 °C; in all cases, a shear rate of $\dot{\gamma} = 10\ s^{-1}$ was applied. It was possible to distinguish between the influence of evaporation of organic volatiles or water and polymerization reactions on the viscosity increase during aging with this setup.
Newtonian flow behavior was observed in the whole investigated temperature range between 20 and 80 °C for all examined pyrolysis oils, except for oil from WS, which exhibits strong shear thinning at temperatures of $T \leq 50$ °C. This latter behavior may be at-

tributed to residual phenolic crystals or aggregates forming a sample-spanning network structure. Oil from CM exhibits three times higher viscosity compared to the oils from BW, WS, and SS at temperatures of T > 50 °C.

The pyrolysis temperature has essentially no effect on viscosity and its temperature dependence, except for BW oil. The temperature dependence of viscosity follows Arrhenius' law and is solely determined by the flow activation energy E_A. This quantity is highest for CM oil and lowest for WS oil. When BW is used as feedstock, absolute viscosity and E_A values are highest if pyrolysis is performed at a temperature of 450 °C, and this is presumably due to the low water content of the oil obtained at this temperature.

A substantial viscosity increase was observed during so-called accelerated aging experiments performed at 80 °C for BW and SS oil aging. Viscosity increased even during storage at 40 °C. This viscosity increase is most pronounced for BW oil and least for WS oil. CM and SS oils show an intermediate viscosity rise.

From a comparison of viscosity measurements performed using an open sample cell and a pressure cell providing an inert gas atmosphere, it can be concluded that aging of BW oil is mostly due to polymerization, whereas aging of WS oil is solely due to evaporation of volatiles. This is corroborated by GC-MS and SEC measurements. For CM and SS oils, both polymerization and evaporation contribute almost equally to the increase of viscosity when an open sample cell is used.

7 Outlook

Within the scope of this thesis plenty new aspects regarding the processing properties of biogenic suspensions and oils were investigated. Thereby, several new questions have opened up. Previously performed experiments revealed a strong increase in low shear viscosity after addition of a second, immiscible fluid into a carbonaceous suspension. Continuing investigations, which build on this topic, should examine a side effect, explicitly the decrease in surface tension, of this stabilization method. The impact of the surface tension drop on atomization has also to be further examined, as the mean droplet size is reduced at low GLR. Capillary suspensions with other stabilizing secondary fluids (e.g. octanoic acid or linolic acid) should be tested for their flow behavior as well as regarding their spraying properties. The effect of the orifice geometry should also be taken into account for the atomization of stabilized slurries and examined in subsequent work. As conventional elongational rheometry is failing for capillary suspensions a new concept of measuring the elongational rheological properties should be applied. Therefor, a hyperbolic flow channel might be implemented into a regular capillary rheometer resulting in an uniaxial elongation of the fluid. First approaches exhibited promising results, but further development, especially regarding the surface texture of those inlets, is necessary.

Another approach to optimize the process could be the use of low viscous pyrolysis oil as secondary fluid for creating a capillary suspension.

The particle shape has a strong impact on the flow behavior of coke water slurries. The effect of this parameter on forming of capillary bridges and the stabilizing effect could lead to new insights into the structure inside the fluid which adjusts after the addition of a secondary fluid. X-ray tomography (μCT) could deliver the required structural information, but a better contrast between porous coke particles and the surrounding fluid has to be achieved. Also fundamental knowledge about the relationship between particle shape, their spatial and orientational distribution in the suspension and flow properties are missing.

8 Kurzfassung

Die vorliegende Arbeit befasst sich mit der Rheologie von biogenen Suspensionen und Ölen. Hierbei wurden experimentelle Studien über das Fließ- und Verarbeitbarkeitsverhalten von Pyrolyseprodukten innerhalb des sogenannten bioliq®-Prozesses durchgeführt. Unter Berücksichtigung der prozessrelevanten Scherraten wurden hier neue Wege zur Charakterisierung und Verbesserung der Verarbeitbarkeit solcher Fluide aufgezeigt. Die Ergebnisse dieser Thesis sind in drei Themengebiete unterteilt:

1. Verbesserung der Sedimentationsstabilität und Zerstäubungseigenschaften von Koks-Wasser-Slurries hergestellt aus Weizenstroh und Buchenholz unter Berücksichtigung der Pumpbarkeit.
2. Phänomenologische Beschreibung des Fließverhaltens von Koks-Wasser-Slurries in Abhängigkeit von Partikelfüllgrad und -form.
3. Rheologische Charakterisierung des Fließverhaltens und der Alterung von Pyrolyseölen hergestellt aus verschiedenen Rohstoffen (Buchenholz, Weizenstroh, Hühnerdung und Klärschlamm) bei unterschiedlichen Temperaturen (350, 400, 450 and 500°C).

Ein neues Konzept zur Verbesserung der Sedimentationsstabilität und Zerstäubung von Koks-Wasser-Slurries für die Energieumwandlung von Biomasse, wie z.B. im bioliq®-Prozess, wurde vorgestellt. Dieses Konzept basiert auf dem Kapillarsuspensionsphänomen. Ein kleiner Anteil einer zweiten, unmischbaren Flüssigkeit wird dabei der Suspension zugegeben. So entsteht ein Netzwerk aus Flüssigkeitsbrücken zwischen den Partikeln, dass die gesamte Probe durchzieht und durch Kapillarkräfte kontrolliert wird. Der Übergang vom flüssigen Zustand zu einer gelartigen Struktur wird begleitet von einem starken Anstieg der sogenannten low shear Viskosität, die die Sedimentation kontrolliert, während die Viskosität bei hohen Scherraten, welche relevant für die Zerstäubung ist, nicht beeinflusst wird. Wässrige Weizenstroh- und Buchenholzkoks Slurries ($\phi_m = 20$ %) wurden als Modellsystem genutzt und Octanol-1 als Zweitfluid ($\phi_{sf} = 0$ - 3.1 vol.%) um dieses Konzept zu demonstrieren. Visuelle Inspektion, Zentrifugationsexperimente sowie bildgebende Magnetresonanztomographie bestätigen die drastisch verbesserte Sedimentationsstabilität. Sogar nach der Lagerung für mehrere Tage konnte keine Sedimentation

beobachtet werden. Dies bietet neue Möglichkeiten für den Transport und die Lagerung von solchen Systemen, z.B. können Transport- und Lagerzeiten verlängert werden, das Rühren der Tanks wird überflüssig, Verstopfung der Rohrleitungen und Düsen wird verhindert, d.h. Prozessstillstandszeiten könnten reduziert und die Prozesseffektivität erhöht werden. Der Einfluss von der Zweitflüssigkeit auf die Zerstäubung wurde unter der Verwendung eines außenmischenden Zweistoffzerstäubers am ITCvgt untersucht, wobei die Gas-Liquid-Ratio (GLR) zwischen 0.5 und 1.5 bei einem konstanten Massenflüssigkeitsstrom von 10 kg h^{-1} variiert wurde. Zum ersten Mal wurden Kapillarsuspensionen im Pilotmaßstab mit Batchvolumen von 40 l hergestellt, um diese Experimente durchführen zu können. Die eingesetzte Zweitphase hat keinen Einfluss auf den Brennwert für die Flugstromvergasung im bioliq®-Prozess, jedoch auf den mittleren Sauterdurchmesser (SMD) der gebildeten Tropfen und auf den resultierenden Spraywinkel. Beide Größen verringern sich durch die Zugabe der Zweitphase. Qualitativ können die hier beobachteten Änderungen bei der Zerstäubung der außergewöhnlichen Verringerung der Oberflächenspannung, hervorgerufen durch die Zugabe des hier verwendeten Zweitfluids, zugeschrieben werden. Die SMD Reduzierung ist für das Weizenstrohkoks stärker als für das Buchenholzkoks und besonders ausgeprägt bei niedrigen GLR. Die Abnahme des Spraywinkel, welche für beide Systeme beobachtet wurde, sollte bei der Reaktorkonstruktion mit berücksichtigt werden. Diese Erkenntnisse legen nahe, dass das Kapillarsuspensionskonzept die Vergasung verbessert und zu einer höheren Prozessvariabilität sowie -effizienz führt.

Da es möglich ist wässrige Koksslurries zu stabilisieren und die Rheologie im niedrigen Scherratenbereich maßzuschneidern, muss der Einfluss des Partikelvolumenfüllgrades, -größenverteilung und -form auf das Fließverhalten von Koks Wasser Slurries untersucht werden, um die Viskosität in einem großen Scherratenbereich gezielt einstellen zu können. Hierzu wurden zwei unterschiedliche Koksfraktionen (Weizenstroh und Buchenholz) mit gleichem mittleren Ausgangspartikeldurchmesser in einer Planetenkugelmühle gemahlen. Beide Kokssorten zeigen eine gleichgroße Abnahme in der Partikelgröße mit zunehmender Mahldauer. Zusätzlich ändern die Weizenstrohkokspartikel ihre Form mit ansteigender Mahldauer, die quantitativ an Hand der Zirkularität der Partikel charakterisiert wurde. Im Gegenzug bleibt die Form der Buchenholzkokspartikel gleich. In beiden Fällen bleibt die Porosität der Partikel konstant ungeachtet der Mahldauer.
Slurries wurden mit diesen Kokspartikeln hergestellt und rheologisch charakterisiert. Für niedrige Masse- bzw. Volumenfüllgrade ($\phi_V \leq 20$ %) verhalten sich die Suspensionen wie newtonische Fluide, während für höhere Partikelbeladungen scherverdünnendes

Fließverhalten auftritt. Der Verlauf der dazugehörigen Viskositätsfunktionen kann mathematisch mit dem Sisko Modell gut beschrieben werden. Für Weizenstrohkoksslurries (WSCS) reduziert sich die Viskosität bei konstantem Massenfüllgrad mit zunehmender Mahldauer der Partikel, was der zunehmenden Zirkularität zugeschrieben wird. Dementsprechend können höhere Partikelmassenanteile bei einem konstanten Viskositätsniveau in den Slurry gemischt werden bei einer gleichbleibend guten Verarbeitbarkeit. Dies ist einhergehend mit einer erhöhten Energiedichte und folglich einem verbesserten Slurry-Brennwert. Im Unterschied hierzu zeigen Buchenholzkoksslurries (BWCS) gleiche Viskositätsfunktionen unabhängig von der Mahldauer der Partikel, da deren Zirkularitätsverteilung unverändert bleibt. Porosität und Dichte der beiden Koksfraktionen bleiben konstant während der Mahlung und die Partikelgröße verringert sich auf die gleiche Weise. Offensichtlich ist die Partikelform der entscheidende Parameter, der die Änderung im Fließverhalten von WSCS herbeiführt.
Der Effekt der Partikelform auf die Koksslurryviskosität wurde quantitativ mittels dem Modell von Santamaria-Holek und Mendoza erfasst, welches die Abhängigkeit der relativen Viskosität vom Partikelvolumenfüllgrad beschreibt. Dieses Modell beinhaltet zwei Parameter, nämlich den maximalen Volumenfüllgrad und die intrinsische Viskosität. Der Erstere ist abhängig von der Partikelgrößenverteilung sowie von der Partikelform, während der Letztere ausschließlich durch die Partikelform bestimmt wird. Folglich stehen beide Parameter stark miteinander in Beziehung und können nicht simultan gefitted werden. Daher wurde die maximale Packungsdichte konstant gehalten und die intrinsische Viskosität $[\eta]$ wurde aus der Anpassung des etablierten phänomenologischen Modells an die experimentellen Daten bestimmt. Die Werte für die intrinsische Viskosität, die durch diese Methode ermittelt wurden, blieben unverändert für das Buchenholzkoks und nahmen für das Weizenstrohkoks ab. Dies ist einhergehend mit der Bildauswertung bei der eine konstante Zirkularität für Buchenholzkoks und ein Anstieg dieses Formparameters für Weizenstrohkoks ermittelt wurde. Ferner wurde eine exzellente Übereinstimmung der Absolutwerte der intrinsischen Viskosität aus der Modellierung der Viskosität von konzentrierten Suspensionen und der direkt gemessenen Werte aus viskosimetrischen Messungen verdünnter Suspensionen gefunden. Diese konsistente Datenanalyse beinhaltet drei voneinander unabhängige Messmethoden und rechtfertigt diese vereinfachte aber robuste Annahme der hier vorgeschlagenen Modellierung der Koksslurryviskosität.

Diese Untersuchungen liefern schließlich den Beleg, dass das Fließverhalten von Koks Wasser Slurries durch die Änderung der Partikelform maßgeschneidert werden kann. Eine Reduktion der Viskosität kann durch das Mahlen von Weizenstrohkokspartikeln

erreicht werden, welche eine wesentlich höhere Partikelbeladung, d.h. Brennwert, bei einem bestimmten Viskositätsniveau ermöglicht bei weiterhin guten Transport- und Vergasungseigenschaften.

Der dritte Teil dieser Thesis befasst sich mit dem Fließverhalten von Pyrolyseölen hergestellt aus vier verschiedenen Rohstoffen: Buchenholz (BW), Weizenstroh (WS), Hühnerdung (CM) und Klärschlamm (SS), pyrolisiert bei 350, 400, 450 und 500 °C. Ein Rotationsrheometer ausgestattet mit einer koaxialen Zylindergeometrie wurde benutzt um diese Öle rheologisch zu charakterisieren. Zusätzlich wurden Alterungsexperimente in einer Probenzelle mit freier Oberfläche bei 40 und 80 °C sowie in einer hermetisch abgedichteten Druckmesszelle unter einer Inertgasatmosphäre bei 80 °C durchgeführt, wobei in allen Fällen eine Scherrate von $\dot{\gamma} = 10\ s^{-1}$ beaufschlagt wurde. Durch dieses Setup war es möglich zwischen dem Einfluss der Evaporation von flüchtigen, organischen Stoffen oder Wasser und Polymerisationsreaktionen auf den Viskositätsanstieg während der Alterung zu differenzieren.
Newtonisches Fließverhalten wurde im gesamten Temperaturbereich zwischen 20 und 80 °C für alle untersuchten Pyrolyseöle beobachtet, bis auf das Öl aus WS, welches starke Scherverdünnung bei Temperaturen $\leq$ 50 °C aufzeigt. Dieses Verhalten könnte durch phenolische Kristalle oder Aggregate, die eine mögliche probendurchziehende Struktur bilden, hervorgerufen werden. Das Öl aus CM zeigt eine dreimal höhere Viskosität verglichen mit Ölen aus BW, WS und SS bei Temperaturen $>$ 50 °C.
Die Pyrolysetemperatur hat keinen wesentlichen Einfluss auf die Viskosität und deren Abhängigkeit von der Temperatur mit Ausnahme für das BW Öl. Die Temperaturabhängigkeit der Viskosität folgt den Gesetzmäßigkeiten von Arrhenius und ist ausschließlich festgelegt durch die Fließaktivierungsenergie E_A. Diese Quantität ist am höchsten für CM Öl und am niedrigsten für WS Öl. Wenn BW als Rohstoff eingesetzt wird, sind die Absolutwerte für die Viskosität und E_A am größten wenn die Pyrolyse bei einer Temperatur von 450 °C durchgeführt wird. Dies hängt vermutlich mit dem niedrigen Wassergehalts des Öls, welches bei dieses Temperatur erhalten wird, zusammen.
Ein beträchtlicher Viskositätsanstieg wird bei sogenannten beschleunigten Alterungsexperimenten, die bei 80 °C durchgeführt werden, für BW und SS Öl beobachtet. Sogar bei 40 °C findet ein Anstieg der Viskosität statt. Dieser Viskositätsanstieg ist am meisten für BW Öl und am wenigsten für WS Öl ausgeprägt. CM und SS Öl haben eine dazwischenliegende Viskositätserhöhung.
Aus einem Vergleich der Viskositätsmessungen in einer Probenzelle mit freier Oberfläche und einer Druckmesszelle unter einer Inertgasatmosphäre kann geschlossen werden, dass

Alterung von BW Öl hauptsächlich durch Polymerisation bestimmt ist, während Alterung von WS Öl ausschließlich durch die Evaporation von flüchtigen organischen Stoffen entsteht. Dies wird durch GC-MS und SEC Messungen bekräftigt. Für CM und SS Öle tragen sowohl Polymerisation als auch die Evaporation ungefähr gleich zur Viskositätserhöhung bei, wenn eine offene Probenzelle genutzt wird.

Bibliography

[Abadio et al., 2004] Abadio, F. D. B., Domingues, A. M., Borges, S. V., and Oliveira, V. M. (2004). Physical properties of powdered pineapple (Ananas comosus) juice - Effect of malt dextrin concentration and atomization speed. *Journal of Food Engineering*, 64(3):285–287.

[Aktas and Woodburn, 2000] Aktas, Z. and Woodburn, E. T. (2000). Effect of addition of surface active agent on the viscosity of a high concentration slurry of a low-rank British coal in water. *Fuel processing technology*, 62(1):1–15.

[Alonso et al., 2010] Alonso, D. M., Bond, J. Q., and Dumesic, J. A. (2010). Catalytic conversion of biomass to biofuels. *Green Chemistry*, 12:1493–1513.

[Alsbou and Helleur, 2014] Alsbou, E. and Helleur, B. (2014). Accelerated aging of bio-oil from fast pyrolysis of hardwood. *Energy and Fuels*, 28(5):3224–3235.

[Arienti and Soteriou, 2009] Arienti, M. and Soteriou, M. C. (2009). Time-resolved proper orthogonal decomposition of liquid jet dynamics. *Physics of Fluids*, 21(112104):1 – 15.

[Ashgriz, 2011] Ashgriz, N. (2011). *Handbook of atomization and sprays: theory and applications*. Springer Science & Business Media.

[Baldwin and Feik, 2013] Baldwin, R. M. and Feik, C. J. (2013). Bio-oil stabilization and upgrading by hot gas filtration. *Energy and Fuels*, 27(6):3224–3238.

[Barnes, 1981] Barnes, H. A. (1981). Dispersion rheology: 1980. *Royal Soc. Of Chem., Industrial Division, London*.

[Barnes et al., 1989] Barnes, H. A., Hutton, J. F., and Walters, K. (1989). *An Introduction to Rheology*. Elsevier, Amsterdam.

[Basu, 2013] Basu, P. (2013). *Biomass Gasification, Pyrolysis and Torrefaction*. Elsevier Inc., London, 2nd edition.

[Batchelor, 1977] Batchelor, G. (1977). The effect of brownian motion on the bulk stress in a suspension of spherical particles. *Journal of fluid mechanics*, 83(01):97–117.

[Batts and Fathoni, 1991] Batts, B. D. and Fathoni, A. (1991). A Literature Review on Fuel Stability Studies with Particular Emphasis on Diesel Oil. *Energy & Fuels*, 5(7):2–21.

[Bayvel and Orzechowski, 1993] Bayvel, L. and Orzechowski, Z. (1993). *Liquid Atomization*. Taylor & Francis, Washington, DC.

[Bhoi et al., 2016] Bhoi, S., Banerjee, T., and Mohanty, K. (2016). Beneficiation of Indian coals using Ionic Liquids. *Fuel Processing Technology*, 151:1–10.

[Bingham, 1917] Bingham, E. C. (1917). *An investigation of the laws of plastic flow*. Number 278. US Government Printing Office.

[Bioliq, 2017] Bioliq (2017). High Pressure Entrained Flow Gasification (bioliq).

[Bitsch et al., 2014] Bitsch, B., Dittmann, J., Schmitt, M., Scharfer, P., Schabel, W., and Willenbacher, N. (2014). A novel slurry concept for the fabrication of lithium-ion battery electrodes with beneficial properties. *Journal of Power Sources*, 265:81–90.

[Bossler and Koos, 2016] Bossler, F. and Koos, E. (2016). Structure of Particle Networks in Capillary Suspensions with Wetting and Nonwetting Fluids. *Langmuir*, 32(6):1489–1501.

[Boylu et al., 2004] Boylu, F., Dinçer, H., and Atesok, G. (2004). Effect of coal particle size distribution, volume fraction and rank on the rheology of coal-water slurries. *Fuel Processing Technology*, 85(4):241–250.

[Brenner, 1974] Brenner, H. (1974). Rheology of a dilute suspension of axisymmetric Brownian particles. *International Journal of Multiphase Flow*, 1(2):195–341.

[Bridgwater, 1999] Bridgwater, A. V. (1999). An introduction to fast pyrolysis of biomass for fuels and chemicals. In *Fast Pyrolysis of Biomass: A Handbook*, volume 1, pages 1–13. CPL Scientific Publishing Services.

[Bridgwater, 2001] Bridgwater, A. V. (2001). *Progress in Thermochemical Biomass Conversion*. Blackwell Science Ltd., London.

[Bridgwater and Peacocke, 2000] Bridgwater, A. V. and Peacocke, G. V. C. (2000). Fast pyrolysis processes for biomass. *Renewable & sustainable energy reviews*, 4(1):1–73.

[Brown et al., 2000] Brown, A. B. D., Clarke, S. M., Convert, P., and Rennie, A. R. (2000). Orientational order in concentrated dispersions of plate-like kaolinite particles under shear. *J. Rheol.*, 44(2):221–233.

[Case et al., 2014] Case, P. A., Wheeler, M. C., and Desisto, W. J. (2014). Effect of residence time and hot gas filtration on the physical and chemical properties of pyrolysis oil. *Energy and Fuels*, 28(6):3964–3969.

[Chaala et al., 2004] Chaala, A., Ba, T., Garcia-Perez, M., and Roy, C. (2004). Colloidal Properties of Bio-oils Obtained by Vacuum Pyrolysis of Softwood Bark: Aging and Thermal Stabiligy. *Energy & Fuels*, 18(3):1535–1542.

[Chen et al., 2011a] Chen, R., Wilson, M., Leong, Y. K., Bryant, P., Yang, H., and Zhang, D. K. (2011a). Preparation and rheology of biochar, lignite char and coal slurry fuels. *Fuel*, 90(4):1689–1695.

[Chen et al., 2011b] Chen, T., Wu, C., Liu, R., Fei, W., and Liu, S. (2011b). Effect of hot vapor filtration on the characterization of bio-oil from rice husks with fast pyrolysis in a fluidized-bed reactor. *Bioresource Technology*, 102(10):6178–6185.

[Coulson et al., 1999] Coulson, J. M., Richardson, J. F., Backhurst, J. R., and Harker, J. H. (1999). *Chemical Engineering Volume 1: Fluid flow, heat transfer and mass transfer*. Butterworth-Heinemann.

[Dahmen et al., 2016] Dahmen, N., Abeln, J., Eberhard, M., Kolb, T., Leibold, H., Sauer, J., Stapf, D., and Zimmerlin, B. (2016). The bioliq process for producing synthetic transportation fuels. *Wiley Interdisciplinary Reviews: Energy and Environment*.

[Dahmen et al., 2015] Dahmen, N., Arnold, U., Djordjevic, N., Henrich, T., Kolb, T., Leibold, H., and Sauer, J. (2015). High pressure in synthetic fuels production. *The Journal of Supercritical Fluids*, 96:124–132.

[Dahmen et al., 2012] Dahmen, N., Henrich, E., Dinjus, E., and Weirich, F. (2012). The bioliq bioslurry gasification process for the production of biosynfuels, organic chemicals, and energy. *Energy, Sustainability and Society*, 2(1):3.

[Diebold, 2000] Diebold, J. (2000). A Review of the Chemical and Physical Mechanisms of the Storage Stability of Fast Pyrolysis Bio-Oils. *NREL Report*, (January):59.

[Diebold and Czernik, 1997] Diebold, J. P. and Czernik, S. (1997). Additives To Lower and Stabilize the Viscosity of Pyrolysis Oils during Storage. *Energy Fuels*, 11(10):1081–1091.

[Dinçer et al., 2003] Dinçer, H., Boylu, F., Sirkeci, a. a., and Ate?ok, G. (2003). The effect of chemicals on the viscosity and stability of coal water slurries. *International Journal of Mineral Processing*, 70(1-4):41–51.

[Dittmann et al., 2013] Dittmann, J., Koos, E., and Willenbacher, N. (2013). Ceramic capillary suspensions: Novel processing route for macroporous ceramic materials. *Journal of the American Ceramic Society*, 96(2):391–397.

[Dittmann et al., 2016] Dittmann, J., Maurath, J., Bitsch, B., and Willenbacher, N. (2016). Highly Porous Materials with Unique Mechanical Properties from Smart Capillary Suspensions. *Advanced Materials*, 28(8):1689–1696.

[Domenech and Velankar, 2014] Domenech, T. and Velankar, S. (2014). Capillary-driven percolating networks in ternary blends of immiscible polymers and silica particles. *Rheologica Acta*, 53(8):593–605.

[Donev et al., 2004] Donev, A., Cisse, I., Sachs, D., Variano, E. a., Stillinger, F. H., Connelly, R., Torquato, S., and Chaikin, P. M. (2004). Improving the density of jammed disordered packings using ellipsoids. *Science (New York, N.Y.)*, 303(5660):990–993.

[Eilers, 1943] Eilers, H. (1943). Die Viskositäts-Konzentrationsabhängigkeit kolloider Systeme in organischen Lösungsmitteln. *Kolloid Zeitschrift*, 102(2):154 – 169.

[Einstein, 1906] Einstein, A. (1906). Eine neue Bestimmung der Moleküldimensionen. *Annalen der Physik*, 324(2):289–306.

[Einstein, 1911] Einstein, A. (1911). Berichtigung zu meiner Arbeit: Eine neue Bestimmung der Moleküldimensionen. *Annalen der Physik*, 339(3):591–592.

[Farris, 1968] Farris, R. J. (1968). Prediction of the Viscosity of Multimodal Suspensions from Unimodal Viscosity Data. *Journal of Rheology*, 12(2):281.

[Fisk et al., 2009] Fisk, C. A., Morgan, T., Ji, Y., Crocker, M., Crofcheck, C., and Lewis, S. A. (2009). Bio-oil upgrading over platinum catalysts using in situ generated hydrogen. *Applied Catalysis A: General*, 358(2):150–156.

[Gao et al., 2016] Gao, W., Zhang, M., and Wu, H. (2016). Fuel properties and ageing of bioslurry prepared from glycerol/methanol/bio-oil blend and biochar. *Fuel*, 176:72–77.

[Ghezelchi et al., 2015] Ghezelchi, M. H., Garcia-Perez, M., and Wu, H. (2015). Bioslurry as a Fuel. 7: Spray Characteristics of Bio-Oil and Bioslurry via Impact and Twin-Fluid Atomizers. *Energy and Fuels*, 29(12):8058–8065.

[Giesekus, 1983] Giesekus, H. (1983). Disperse systems: dependence of rheological properties on the type of flow with implications for food rheology. In Jowitt, R., editor, *Physical Properties of Foods*, chapter 13, pages 205 – 220.

[Glasstone et al., 1941] Glasstone, S., Laidler, K. J., and Eyring, H. (1941). *The Theory of Rate Processes*. McGraw-Hill, New York.

[Günther, 1984] Günther, R. (1984). *Verbrennung und Feuerung*. Springer, Berlin.

[Haber and Brenner, 1984] Haber, S. and Brenner, H. (1984). Rheological properties of dilute suspensions of centrally symmetric Brownian particles at small shear rates. *Journal of Colloid and Interface Science*, 97:496–514.

[Hamaker, 1937] Hamaker, H. (1937). The London van der Waals attraction between spherical particles. *Physica*, 4(10):1058–1072.

[Hashimoto, 1999] Hashimoto, N. (1999). CWM: Its Past, Present and Future. *Coal Preparation*, 21(1):3–22.

[He et al., 2011] He, Q., Wang, R., Wang, W., Xu, R., and Hu, B. (2011). Effect of particle size distribution of petroleum coke on the properties of petroleum coke-oil slurry. *Fuel*, 90(9):2896–2901.

[Henrich et al., 2015] Henrich, E., Dahmen, N., Dinjus, E., and Sauer, J. (2015). The role of biomass in a future world without fossil fuels. *Chemie-Ingenieur-Technik*, 87(12):1667–1685.

[Hergert and Wriedt, 2012] Hergert, W. and Wriedt, T. (2012). *The Mie Theory*. Springer, Berlin.

[Higman and Burgt, 2003] Higman, C. and Burgt, M. V. D. (2003). *Gasification*. Elsevier, Amsterdam, 2nd edition.

[Hochman et al., 2010] Hochman, B. G., Rajagopal, D., and Zilberman, D. (2010). American Economic Association Are Biofuels the Culprit ? OPEC, Food, and Fuel. *The American Economic Review*, 100(2):183–187.

[Hoffmann et al., 2014] Hoffmann, S., Koos, E., and Willenbacher, N. (2014). Using capillary bridges to tune stability and flow behavior of food suspensions. *Food Hydrocolloids*, 40:44–52.

[Hogan, 1997] Hogan, E. (1997). Bioenergy development program–thermochemical conversion. In *Fuel and Energy Abstracts*, volume 38, pages 163–163. Elsevier.

[Hu et al., 2013] Hu, X., Wang, Y., Mourant, D., Gunawan, R., Lievens, C., Chaiwat, W., Gholizadeh, M., Wu, L., Li, X., and Li, C.-Z. (2013). Polymerization on Heating up of Bio-Oil: A Model Compund Study. *AIChE Journal*, 59(3):888–900.

[Iglesias Gonzalez et al., 2011] Iglesias Gonzalez, M., Kraushaar-Czarnetzki, B., and Schaub, G. (2011). Process comparison of biomass-to-liquid (BtL) routes Fischer-Tropsch synthesis and methanol to gasoline. *Biomass Conversion and Biorefinery*, 1(4):229–243.

[Im et al., 2004] Im, K.-S., Lai, M.-C., and Yu, S.-T. J. (2004). Simulation of Spray Transfer Processes in Electrostatic Rotary Bell Sprayer. *Journal of Fluids Engineering*, 126(3):449–456.

[Jakobs et al., 2015] Jakobs, T., Djordjevic, N., Sanger, A., Zarzalis, N., and Kolb, T. (2015). Influence of Reactor Pressure on Twin-Fluid Atomization: Basic Investigations on Burner Design for High-Pressure Entrained Flow Gasifier. *Atomization and Sprays*, 25(12):1081–1105.

[Jampolski et al., 2017a] Jampolski, L., Jakobs, T., Kolb, T., and Willenbacher, N. (2017a). Coke slurries with improved higher heating value and good processability via particle shape design. *Chemical Engineering & Technology*.

[Jampolski et al., 2017b] Jampolski, L., Morgano, M. T., Seifert, H., Kolb, T., and Willenbacher, N. (2017b). Flow Behavior and Aging of Pyrolysis Oils from Di ff erent Feedstocks. *Energy & Fuels*, 31(5):5165–5173.

[Jampolski et al., 2016] Jampolski, L., Sänger, A., Jakobs, T., Guthausen, G., Kolb, T., and Willenbacher, N. (2016). Improving the processability of coke water slurries for entrained flow gasification. *Fuel*, 185:102–111.

[Jeffery, 1922] Jeffery, G. (1922). The Motion of Ellipsoidal Particles Immersed in a Viscous Fluid. *Proceedings of the Royal Society A*, 102:161–179.

[Jiang and Ellis, 2010] Jiang, X. and Ellis, N. (2010). Upgrading bio-oil through emulsification with biodiesel: Thermal stability. *Energy and Fuels*, 24(4):2699–2706.

[Junming et al., 2008] Junming, X., Jianchun, J., Yunjuan, S., and Yanju, L. (2008). Bio-oil upgrading by means of ethyl ester production in reactive distillation to remove water and to improve storage and fuel characteristics. *Biomass and Bioenergy*, 32(11):1056–1061.

[Kaltschmitt et al., 2009] Kaltschmitt, M., Hartmann, H., and Hofbauer, H. (2009). *Energie aus Biomasse - Grundlagen, Technik und Verfahren*. Springer, Heidelberg Dordrecht London NewYork, 2nd editio edition.

[Kapur et al., 1985] Kapur, J., Sahoo, P., and Wong, A. (1985). A new method for gray-level picture thresholding using the entropy of the histogram. *Computer Vision, Graphics, and Image Processing*, 29(1):140.

[Kim et al., 2012] Kim, T. S., Kim, J. Y., Kim, K. H., Lee, S., Choi, D., Choi, I. G., and Choi, J. W. (2012). The effect of storage duration on bio-oil properties. *Journal of Analytical and Applied Pyrolysis*, 95:118–125.

[Koike et al., 2016] Koike, N., Hosokai, S., Takagaki, A., Nishimura, S., Kikuchi, R., Ebitani, K., Suzuki, Y., and Oyama, S. T. (2016). Upgrading of pyrolysis bio-oil using nickel phosphide catalysts. *Journal of Catalysis*, 333:115–126.

[Koos, 2014] Koos, E. (2014). Capillary suspensions: Particle networks formed through the capillary force. *Current Opinion in Colloid and Interface Science*, 19(6):575–584.

[Koos et al., 2012] Koos, E., Johannsmeier, J., Schwebler, L., and Willenbacher, N. (2012). Tuning suspension rheology using capillary forces. *Soft Matter*, 8(24):6620.

[Koos and Willenbacher, 2011] Koos, E. and Willenbacher, N. (2011). Capillary forces in suspension rheology. *Science (New York, N.Y.)*, 331(6019):897–900.

[Krieger and Dougherty, 1959] Krieger, I. M. and Dougherty, T. J. (1959). A Mechanism for Non-Newtonian Flow in Suspensions of Rigid Spheres. *Transactions of the Society of Rheology*, 3:137 – 152.

[Kufferath et al., 1999] Kufferath, A., Wende, B., and Leuckel, W. (1999). Influence of liquid flow conditions on spray characteristics of internal-mixing twin-fluid atomizers. *International Journal of Heat and Fluid Flow*, 20:513–519.

[Lefebvre, 1990] Lefebvre, A. H. (1990). *Atomization and Sprays*, volume 45.

[Lefebvre, 2006] Lefebvre, A. H. (2006). *Atomization*. Begellhouse.

[Lin, 2003] Lin, S. (2003). *Breakup of Liquid Sheets and Jets*. Cambridge University Press, Cambridge.

[Lowell and Shields, 1991] Lowell, S. and Shields, J. E. (1991). *Powder surface area and porosity*. Chapman and Hall, London, 3rd edition.

[Mansour and Chigier, 1995] Mansour, A. and Chigier, N. (1995). Air-blast atomization of non-Newtonian liquids. *Journal of Non-Newtonian Fluid Mechanics*, 58(2-3):161–194.

[Maron and Pierce, 1956] Maron, S. H. and Pierce, P. E. (1956). Application of ree-eyring generalized flow theory to suspensions of spherical particles. *Journal of colloid science*, 11(1):80–95.

[Matas and Cartellier, 2013] Matas, J.-P. and Cartellier, A. (2013). Flapping instability of a liquid jet. *Comptes Rendus Mécanique*, 341(1-2):35–43.

[Maurath et al., 2015] Maurath, J., Dittmann, J., Schultz, N., and Willenbacher, N. (2015). Fabrication of highly porous glass filters using capillary suspension processing. *Separation and Purification Technology*, 149:470–478.

[Metzner, 1985] Metzner, A. B. (1985). Rheology of Suspensions in Polymeric Liquids. *Journal of Rheology*, 29(6):739.

[Nawab and Mason, 1958] Nawab, M. A. and Mason, S. G. (1958). The Viscosity of Dilute Suspensions of Thread-like Particles. *The Journal of Physical Chemistry*, 62(10):1248–1253.

[Nicoleit et al., 2016] Nicoleit, T., Dahmen, N., and Sauer, J. (2016). Production and Storage of Gasifiable Slurries Based on Flash-Pyrolyzed Straw. *Energy Technology*, 4(1):221–229.

[Nolte and Liberatore, 2010] Nolte, M. W. and Liberatore, M. W. (2010). Viscosity of biomass pyrolysis oils from various feedstocks. *Energy and Fuels*, 24(12):6601–6608.

[Nolte and Liberatore, 2011] Nolte, M. W. and Liberatore, M. W. (2011). Real-Time Viscosity Measurements during the Accelerated Aging of Biomass Pyrolysis Oil. *Energy & Fuels*, 25(7):3314–3317.

[Oasmaa et al., 2016] Oasmaa, A., Fonts, I., Pelaez-Samaniego, M. R., Garcia-Perez, M. E., and Garcia-Perez, M. (2016). Pyrolysis Oil Multiphase Behavior and Phase Stability: A Review. *Energy and Fuels*, 30(8):6179–6200.

[Oasmaa and Peacocke, 2001] Oasmaa, A. and Peacocke, C. (2001). A guide to physical property characterisation of biomass-derived fast pyrolysis liquids. *VTT Publications*, (450):2–65.

[Oasmaa, A., Kuoppala, 2003] Oasmaa, A., Kuoppala, E. (2003). Fast pyrolysis of forestry residue: Storage stability of liquid fuel. *Energy Fuel*, (17):1075–1084.

[Oh et al., 2016] Oh, S., Shin, D.-j., Choi, H. S., and Choi, J. W. (2016). Storage performance of bio-oil after hydrodeoxygenative upgrading with noble metal catalysts. *Fuel*, 182:1–11.

[Olson, 2011] Olson, E. (2011). Particle shape factors and their use in image analysis-part 1: Theory. *Journal of GXP Compliance*, 15(3):85–96.

[Ortega et al., 2011] Ortega, J. V., Renehan, A. M., Liberatore, M. W., and Herring, A. M. (2011). Physical and chemical characteristics of aging pyrolysis oils produced from hardwood and softwood feedstocks. *Journal of Analytical and Applied Pyrolysis*, 91(1):190–198.

[Pabst et al., 2006] Pabst, W., Gregorová, E., and Berthold, C. (2006). Particle shape and suspension rheology of short-fiber systems. *Journal of the European Ceramic Society*, 26(1-2):149–160.

[Papachristodoulou and Trass, 1984] Papachristodoulou, G. and Trass, O. (1984). Rheological Properties of Coal-Oil Mixture Fuels. *Powder Technology*, 40(1 - 3):353 – 362.

[Patel, 2006] Patel, M. R. (2006). *Wind and Solar Power Systems: Design, Analysis, and Operation*. Taylor & Francis, New York, 2nd editio edition.

[Pawlik, 2005] Pawlik, M. (2005). Polymeric dispersants for coal-water slurries. *Colloids and Surfaces A: Physicochemical and Engineering Aspects*, 266(1-3):82–90.

[Pawlik et al., 1997] Pawlik, M., Laskowski, J. S., and Liu, H. (1997). Effect of Humic Acids and Coal Surface Properties on Rheology of Coal-Water Slurries. *Coal Preparation*, 18(3-4):129–149.

[Pfitzer et al., 2016] Pfitzer, C., Dahmen, N., Troger, N., Weirich, F., Sauer, J., Gunther, A., and Muller-Hagedorn, M. (2016). Fast pyrolysis of wheat straw in the bioliq pilot plant. *Energy & Fuels*, 30(10):8047–8054.

[Pietsch and Rumpf, 1967] Pietsch, W. and Rumpf, H. (1967). Haftkraft, Kapillardruck, Flüssigkeitsvolumen und Grenzwinkel einer Flüssigkeitsbrücke zwischen zwei Kugeln. *Chemie Ingenieur Technik*, 39(15):885–893.

[Pollack and Cuzzi, 1980] Pollack, J. B. and Cuzzi, J. N. (1980). Scattering by Nonspherical Particles of Size Comparable to a Wavelength: A New Semi-Empirical Theory and Its Application to Tropospheric Aerosols. *Journal of the Atmospheric Sciences*, 37(4):868–881.

[Rallison, 1978] Rallison, J. M. (1978). The effects of Brownian rotations in a dilute suspension of rigid particles of arbitrary shape. *Journal of Fluid Mechanics*, 84(02):237–263.

[Rayleigh, 1878] Rayleigh, L. (1878). On the instability of jets. *Proceedings of the London mathematical society*, 1(1):4–13.

[Raynal et al., 1997] Raynal, L., Villermaux, E., Lasheras, J., and Hopfinger, E. (1997). Primary instability in liquid gas shear layers. *11th International Symposium on Turbulent Shear Flows*, 3:271 – 275.

[Reitz, 1978] Reitz, R. D. (1978). Atomization and other breakup regimes of a liquid jet.

[Rizkalla and Lefebvre, 1975] Rizkalla, A. A. and Lefebvre, A. H. (1975). Influence of Liquid Properties on Airblast Atomizer Spray Characteristics. *Journal of Engineering for Power*, 97(2):173.

[Roh et al., 1995] Roh, N.-S., Shin, D.-H., Kim, D.-C., and Kim, J.-D. (1995). Rheological mixtures behaviour of coal-water mixtures: 1. Effects of coal type, loading and particle size. *Fuel*, 74(8):1220–1225.

[Rubio-Hernández et al., 2006] Rubio-Hernández, F. J., Ayúcar-Rubio, M. F., Velázquez-Navarro, J. F., and Galindo-Rosales, F. J. (2006). Intrinsic viscosity of SiO2, Al2O3 and TiO2 aqueous suspensions. *Journal of Colloid and Interface Science*, 298(2):967–972.

[Sänger et al., 2014] Sänger, A., Jakobs, T., Djordjevic, N., and Kolb, T. (2014). Effect of primary instability of a high viscous liquid jet on the spray quality generated by a twin-fluid atomizer. *ILASS Europe, 26th Annual Conference on Liquid Atomization and Spray Systems*.

[Santamaría-Holek and Mendoza, 2010] Santamaría-Holek, I. and Mendoza, C. I. (2010). The rheology of concentrated suspensions of arbitrarily-shaped particles. *Journal of Colloid and Interface Science*, 346(1):118–126.

[Santo et al., 2006] Santo, U., Seifert, H., Kolb, T., Wiemer, H., Krebs, L., Pantouflas, E., and Zarzalis, N. (2006). Conversion of biomass based slurry in an entrained flow gasifier–characterisation of combustion behaviour. In *7th European Conference on Industrial Furnaces and Boilers (INFUB), Porto, Portugal*.

[Schneider et al., 2016] Schneider, M., Koos, E., and Willenbacher, N. (2016). Highly conductive, printable pastes from capillary suspensions. *Scientific Reports*, 6(August):31367.

[Scholze and Meier, 2001] Scholze, B. and Meier, D. (2001). Characterization of the water-insoluble fraction from pyrolysis oil (pyrolytic lignin). Part I. PY-GC/MS, FTIR, and functional groups. *Journal of Analytical and Applied Pyrolysis*, 60(1):41–54.

[Schubert, 1984] Schubert, H. (1984). Capillary forces-modeling and application in particulate technology. *Powder Technology*, 37(1):105–116.

[Servais et al., 2002] Servais, C., Jones, R., and Roberts, I. (2002). The influence of particle size distribution on the processing of food. *Journal of Food Engineering*, 51(3):201–208.

[Shin and Shen, 2007] Shin, Y. J. and Shen, Y. H. (2007). Preparation of coal slurry with organic solvents. *Chemosphere*, 68(2):389–393.

[Shivaram et al., 2013] Shivaram, P., Leong, Y. K., Yang, H., and Zhang, D. K. (2013). Flow and yield stress behaviour of ultrafine Mallee biochar slurry fuels: The effect of particle size distribution and additives. *Fuel*, 104:326–332.

[Sims et al., 2010] Sims, R. E. H., Mabee, W., Saddler, J. N., and Taylor, M. (2010). An overview of second generation biofuel technologies. *Bioresource Technology*, 101(6):1570–1580.

[Sirignano and Mehring, 2000] Sirignano, W. A. and Mehring, C. (2000). Review of theory of distortion and disintegration of liquid streams. *Progress in Energy and Combustion Science*, 26(4):609–655.

[Sisko, 1958] Sisko, A. W. (1958). The flow of lubricating greases. *Industrial and Engineering Chemistry*, (50):1789 – 1792.

[Slopiecka et al., 2012] Slopiecka, K., Bartocci, P., and Fantozzi, F. (2012). Thermogravimetric analysis and kinetic study of poplar wood pyrolysis. *Applied Energy*, 97:491–497.

[Song and Springer, 1996] Song, B. and Springer, J. (1996). Determination of Interfacial Tension from the Profile of a Pendant Drop Using Computer-Aided Image Processing2. Experimental. *Journal of Colloid and Interface Science*, 184:77–91.

[Tadros, 2010] Tadros, T. F. (2010). *Rheology of Dispersions: Principles and Applications*.

[Taylor, 1932] Taylor, G. I. (1932). The Viscosity of a Fluid Containing Small Drops of Another Fluid. *Proceedings of the Royal Society of London A*, 138:41–48.

[Thomas, 1965] Thomas, D. G. (1965). Transport characteristics of suspension: VIII. A note on the viscosity of Newtonian suspensions of uniform spherical particles. *Journal of Colloid Science*, 20(3):267 – 277.

[Tiwari et al., 2004] Tiwari, K. K., Basu, S. K., Bit, K. C., Banerjee, S., and Mishra, K. K. (2004). High-concentration coal-water slurry from Indian coals using newly developed additives. *Fuel Processing Technology*, 85(1):31–42.

[Tomasi Morgano et al., 2015] Tomasi Morgano, M., Leibold, H., Richter, F., and Seifert, H. (2015). Screw pyrolysis with integrated sequential hot gas filtration. *Journal of Analytical and Applied Pyrolysis*, 113:216–224.

[Trinh et al., 2013] Trinh, T. N., Jensen, P. A., Kim, D. J., Knudsen, N. O., Sørensen, H. R., and Hvilsted, S. (2013). Comparison of lignin, macroalgae, wood, and straw fast pyrolysis. *Energy and Fuels*, 27(3):1399–1409.

[Tsai and Vu, 1986] Tsai, S. C. and Vu, T. (1986). Atomization of coal-water slurry using twin-fluid jet atomizer. *Fuel*, 66(11):1596–1602.

[Tu et al., 2015] Tu, Y., Xu, Z., and Wang, W. (2015). Method for evaluating packing condition of particles in coal water slurry. *Powder Technology*, 281:121–128.

[Tudor et al., 1996] Tudor, P. R., Atkinson, D., Crawford, R. J., and Mainwaring, D. E. (1996). The effect of adsorbed and non-adsorbed additives on the stability of coal-water suspensions. *Fuel*, 75(4):443–452.

[Turian et al., 2002] Turian, R. M., Attal, J. F., Sung, D.-j., and Wedgewood, L. E. (2002). Properties and rheology of coal water mixtures using different coals. *Fuel*, 81:2019–2033.

[Turian et al., 1992] Turian, R. M., Hsu, F.-L., Avramidis, K. S., Sung, D.-J., and Allendorfer, R. K. (1992). Settling and rheology of suspensions of narrow-sized coal particles. *AIChE Journal*, 38(7):969–987.

[Umar et al., 2009] Umar, D. F., Usui, H., Komoda, Y., and Muta'alim (2009). Effect of dispersing and stabilizing additives on rheological characteristics of the upgraded brown coal water mixture. *Fuel Processing Technology*, 90(4):611–615.

[Usui et al., 1997] Usui, H., Saeki, T., Hayashi, K., and Tamura, T. (1997). Sedimentation Stability and Rheology of Coal Water Slurries. *Coal Preparation*, 18(3-4):201–214.

[Villermaux, 1998] Villermaux, E. (1998). Mixing and Spray Formation in Coaxial Jets. *Journal of Propulsion and Power*, 14(5):807–817.

[Weitz, 2004] Weitz, D. A. (2004). Packing in the spheres. *Science (New York, N.Y.)*, 303(5660):968–969.

[Wellinger et al., 2013] Wellinger, A., Murphy, J., and Baxter, D. (2013). *The Biogas Handbook: Science, production and applications*. Woodhead Publishing Limited, Cambridge.

[Widayatno et al., 2016] Widayatno, W. B., Guan, G., Rizkiana, J., Yang, J., Hao, X., Tsutsumi, A., and Abudula, A. (2016). Upgrading of bio-oil from biomass pyrolysis over Cu-modified β-zeolite catalyst with high selectivity and stability. *Applied Catalysis B: Environmental*, 186:166–172.

[Wright et al., 2008] Wright, M. M., Brown, R. C., and Boateng, A. A. (2008). Distributed processing of biomass to bio-oil for subsequent production of Fischer-Tropsch liquids. *Biofuels, Bioproducts and Biorefining*, 2(3):229–238.

[Xu et al., 2013a] Xu, J., Chen, L., Choi, H., Konish, H., and Li, X. (2013a). Assembly of metals and nanoparticles into novel nanocomposite superstructures. *Scientific reports*, 3:1730.

[Xu et al., 2013b] Xu, M., Liu, H., Zhao, H., and Li, W. (2013b). How to Decrease the Viscosity of Suspension with the Second Fluid and Nanoparticles? *Scientific reports*, 3:3137.

[Xu et al., 2009a] Xu, R., Zhuang, W., He, Q., Cai, J., and Hu, B. (2009a). Effects of Chemical Structure on the Properties of Carboxylate-Type Copolymer Dispersant for Coal-Water Slurry. *Environmental and Energy Engineering*, 55(9):2461 – 2467.

[Xu et al., 2009b] Xu, Y., Wang, T., Ma, L., Zhang, Q., and Wang, L. (2009b). Upgrading of liquid fuel from the vacuum pyrolysis of biomass over the Mo-Ni/γ-Al2O3 catalysts. *Biomass and Bioenergy*, 33(8):1030–1036.

[Yamamoto and Matsuoka, 1999] Yamamoto, S. and Matsuoka, T. (1999). Dynamic simulation of rod-like and plate-like particle dispersed systems. *Computational Materials Science*, 14(1-4):169–176.

[Yang et al., 2016] Yang, X., Tu, Y., Ren, Y., and Xu, Z. (2016). Optimization of packing state in brown coal water slurry based on the two-grade fractal model. *Fuel*, 168:54–60.

[Yang et al., 2015] Yang, Z., Kumar, A., and Huhnke, R. L. (2015). Review of recent developments to improve storage and transportation stability of bio-oil. *Renewable and Sustainable Energy Reviews*, 50:859–870.

[Yu et al., 2007] Yu, F., Ruan, R., Deng, S., Chen, P., Liu, Y., Wan, Y., Olson, A., and Kittelson, D. (2007). Physical and Chemical Properties of Bio-Oils From Microwave Pyrolysis of Corn Stover Physical and Chemical Properties of Bio-Oils From Microwave Pyrolysis of Corn Stover. 136(August 2016).

[Zarraga et al., 2000] Zarraga, I. E., Hill, D. a., and Leighton, D. T. (2000). The characterization of the total stress of concentrated suspensions of noncolloidal spheres in Newtonian fluids. *Journal of Rheology*, 44(3):671.

[Zhang et al., 2015a] Zhang, J., Zhao, H., Li, W., Xu, M., and Liu, H. (2015a). Multiple Effects of the Second Fluid on Suspension Viscosity. *Scientific reports*, 5:16058.

[Zhang et al., 2016] Zhang, J., Zhao, H., Wang, C., Li, W., Xu, J., and Liu, H. (2016). The influence of pre-absorbing water in coal on the viscosity of coal water slurry. *Fuel*, 177:19–27.

[Zhang et al., 2013] Zhang, M., Liaw, S. B., and Wu, H. (2013). Bioslurry as a fuel. 5. Fuel properties evolution and aging during bioslurry storage. *Energy and Fuels*, 27(12):7560–7568.

[Zhang et al., 2007] Zhang, Q., Chang, J., Wang, T., and Xu, Y. (2007). Review of biomass pyrolysis oil properties and upgrading research. *Energy Conversion and Management*, 48(1):87–92.

[Zhang et al., 2006] Zhang, Q., Chang, J., Wang, T. J., and Xu, Y. (2006). Upgrading bio-oil over different solid catalysts. *Energy and Fuels*, 20(6):2717–2720.

[Zhang et al., 2015b] Zhang, Y., Allen, M. C., Zhao, R., Deheyn, D. D., Behrens, S. H., and Meredith, J. C. (2015b). Capillary foams: Stabilization and functionalization of porous liquids and solids. *Langmuir*, 31(9):2669–2676.

[Zhang et al., 2014] Zhang, Y., Wu, J., Wang, H., Meredith, J. C., and Behrens, S. H. (2014). Stabilization of liquid foams through the synergistic action of particles and an immiscible liquid. *Angewandte Chemie - International Edition*, 53(49):13385–13389.

[Zhao et al., 2014] Zhao, H., Hou, Y. B., Liu, H. F., Tian, X. S., Xu, J. L., Li, W. F., Liu, Y., Wu, F. Y., Zhang, J., and Lin, K. F. (2014). Influence of rheological properties on air-blast atomization of coal water slurry. *Journal of Non-Newtonian Fluid Mechanics*, 211:1–15.

[Zhao et al., 2012] Zhao, H., Liu, H. F., Xu, J. L., Li, W. F., and Cheng, W. (2012). Breakup and atomization of a round coal water slurry jet by an annular air jet. *Chemical Engineering Science*, 78:63–74.